ESTI ESCR 2018

JOINT MEETING OF ESTI AND ESCR

MAY 24-26, 2018
GENEVA, SWITZERLAND

ONLINE ABSTRACT SYLLABUS

ESTI European Society of Thoracic Imaging

EUROPEAN SOCIETY OF **CARDIOVASCULAR RADIOLOGY**

Abstracts appear as submitted to the abstract/poster submission system and have not been checked for correctness and completeness.

INVITED ABSTRACTS

The role of imaging in current guidelines

M. R. Rees; Gwynedd/UK

Body: The current ESC/EACTS guidance for the management of aortic valve disease state that: The diagnosis of severe AS requires consideration of aortic valve area, flow rate, pressure gradients, left ventricular (LV) function, the degree of valve calcification, and blood pressure.
The strongest indication for intervention remains symptoms (spontaneous or on exercise testing).
Predictors of rapid symptom development can justify early surgery in asymptomatic patients, particularly when surgical risk is low.
Although current data favour transcatheter aortic valve replacement (TAVR) in elderly patients who are at increased risk for surgery (particularly if transfemoral access is feasible), the decision between TAVR and surgical AVR (SAVR) should be made by a Heart Team after careful, comprehensive evaluation of the patient, weighing individual risks and benefits.
A heart team discussion is recommended to discuss whether surgical repair of the aortic valve is possible
The ESC guidelines recommend analysis of the entire aorta at first diagnosis using CT or MRI.
After transcatheter or surgical valve replacement, echocardiography should be routinely performed within 30 days (preferably around 30 days) to establish baseline valve function, 1 year after implantation, and annually thereafter.
Take Home Points: The ESC guidelines recommend that the whole of the aorta is imaged prior to aortic valve surgery and this should be carried out via CT or MRI.
Cross-sectional imaging is increasingly important in the workup of patients with aortic valve disease but this is currently additional to cardiac ultrasound imaging

When and how to use CT

K. Nikolaou; Tübingen/DE

Body: Valvular heart disease and coronary heart disease (CHD) are highly prevalent in the general population and often coincide in the same patient. Cardiac computed tomography (CT) makes it possible to noninvasively rule out coronary disease, e.g., before valve surgery, and to potentially avoid invasive heart catheterization in patients with suspicion for CHD. However, the same imaging test also provides complex anatomical and functional information on the heart valves that may complement the information from echocardiography and Magnetic Resonance Imaging, making it possible to also characterize the etiology and severity of prevalent valvular disease. Moreover, for trans-catheter aortic valve replacement (TAVR / TAVI), CT has become the method of choice for pre-interventional planning of the procedure. In this session, the anatomy of the heart valves as displayed on a cardiac CT scan, and the technical requisites of cardiac CT for the study of the valves will be presented. Also, the usefulness of CT in the preoperative / pre-interventional study of the coronary arteries and of valvular disease will be discussed.
Take Home Points:
- Which information on the heart valves is present on a regular CT coronary angiography scan?
- What kind of cardiac CT scan can reveal what kind of information on cardiac valves?
- How important is cardiac CT scanning for presurgical and pre-interventional planning in patients with valvular heart disease?
- What complementary information can CT provide on the heart valves as compared to echocardiography and / or MRI?

When and how to use MRI

M. Hrabak Paar; Zagreb/HR

Body: MRI is a valuable tool in evaluation of valvular heart disease in patients with inadequate echocardiographic quality or discrepant results. It is the only technique capable of true in-vivo quantification of valvular regurgitation using phase-contrast imaging, therefore we can use it for accurate assessment of regurgitation severity. The severity of valvular stenosis can be estimated by planimetry of the valve opening or measurement of the peak antegrade velocity through the valve using phase-contrast imaging, but the MRI-measured peak velocity is usually underestimated due to partial volume averaging. Another advantage of MRI is the possibility to assess the impact of valvular disease on the cardiac chambers and large vessels, including atrial and ventricular volumes, systolic function and abnormalities of the ascending aorta and pulmonary arteries. As a reference standard for pulmonary valve assessment and evaluation of right ventricular volumes and function, MRI should be used for evaluation of patients with insufficiency of the tricuspid or pulmonary valves. Evaluation of myocardial fibrosis in patients with valvular disease has a prognostic impact, focal fibrosis can be assessed using late gadolinium enhancement, whereas diffuse interstitial fibrosis can be better evaluated using T1 mapping techniques and extracellular volume calculation.

Aortic stenosis – antegrade jet at the level of the aortic valve in systole (arrow).

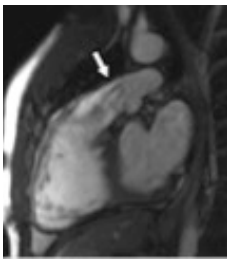

Pulmonary insufficiency – retrograde jet through the pulmonary valve in diastole (arrow) in a patient after Tetralogy of Fallot repair.

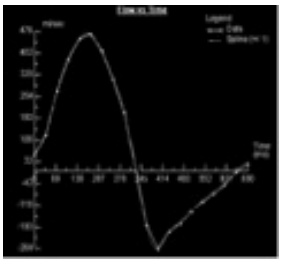

Pulmonary insufficiency – flow versus time curve depicting severe regurgitation with regurgitant fraction of 45%.

Take Home Points:

1. MRI is better for assessment of regurgitant than stenotic valvular lesions.
2. Besides assessment of valvular disease severity, in patients with valvular heart disease the impact of the pressure or volume overload on the cardiac chambers should be estimated, including volumes, systolic function and myocardial fibrosis.
3. MRI is the gold standard for assessment of the pulmonary valve disease.

Screening in pulmonary diseases: Dose issues

D. Tack; Braine-L'Alleud/BE

Body: Lung cancer is the most frequent cause of tumor-associated death and only has a good prognosis if detected at a very early tumor stage. The American National Lung Screening Trial (NLST) could prove that low-dose computed tomography (CT) screening is able to reduce lung cancer mortality by 20 %. There are a number of open or not yet satisfactorily answered questions, such as the definition of the appropriate screening population, the management of nodules detected by screening and the risk of cumulative radiation exposure. There are numerous pitfalls in calculating benefit/risks ratios because of uncertainties in real risks at low-dose, and of quantifying the radiation dose delivered to individuals. In addition, these ratios do not remain stable over time, mainly because of technology improvements enabling to scan at further reduced dose.
Take Home Points:
Benefit/risk ratio is in favour of screening.
Benefit/risk ratio increases when new thechnology enable new dose reductions.

Overdiagnosis of lung cancer and false positives in low-dose CT-screening

J. Brodersen; Copenhagen/DK

Body: Medical screening can lead to intended benefits and to unintended harms. In lung cancer screening with low-dose CT-scans the most frequent harm is false positives and the most severe harm is overdiagnosis.
The objective is this presentation is to present how the psychosocial consequences of false positives were investigated and how the degree of overdiagnosis of lung cancer was estimated in the Danish Lung Cancer Screening Trail.
Take Home Points: False positives is a very frequent harm in low-dose CT-screeing for lung cancer and might lead to substantial negative posychosocial consequences.
The Danish Lung Cancer Screening Trail raises the concern that overdiagnosis in lung cancer screening may be larger than what was previously reported in two trials.

Early recognition of CTEPH - The central role of the radiologist

G. Robinson; Bath/UK

Body: Untreated and undiagnosed chronic thromboembolic pulmonary hypertension can be fatal. CT signs of CTEPH can be subtle and are missed.
Increasing numbers of CT Pulmonary angiograms are being performed, some where CTEPH is on the differential, others where the clinician has not considered the diagnosis.
The radiologist plays a central role in early recognition; with a ‚negative' report the diagnosis of CTEPH may not be considered again.
We will review: Prognosis, incidence and prevalence of CTEPH. Normal pulmonary artery anatomy. CT Signs of CTEPH. Role of other imaging. Treatment options and workup.

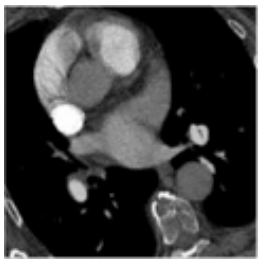

Image 1: CTPA. Left lower lobe web and middle lobe occlusion

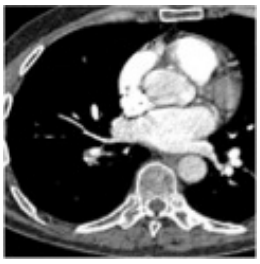

Image 2a: CTPA. Right lower lobe web

Image 2b: MRPA. Right lower web. Surgical work up.

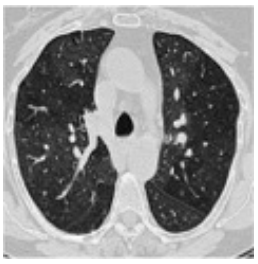

Image 3: CTPA. Mosaic lung and large segmental pulmonary arteries. Distal CTEPH.

Take Home Points: CTEPH is under-diagnosed. The radiologist should consider the diagnosis when reporting CTPA. The signs can be subtle and are missed. Understanding of normal anatomy is critical. Pulmonary endarterectomy is the treatment option of choice and curative in many. Medical treatments are available for non-operative cases.

And the right ventricle? Indicators of stress and failure

K.-F. Kreitner; Mainz/DE

Body: Pulmonary hypertension is a right heart failure syndrome. In early-stage PAH, the right ventricle tends to remain adapted to afterload with increased contractility and little or no increase in right heart chamber dimensions. However, less than optimal RV arterial coupling may already cause a decreased aerobic exercise capacity by limiting maximum cardiac output. In more advanced stages, RV systolic function cannot remain matched to afterload and dilatation of the right heart chamber progressively develops. In addition, diastolic dysfunction occurs due to myocardial fibrosis and sarcomeric stiffening. All these changes lead to limitation of RV flow output, increased right-sided filling pressures and under-filling of the left ventricle, with eventual decrease in systemic blood pressure and altered systolic ventricular interaction. These pathophysiological changes account for exertional dyspnoea and systemic venous congestion typical of PH. Complete evaluation of RV failure requires multiple imaging modalities. MRI and CT are capable of determining the etiology and pathophysiology of PH, and can be very useful in the management of patients with PH. Exciting new techniques such as RV tissue characterization with T1-mapping, 4D flow of RV and pulmonary arteries, and CT lung perfusion imaging are paving the way for a new era of imaging in PH. These imaging modalities complement echocardiography and invasive hemodynamic testing, and may be useful as surrogate endpoints for early-phase PH clinical trials. Treatment of RV failure in PH relies on: decreasing afterload with drugs targeting pulmonary circulation; fluid management to optimise ventricular diastolic interactions; and inotropic interventions to reverse cardiogenic shock.
Take Home Points: MR and CT get nmore and more important in assessment of the right ventrcle in patients with PH. MR furthermore provides prognostic information.

Noninvasive measurement of pulmonary artery pressure: Fact or fiction

J. Vogel-Claussen; Hanover/DE

Body: Pulmonary hypertension (PH) is a condition of varied aetiology, commonly associated with a poor clinical outcome. Patients are categorised on the basis of pathophysiological, clinical, radiological and therapeutic similarities. Recent advances in quantitative MR and CT imaging allow for a better initial characterization and measurement of the morphologic and flow related changes that accompany the response of the heart-lung axis to prolonged elevation of pulmonary arterial pressure and resistance and provide a reproducible, comprehensive and non-invasive means of assessing the course of the disease and response to treatment. Typical features of pulmonary arterial hypertension (PAH) occur primarily as a result of increased pulmonary vascular resistance and resultant increased RV afterload. Several MRI derived diagnostic markers have emerged, such as ventricular mass index (VMI), interventricular septal configuration and average pulmonary artery velocity having reported diagnostic accuracy similar to Doppler echocardiography.
Take Home Points:
To learn about noninvasive pulmonary pressure estimation using Doppler echocardiography.
To learn about noninvasive pulmonary pressure estimation using MRI.
To learn about noninvasive pulmonary pressure estimation using CT.

Imaging the lungs in the non HIV immuno-comprimised patient

T. Franquet; Barcelona/ES

Introduction

Pulmonary infection is a major cause of morbidity and mortality in patients with impaired immune function. In the last several decades, AIDS epidemic, advances in the treatment of cancer, organ transplantation, and immunosuppressive therapy has resulted in large numbers of patients who develop abnormalities in their immune system. Mildy impaired host immunity as it occurs in chronic debilitating illness, diabetes mellitus, malnutrition, alcoholism, advanced age, prolonged corticosteroid administration and chronic obstructive lung disease have also been regarded as predisposing factors of pulmonary infections.

Pattern recognition of pulmonary infection in the immunocompromised non-HIV patient.

High-resolution CT can be helpful in the detection, differential diagnosis, and management of immunocompromised patients with pulmonary complications (5). Although accurate clinical information is essential to narrow the differential diagnosis, it is often still impossible to determine the cause of parenchymal abnormalities in this group of patients. Combination of pattern recognition with knowledge of the clinical setting is the best approach to pulmonary infectious processes. A specific pattern of involvement can help suggest a likely diagnosis in many instances.

The most common patterns seen at HRCT in acute pulmonary infections in these patients include nodules, tree-in-bud appearance, ground-glass attenuation, consolidation and airway disease.

Nodules

Angioinvasive aspergillosis occurs almost exclusively in immunocompromised patients with a severe neutropenia. The characteristic CT findings consist of nodules surrounded by a halo of ground-glass attenuation (halo sign) or pleural based wedge-shaped areas of consolidation. In severely neutropenic patients the halo sign is highly suggestive of angioinvasive aspergillosis. The ground-glass halo reflects the presence of hemorrhage surrounding the nodule. A similar appearance has been described in a number of other conditions including infection by Mucorales, Candida, herpes simplex and cytomegalovirus. Viral infection occurs in organ and bone marrow transplant patients. CMV infection usually develops between 1 and 4 months after transplantation. The HRCT findings of CMV infection are variable consisting of lobar consolidation, diffuse and focal parenchymal haziness, and multiple small nodules with associated areas of ground-glass attenuation ("halo").

Opportunistic fungi constitute the second most common group of pathogens with a higher probability of causing infection in allogeneic than in autologous transplant recipients. Fungi that frequently produce nodular opacities include Cryptococcus, Coccidioides, Blastomyces, Aspergillus, and Mucorales.

Nontuberculous mycobacteria infection may present as nodular lesions on the chest radiograph. The nodules may be single or multiple and are frequently associated with centrilobular nodules and branching opacities resulting in a "tree-in-bud" appearance.

"Tree-in-bud" pattern

The "tree-in-bud" pattern, first described in diffuse panbronchiolitis and endobronchial spread of tuberculosis, represent bronchioles filled with mucus or inflammatory material resulting in centrilobular tubular, branching, or nodular structures. A variety of bacterial, mycobacterial, fungal, and viral pathogens may cause bronchogenic dissemination and bronchiolar impaction by mucus or pus, resulting in typical "tree-in-bud" appearance.

Aspergillus bronchiolitis is characterized on HRCT by the presence of centrilobular nodules and branching linear or nodular opacities giving an appearance resembling a "tree-in-bud". The centrilobular nodules have a patchy distribution in the lung and are similar to those seen in a number of different infectious conditions, including endobronchial spread of pulmonary tuberculosis, M. Avium-intracellulare, viral and mycoplasma pneumonia.

Ground-glass opacity

Ground-glass opacity is defined as a localized increase in lung attenuation that allows visualization of vascular structures coursing through the affected region. Ground glass attenuation is a common but nonspecific HRCT finding in the non-HIV immunocompromised patients. This finding may represent either alveolar or interstitial disease and may also be associated with different entities.

In immunocompromised patients the differential diagnosis includes infections such as PCP, CMV and Mycoplasma, drug induced lung disease, pulmonary hemorrhage and cryptogenic organizing pneumonia.

Consolidation

Focal or multifocal areas of consolidation in non HIV patients may be seen with various infections. Bacterial infections are more frequent than fungal infections in non-HIV immunocompromised patients. Infections caused by fungi are most commonly seen in neutropenic patients with hematological diseases. A distinct form of aspergillus infection called semi-invasive or chronic necrotizing aspergillosis, may be seen in patients with chronic debilitating illness, diabetes mellitus, malnutrition, alcoholism, advanced age, prolonged corticosteroid administration, and chronic obstructive lung disease. This uncommon form of Aspergillosis may progress slowly over months or years. Radiologically, unilateral or bilateral segmental areas of consolidation with or without cavitation and/or adjacent pleural thickening, and multiple nodular opacities are demonstrated. Mycobacterial infection may also cause focal areas of consolidation, with or without cavitation.

Airway disease

Diseases of the airways are becoming increasingly more frequently recognized in immunocompromised non-HIV patients. Infectious causes for airway disease include bacterial bronchitis, tuberculous involvement of the airway, and necrotizing tracheobronchial aspergillosis. Necrotizing bronchial aspergillosis is a rare form of invasive aspergillosis that may be seen on CT

as an endobronchial mass, an obstructive pneumonitis and/or collapse, or as a hilar mass. The diagnosis of this form of aspergillus infection is usually based on the presence of abnormal chest radiograph and bronchoscopic biopsy specimen consistent with tissue invasion.

Suggested articles

Brown MJ, Miller RR, Müller NL. Acute lung disease in the immunocompromised host: CT and pathologic findings. Radiology 1994;190:247-254

Fishman JA, Rubin RH. Infection in organ transplant recipients. N Engl J Med 1998;338:1741-1751

Primack SL, Müller NL. HRCT in acute diffuse lung disease in the immunocompromised patient. Radiol Clin North Am 1994; 32:731-744.

Aquino SL, Gamsu G, Webb WR, Kee ST. Tree-in-bud pattern: frequency and significance on thin section CT. J Comput Assist Tomogr 1996; 20:594-599

Franquet T, Müller NL, Giménez A, Guembe P, de la Torre J, Bagué S. Spectrum of pulmonary aspergillosis : histologic, clinical, and radiologic findings. RadioGraphics 2001;21:825-837.

Erasmus JJ, McAdams HP, Farrell MA, Patz, Jr. EF. Pulmonary nontuberculous mycobacterial infection: radiologic manifestations. RadioGraphics 1999; 19:1487-1503.

Take Home Points:

1) Radiologists must be familiar with the various types of immunosupression
2) Patient's history, demographic characteristics, and host immunity are necessary and may influence the radiologic approach
3) Certain imaging findings may suggest specific disease processes (e.g., „Halo sign" in neutropenic patients.

Angioinvasive aspergillosis. Axial CT scan shows a dense nodule surrounded by a „halo" of ground-glass opacity.

EDAC and Tracheobronchomalacia

J. A. J. J. Verschakelen, W. de Wever, J. Coolen, A. Dubbeldam, C. Dooms; Leuven/BE

Body: Excessive dynamic airway collapse (EDAC) and tracheobronchomalacia (TBM) are two distinct functional conditions that affect the trachea and main bronchi and that are characterized by generalized or focal airway wall weakness. In TBM the weakness of the airway is due to impaired cartilage integrity. In EDAC the cartilage is intact and the airway weakness is possibly related to a reduction and/or atrophy of the elastic fibers resulting in a bulging of the membranous part of the airway into the lumen. Hence, both entities have different morphology on imaging studies and bronchoscopy.

While TBM is a true central airways cartilaginous disease, most EDAC are seen as a consequence of peripheral airway obstruction from emphysema, chronic bronchitis or asthma associated with airway inflammation. EDAC has also been described in obese patients.

Narrowing of the central airways during expiration is, however, also seen in normal individuals and the frontier between normal and abnormal narrowing is not always clear. In addition, it has been shown that even in patients with COPD the degree of narrowing may be independent of disease severity and not correlated with physiologic parameters.

This presentation will summarize the current insights in TBM and EDAC and will discuss the potential role of imaging in the diagnosis of these entities

Take Home Points:

1. Tracheobronchomalacia and EDAC have different morphology on imaging studies and bronchoscopy.
2. Tracheobronchomalacia is a true central airways cartilaginous disease.
3. EDAC is characterized by excessive bulging of the posterior membrane inside the central airway lumen.
4. EDAC may be seen in normal individuals and may not interfere with airflow.

Non tuberculous mycobacterium infection: Role of imaging

A. Christe; Berne/CH

Body: Mycobacterium avium-intracellulare (MAC) ist the most frequent representative of Non Tuberculous Mycobacterium Infection (NTM: ~60% MAC). It is not possible to radiologically distinguish MAC from other NTM like Mycobacterium kansasii. MAC basically appears in two forms: Classic upper lobe fibro-cavitary pattern Nodular bronchiectatic form.

The first pattern is typically seen in middle aged men with underlying COPD and some sort of immunocompromise. In its appearance the distribution and CT patterns remind of a typical tuberculousis infection with upper lobe predominance, cavities, surrounding tree-in-bud opacities and fibrosis. The second form is usually seen in older women, who suppress their cough reflex voluntarily (Lady Windermere syndrome). Usually the middle lobe and the lingula are affected with bronchiectasis and associated centrilobular nodules. MAC is also one etiology of the right middle lobe syndrome. Other causes may be chronic bronchitis, granulomatous inflammation or organizing pneumonia which lead to bronchiectasis with atelectasis.

Since colonization of the airways by MAC is frequent and isolation of MAC does not have to be pathological, the role of imaging is to find typical MAC patterns in chest CT. The correlation of both reveals the diagnosis. Patients with MAC infection are not contagious, unlike those with Tbc.

Syndromes assocoated with NTM.

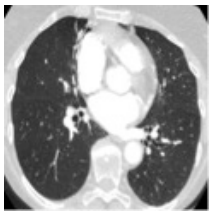

Lady Windermere syndrome with middle lobe MAC affection

Take Home Points: Classic upper lobe fibro-cavitary pattern in smoking men Nodular bronchiectatic form in the middle lobe and lingula in older women (Lady Windermere)

Organising Pneumonia

M. Occhipinti; Florence/IT

Body: Organizing pneumonia (OP) is a histopathological response pattern to lung inflammation. Many different clinical conditions can cause lung inflammation and this in turn can evolve into different outcomes. Clinical conditions leading to OP include bacterial and viral infections, drugs, connective tissue diseases, immunological disorders, organ transplants, radiation, and other minor entities. The parenchymal answer to these miscellanea has clearly defined histopathological findings, whereas the radiological appearance is characterized by heterogeneous patterns. The typical pattern consists of peripheral parenchymal consolidations with air bronchogram, but atypical patterns are far from being uncommon. Imaging with computed tomography plays a key role in both diagnosis and follow-up of OP, determining also patient prognosis. OP can rapidly resolve after corticosteroid treatment, it can relapse, or even progress into irreversible fibrosis. OP can also coexist with lung fibrosis, in an overlap entity characterized by worse prognosis than OP alone. Recognition of signs of relapse and fibrosis is helpful in the management of the patient. In particular, both radiological and clinical determinants of OP relapse, such as neutrophil percentage in the bronchoalveolar lavage, the extent of consolidation on CT, the level of fibrin deposition in lung biopsy specimens, and the duration of therapy have been recently investigated to help physicians in targeting patient's therapy.
Take Home Points: OP is a non-specific response to lung injury Imaging plays a key role in both diagnosis and follow-up of OP Typical patterns as well as atypical patterns of OP need to be borne in mind to avoid misinterpreting the disease Clinical and radiological determinants of OP relapse are helpful in patients management

TNM 8 Update

A. R. Larici; Rome/IT

Body: Lung cancer is a leading cause of cancer related mortality worldwide. A correct staging is the prerequisite for an adequate management of patients. Recently the 8th edition of TNM classification introduced relevant changes of descriptors T and M. Regarding T, it has been demonstrated by survival analyses that from 1 to 5 cm of diameter every centimeter counts, and that larger tumors are best aligned with either T3 (tumor size of more than 5 to 7 cm) or T4 (tumor size of more than 7 cm). This finding further confirms the common intuition that the larger the tumor, the worse the prognosis. Regarding M, the category of intrathoracic lesions is remained M1a, while extrathoracic lesions has been distinguished in M1b and M1c to indicate respectively one (oligometastatic disease) and more than one lesion. In this context it is advisable that radiologists report the number of lesions if only one organ is involved and the number of organs if many. This approach has a relevant clinical impact because oligometastatic disease nowadays is managed and treated differently respect to an extensive M stage disease. The N descriptors are unchanged, but it has been demonstrated that the number of involved nodal stations and nodal zones has prognostic impact. Several limitations still remains, such as the lymph node groups and the number of lymph nodes involved not included in TNM, the categorization of lymphangitic carcinomatosis as an independent descriptor and the evaluation of multiple lung lesions. Certainties and controversies on the topic will be argued in this session, taking into account that cancer staging should be always considered a multidisciplinary process.
Take Home Points:
- Reclassification of some T descriptors with more relevance to tumor size and identification of three different M groups
- Acknowledgment of the importance of N disease quantification
- More stage groupings for better prognostic stratification
- More recommendations for uniform staging although with some persistent limitations

Imaging after radiotherapy

B. Ghaye; Brussels/BE

Body: Radiation-induced lung disease (RILD) is frequent after therapeutic irradiation of thoracic malignancies. Many technique-, treatment-, tumor- and patient-related factors influence the degree of injury sustained by the lung after irradiation. Based on the time interval after the completion of the treatment RILD presents as early and late features characterized by inflammatory and fibrotic changes, respectively. They are usually confined to the radiation port. Though the typical pattern of RILD is easily recognised after conventional 2-D radiation therapy (RT), RILD may present with atypical patterns after more recent type of 3D- or 4D-RT treatment. Three atypical patterns are reported: the modified conventional, the mass-like and the scar-like patterns. Knowledge of the various features and patterns of RILD is important for correct diagnosis and appropriate care. RILD should be differentiated from recurrent tumoral disease, infection and radiation-induced tumors. Due to RILD, the follow-up after RT may be difficult as RECIST criteria may be unreliable to assess tumor response particularly after stereotactic ablation RT (SABR/SBRT). Long-term follow-up should be based on clinical examination and morphological or/and functional investigations including CT, PET-CT, pulmonary functional tests, MRI and PET-MRI. Refinement in morphological criteria to accurately depict early recurrence is still necessary.

Take Home Points:

- Any thoracic tissue exposed to radiations can show radiological features of radiation injury; in particular lung injury is frequent after thoracic radiation therapy (RT) and features of radiation-induced lung disease (RILD) are important to know.
- Two major features are characteristics of RILD: confinement to the fields of radiation and nonconformity to anatomic boundaries (i.e. the fissures).
- Knowledge of the treatment planning, including the beams arrangement and the dose distribution, may aid in the interpretation.
- RILD presents as early and late features based on the time interval after the completion of the treatment.
- The inflammatory early phase appears between 1 and 3 months after the end of the treatment and lasts up to 6 months. With stereotactic ablation RT (SABR), it may appear around the 4th month after completion of RT.
- The fibrosing late phase results from an unresolved early phase and may last for 6 to 12 months or even 24 months in some conditions. Lesions are usually considered as stable and definite after 2 years.
- Technique-, treatment-, tumor- and patient-related factors influence the degree of injury sustained by the lung after irradiation.
- Advances in RT techniques allow to precisely create shaped dose distribution closely conforming to the target volume while minimizing the dose to critical normal tissue, and therefore changing the pattern of RILD, named as modified conventional, mass-like and scar-like patterns.
- Long-term follow-up up to 5 years after RT should be based on morphological or/and functional investigations (CT, PET-CT, pulmonary functional tests, MRI and PET-MRI).
- RILD should be differentiated from recurrent tumoral disease, infection and radiation-induced tumors

Imaging after precision chemotherapy in the modern era of cancer therapy

M.-P. Revel; Paris/FR

Body: To avoid continuing anti-cancer treatment with no efficacy, the accurate assessment of therapeutic response is essential, with a major role of imaging. The Response Evaluation Criteria in Solid Tumors (RECIST) version 1.1 is the most commonly used criteria to assess tumor response under chemotherapy in lung cancer patients. Up to 5 measurable target lesions are to be defined on the baseline CT. Partial response is defined as at least 30% decrease in the sum of diameters (longest axial transverse diameters) of target lesions, taking as reference baseline sum diameters. However, morphological measurement has limitation for targeted therapies inducing necrosis or cystic changes without necessarily producing tumor shrinkage. Positron emission tomography (PET) with 18F-fluorodeoxyglucose (FDG) has been widely adopted as a tool for evaluating metabolic activity in tumors. The PET Response Criteria in Solid Tumors (PERCIST) was proposed as a new method for the quantitative assessment of metabolic changes, and FDG PET may also be performed to detect earlier tumor responses to anti-cancer therapies. However, the assessments of tumor responses have shown considerable difference between the PERCIST and RECIST criteria in several studies. Therefore, the advantage of the PERCIST over the RECIST criteria need to be further evaluated. Immune checkpoint inhibitors now belong to the therapeutic landscape of lung cancer. The evaluation of tumor response to these new agents must be performed by using adapted criteria. Indeed, at least 6% of patients experience response to this treatment despite the apparition of new lesions or initial increase of target lesions, due to the afflux of T cells around the tumor cells. Any apparent progression should thus be confirmed at 4 weeks, to distinguish between pseudo progression and true progression, which is the main difference between RECIST and iRECIST criteria (for immune-related Response Evaluation Criteria in Solid Tumor).

Take Home Points:

- RECIST 1.1 criteria should be used for assessing tumor response under chemotherapy
- PET CT might be used to detect earlier tumor responses
- First progession under immunotherapy should be confirmed at 4 weeks to distinguish between pseudo and true progression

Challenges of Artificial Intelligence and Teleradiology

S. Wildermuth; St. Gallen/CH

Body: The field of medical imaging has witnessed a revolution thanks to the digital transformation initiatives and availability of advanced clinical applications in imaging. New imaging techniques are helping Radiologists and other diagnosticians with greater anatomical and clinical details, highlighting the need for fast access to imaging reports and results and collaborative workflows. Sophistication of artificial intelligence (AI) has allowed for detailed quantification of radiographic characteristics of tissues using predefined engineered algorithms or deep learning methods. However, there are critical challenges associated with the analysis of medical imaging data. While some of these challenges are specific to the imaging field, many others are generic and have already been addressed in other quantitative fields. These pitfalls will be identified and recommendations for analysis strategies of medical imaging data including data normalization will be discussed.
Pulmonary imaging, with chest radiography and computed tomography, has always been one of the focus areas in computer aided diagnosis (CAD). Over the last years, machine learning became the dominant technology for tackling CAD in the lungs, generally producing better results than do classical rule-based approaches. In a rapidly changing field, we have seen how even better results can be obtained with deep learning. The key differences among rule-based processing, machine learning, and deep learning are presented for various applications of CAD in the chest.
Augmented Intelligence is the intersection of machine learning and advanced applications, where clinical knowledge and medical data converge on a single platform. The potential benefits of Augmented Intelligence are realized when it is used in the context of workflows and systems that healthcare practitioners operate and interact with. Unlike Artificial Intelligence, which tries to replicate human intelligence, Augmented Intelligence works with and amplifies human intelligence.
Teleradiology: The rapid development of telecommunication tools as well as a fundamental change in practice and healthcare economics will certainly influence teleradiology in the upcoming years. The challenges for experts and policy makers in promoting appropriate criteria and guidelines for adequate use of teleradiology in clinical practice should be solved in reasonable time among different countries in Europe. It will finally be discussed why little attention has been given to the possible use of teleradiology in enhancing quality and safety of radiological practice.
Take Home Points: Compare differences in CAD, Artificial Intelligence (AI) and Augmented Intelligence Understand concepts and challenges of AI applications in chest radiology Provide insight into current trends and solutions for teleradiology Understand challenges of insourcing and outsourcing teleradiology concepts

Imaging in ECMO

A. Nair; London/UK

Body: The advent of extracorporeal membranous oxygenation (ECMO) as a bridging therapy for patients with severe respiratory failure has revolutionised the care of such patients. ECMO helps to maintain gaseous exchange while therapies aimed at treating the underlying cause of the respiratory failure are initiated; in this way ECMO "buys time" while simultaneously diminishing the reliance on high levels of ventilatory pressure (and its associated complications).
In this presentation, the technical aspects of ECMO administration are briefly reviewed. We then focus on imaging protocol and techniques, especially CT techniques, for evaluating the ECMO patient, including the assessment of recruitability and complications. The role of imaging in distinguishing the underlying aetiology of severe respiratory failure in such patients is also discussed, as well as potential roles for prognostication. Finally, we outline some areas of future imaging research in this novel field.
Take Home Points: CT imaging in ECMO aims to provide a baseline assessment of lung parenchyma and recruitment assessment using low and high-pressure ventilation imaging. CT is also used to exclude any sites of intracranial or intracorporeal haemorrhage prior to commencing an ECMO circuit, since the circuit requires a degree of anticoagulation. Serial imaging can help in identifying the underlying aetiology of severe respiratory failure as well as assess complications and prognosis.

Acute aortic imaging

A. Oikonomou; Toronto, ON/CA

Body: The term "acute aortic syndrome" (AAS) includes a heterogeneous group of entities related to non-traumatic life threatening pathologies of the thoracic aorta, namely acute aortic dissection (AAD), intramural hematoma (IMH) and penetrating atherosclerotic ulcer (PAU). These entities share similar clinical presentations and may mimic other causes of chest pain, such as myocardial infarction, esophageal perforation or pulmonary embolism. Inflammatory and traumatic etiologies of acute aortic entities are not considered as part of the clinical spectrum of AAS, as they both demonstrate distinct pathophysiological and clinical features.
The most important risk factor is hypertension especially in the elderly population. AAS has a high associated mortality and morbidity rate, which mandates early diagnosis and management. The typical clinical presentation is tearing severe chest pain with

maximal intensity at the time of onset. AAS is classified as type A (Stanford) involving the ascending aorta and type B distal to the origin of the left subclavian artery. If left untreated type A AAS has more than 50% mortality and therefore needs urgent medical intervention, while the mortality rate of after medical treatment of type B aortic dissection is clsoe to 10%.
MDCT is the modality of choice for imaging AAS with sensitivity and specificity reaching 100 and 99% respectively. Use of ECG gating is critical for reducing cardiac motion artifacts. Precontrast image acquisition is essential for diagnosis of IMH and intrapleural or intrapericardial rupture. In case of renal failure or contrast allergy MRI is an alternative imaging modality although its role is more crucial for the long term follow up of AAS. Transthoracic and transesophageal echocardiography provides a widely available and portable option at the bedside.
AAD is caused by a disruption of the intima and inner layer of the media enabling blood to split the aortic media creating a false and a true lumen. Therefore the cardinal imaging features of AAS are the the intimomedial flap and a double-channel aorta. Attention to various artifacts that mimic AAD must be made. Certain imaging features are helpful to differentiate true from false lumen, such as the cobweb and beak sign and the lower density of the false compared to the true lumen.
IMH was originally thought to be caused by hemorrhage within the media due to rupture of vasa vasorum, however recently it is believed to result from microscopic tears in the intima as seen in surgery or autopsy. On unenhanced CT, IMH appears as high density crescent-shaped thickening of the aortic wall which does not enhance on post contrast images. No flap is seen. Differentiation between intramural hematoma and thrombosed aortic dissection can be challenging.
PAU is caused when an atherosclerotic lesion ulcerates and penetrates the internal elastic intima and allows contained hematoma formation within the media. It is most commonly seen in the sescending thoracic aorta, in areas of increased atherosclerosis. On enhanced CT a PAU is seen a high density outpouching ulcer of the aortic wall with jagged edges and initmal calcification in an area of extensive atherosclerosis.
Take Home Points:
1. Acute aortic syndrome encomapsses three different entities, namely acute aortic dissection, intramural hematoma and penetrating atherosclerotic ulcer that share similar clinical presentation and may have overlap of imaging findings or occur in isolation.
2. ECG-gated multidector CT is the modality of choice for the diagnosis and classification of AAS. Echocardiography is critical for prompt diagnosis at the bedside and MR angiography plays significant role in the longterm follow up of these patients.
3. Specific imaging findings help the radiologist to reach an accurate diagnosis and identify specific features that have prognostic significance.

MRI parametric mapping for perfusion and tissue characterisation: Clinical tool or work in progress

S. E. Petersen; London/UK

Body: Cardiovascular magnetic resonance (CMR) has come of age. CMR is non-invasiveness and does not require radiation, but its major strength is the ability to characterise and quantify myocardial tissue and myocardial blood flow comprehensively. This invited presentation will discuss the potential and the current evidence regarding CMR parametric mapping for diagnosis, risk stratification and treatment monitoring. The quantitative approaches discussed will include rest and stress myocardial perfusion and tissue characterisation techniques, such as native T1, T2, T2*, extracellular volume fraction (ECV).
Take Home Points: CMR parametric mapping can quantify perfusion and myocardial tissue characteristics CMR parametric mapping holds promise for diagnosis, risk stratification and treatment monitoring CMR parametric mapping may benefit patients by contributing to the personalised or stratified medicine agenda

Workup of Acute Coronary Syndrome

R. Salgado; Edegem/BE

Body: Acute chest pain remains a frequent reason for consulting the emergency department. Nevertheless, up to 20% of patients with myocardial infarction have atypical symptoms. Also, ECG and biomarkers are not always specific or diagnostic, leaving the treating physician with an inconclusive diagnosis and the inability to safely discharge a patient.
Recent studies using CT-angiography in the department have shown that this imaging modality can help in the stratification of patients suspected of acute coronary syndrome but with otherwise inconclusive examinations. Furthermore, its diagnostic efficacy can be further improved by combined the CT results with new biomarkers like high-sensitive troponins.
During the lecture, we will review the evolving role of CT in acute coronary syndrome, with practical guidelines for clinical implementation.
Take Home Points:
1. Some patients suspected of an acute coronary syndrome have an inconclusive intitial work-up.
2. Cardiac-CT can help in the safely discharge from the emergency department of selected patients.
3. New biomarkers like high-sensitive troponins further help in the correct triage of patients.

The Role of CT in Acute Pulmonary Embolism

G. Aviram; Tel-Aviv/IL

Body: Pulmonary embolism (PE) is life threatening condition, demanding early and accurate diagnosis, since both false negative (missing PE) and false poitive (unnessecary anticoagulation), can be harmful. Management decisions upon PE diagnosis, can largely span between immediate thrombolysis with addmisson to intensive care unit, to early discharege for home treatment, based on the patient's status and PE severity.
Appropriate triage of patients using clinical prediction rules and D-dimer can reduce unnecessary use of imaging, and recently D-dimer cut-off values were age-adjusted, reducing the number of older patients "PE unlikely" probability, that will need imaging for suspected PE. On the other hand, patients with "high clinical probability for PE, are directly referred for imaging.
CT pulmonary angiography (CTPA) is the modality of choice for PE diagnosis. Debates exist with regard to the appropriate diagnostic yield of CTPA, and the clinical significance of isolated subsegmental emboli. Risk stratification of patients diagnosed with acute PE is based upon history, clinical assessment, biomarkers and imaging. CTPA can contribute substantially for immediate risk assessment, by demonstrating the dimensions of the cardiac chambers, and provision of some dynamic parameters which reflect the increased pressures in the right heart, like reflux of the contrast to the IVC.
Take Home Points: In this presentation we will discuss current issues related to acute PE diagnosis by CTPA, and how CTPA can contribute to risk assessment, thus leading to improved and prompt therapeutic decisions.

Review of methodology (parametric tissue mapping: T1-; T2-; T2*- and ECV)

N. Kachenoura; Paris/FR

Body: The number of studies involving cardiac magnetic resonance (CMR) parametric tissue mapping and ECV estimation increased substantially in the last decade. Indeed, present CMR literature is dedicated to the usefulness of myocardial T1-, T2-, T2* and ECV-mapping in various pathological conditions. Accordingly, this presentation will focus on summarizing: 1) technical aspects of myocardial tissue mapping including drawbacks, limitations and recommendations, 2) main clinical findings in terms of associations with histological tissue evaluation and in terms of ability to characterize myocardial involvement in various pathological conditions.
Take Home Points: Myocardial parametric mapping provide valuable clinical parameters Need of self-reference values (Control population) Achieve studies with the same sequence and same scheme Define a unique and common sequence (multicenter studies) Favour multi-parametric interpretation Improve fitting algorithms and include fat suppression Progression towards 3D mapping to avoid sampling errors

Are my mapping results normal or abnormal: A practical approach

N. Kawel-Boehm; Chur/CH

Body: The situation in clinical practice where mapping results of a single individual have to be classified as normal or abnormal differs from the research scenario where the mean value of an entire study group of subjects with a certain disease is compared to the mean value of a group of healthy individuals. To classify values of a single subject as normal or abnormal, reference ranges are required.
Since measurements of T1 and T2 time vary with several technical, acquisition related, physiological and postprocessing related parameters, no uniform reference ranges exist but site specific reference values have to be established.
According to current guidelines, the extracellular volume fraction (ECV) can be compared to reference ranges published in the literature using the same CMR system and pulse sequence.
Regarding T2* mapping used to assess myocardial iron overload, measurements can be classified in three different risk categories.
Take Home Points:
- Site specific reference ranges have to be established for T1 and T2 mapping.
- ECV can be compared to reference ranges from the literature using the same CMR system and pulse sequence.
- T2* values can be classified in three different risk categories.

Remote expert opinion in Idiopathic Pulmonary Fibrosis

G. Sommer; Basel/CH

Body: We present a program for remote expert reading of CT images in patients with suspected idiopathic pulmonary fibrosis (IPF). The program was launched at University Hospital Basel in 2016 as a web-based service for medical doctors, mainly pulmonologists, in eastern European countries. The goal of the program is to support local interdisciplinary boards for IPF with expert opinion for CT interpretation according to current guidelines. Referring physicians can upload CT data and related clinical information via a secured website hosted by a swiss internet provider (Swisscom). Images are transmitted to our local picture archiving and

communication system (PACS) and automatically integrated into our radiology information system (RIS). Images are reviewed by a radiologist and a pulmonologist in consensus, both with specific expertise in interstitial lung diseases. Findings are classified according to current ATS/ERS/JRS/ALAT guidelines in structured reports. Until January 2018, 463 cases from 54 referring physicians in 11 countries were reviewed including larger centers and university hospitals. The patterns identified on CT were "usual interstitial pneumonia (UIP)" in 166 cases (36%), "possible UIP" in 83 cases (18%) and "inconsistent with UIP" in 211 cases (46%). Reports are finalized once a week, resulting in a turnaround time of < 4 days on average. In a recent survey, all referrers considered this turnaround time appropriate and stated that reports had significant impact on patient management. Difficulties encountered in the program were mainly of technical nature and mostly related to the electronic file format and the acquisition quality of the uploaded datasets.

Take Home Points:

- CT plays a key role in diagnosis of pulmonary fibrosis, criteria are defined in the ATS/ERS/JRS/ALAT guidelines from 2011.
- 2nd opinion remote expert reading provides standardized reporting of CT according to current guidelines and thereby supports development of local expertise in participating centers.
- Remote assessment of CT data, however, does not replace local interdisciplinary panels in making the final diagnosis.

Web-based Education

T. C. McLoud; Boston, MA/US

Body: Traditionally radiologists have learned by traditional means (textbooks,journals, and case based reviews and standard lectures and courses.) Web based education provides a vehicle for „adult learning" ie self directed,self managed and goal oriented. Content can include „teaching files" or interactive modules which permit self assessment. Web based material can be available at the „point of care" as the radiologist interprets cases (STATDX). Web based modules may provide animated annotation, pretest and post test features and feedback. Several commercial products provide many of these features, RADPRIMER, E-anatomy, Qevlar. ACR case in point provides daily quizzes for the practicing radiologist. Other applications can be added to standard lectures formats with audience response systems (RSNA diagnosis live, Poll everywhere) which permit the audience to respond to proposed questions using their electronic devices (I-phone).

Take Home Points:

1. Education in radiology has changed.
2. Interactive learning with self assessment are important components.
3. Web based programs provide both point of care information and self assessment
4. Audience response systems which use the web for polling response to questions allow participants to assess their level of knowledge and compare their performance with others.

Imaging work up in Lung Volume Reduction

M. Silva; Parma/IT

Body: Several lung volume reduction (LVR) techniques have been increasingly evaluated in patients with advanced pulmonary emphysema. The radiologist plays a pivotal role in the characterization of parenchymal damage and, thus, assessment of eligibility criteria. This review aims to discuss the most common LVR techniques, namely LVR surgery, endobronchial valves, and coils LVR, with emphasis on the role of computed tomography (CT). Several trials have recently highlighted the importance of regional quantification of emphysema by computerized CT-based segmentation of hyperlucent parenchyma, which is strongly recommended for candidates to any LVR treatment. In particular, emphysema distribution pattern and fissures integrity are evaluated to tailor the choice of the most appropriate LVR technique. Furthermore, a number of CT measures have been tested for the personalization of treatment, according to imaging detected heterogeneity of parenchymal disease.
CT characterization of heterogeneous parenchymal abnormalities provides criteria for selection of the preferable treatment in each patient and improves outcome of LVR as reflected by better quality of life, higher exercise tolerance, and lower mortality.
Take Home Points: Accurate regional quantification of pulmonary emphysema is required for selection of the appropriate technique and targeting of lung volume reduction. Atelectasis postendobronchial valves lung volume reduction is positive predictive factor, which is observed in a minority of cases. Fissural integrity drives the choice between endobronchial valves or lung volume reduction with coils. Any LVR treatment may be associated with radiologic changes that need to be carefully interpreted to distinguish between complications and normal evolution. The predictive value of several computerized quantitative CT measures has been recently tested; amongst these, measures of lung perfusion seem the most promising ones.

Quantitative imaging in COPD

P. A. Grenier; Paris/FR

Body: Visual and quantitative CT (QCT) evaluation of CT images in COPD patients contribute to a personalized approach to the treatment of patients with COPD. QCT is useful for identifying and sequentially evaluating the extent of emphysematous destruction, changes in airway dimensions and expiratory air trapping.
Emphysema can be objectively measured using density mask analyses and quantifying the fraction of low attenuation areas of the lung below a selected Hounsfield unit density threshold. The most accepted threshold by using MDCT with thin collimation is -950 HU. As an alternative the percentile density that is a density value below which a given percentage of the lung pixels fall, may be measured. The 15th percentile has proved to be the most sensitive index for assessing emphysema progression. QCT analysis of emphysema extent may be done at regional and lobar distribution. Sources of variation in density based measures include inspired lung volume, scanner make and model, increased body mass index (BMI) and increased lung density in individuals who are current smokers. Regular calibration using a CT phantom is needed. Adjustment for tracheal air attenuation may limit the variation due to scanner marker and model. The tube current should be maintained upper than 50 mAs. The extent of emphysema is more consistent across different tube currents when using iterative reconstruction algorithms. Lung densitometry is highly reproducible when is corrected for differences in lung volume (% emphysema on the follow-up scans corrected using the achieved lung volume on the baseline scan). The extent of emphysema appears to increase quite rapidly after smoking cessation reflecting a fall in lung attenuation, and emphysema measurements increase with increasing body-mass index. As a result, longitudinal analysis of emphysema must adjust for both smoking status and BMI both of which may change over time. When sources of variation are controlled and keeping the same acquisition and reconstruction parameters, a change of 1.1% in the emphysema extent with 95% probability can be detected by using MDCT. QCT analysis of emphysema extent correlates significantly with both FEV1/FVC as well as FEV1, and predicts COPD exacerbations that require hospitalization. Quantitative emphysema is associated with lower respiratory quality of life and with increased all-cause mortality in patients with COPD.
Gas trapping on expiratory CT has been used as a surrogate for small airway disease. Percentage of low attenuation area at -856 HU or -850HU at end-expiration provides remarkably high correlations with predicted FEV1% and FEV1/FVC ratio. Expiration to inspiration ratio of mean lung density is most suitable for detecting air trapping in smokers and performs significantly better than other quantitative measures. However these metrics are influenced by underlying emphysema. By using parametric response mapping (PRM), an application of image matching in which inspiratory and expiratory images are deformed and co-registered voxel-to-voxel, double thresholding lung densitometry allows to separate voxels of emphysema (-950 HU insp and -856 HU exp), voxels of functional small airway disease (fSAD) (> -950 HU insp and < -856 exp) and voxels of normal lung (> -950 HU insp and > -856 exp). PRMs may provide spatial information on the distribution of emphysema and small airway disease, thus permitting measurement and tracking of these disease components separately. PRM fSAD is significantly associated with subsequent FEV1 decline particularly in mild-to-moderate stage disease. This association is evident in GOLD 0 subjects even before the development of spirometrically detected airflow obstruction.
Inflammation and remodeling processes arise in the small airways but similarly affect the large airways. Airway remodeling in the segmental and subsegmental airway is used as a surrogate measure of small airway remodeling. Airway wall thickness (AWT), airway wall area % (WA%) are the commonest metrics used. Summary measures of airway size are provided by the Pi 10 and Pi 15 which are the square roots of the wall areas of theoretical airways with internal perimeter 10 mm and 15 mm respectively, obtained from measurements of dimensions of all bronchi measured. These measures of airway thickness are associated with exercise capacity, chronic bronchitis and bronchodilator responsiveness. Bronchial wall thickening was associated with increased rate of exacerbation. The increase of WA% with worsening COPD has proved to be a combination of reduced airway size and luminal encroachment by thickened airway walls.
Central airway collapse on expiratory CT scan defined as a reduction of more than 50% in tracheal cross sectional area on expiratory CT was observed in 5% of all smokers and was more prevalent in those with COPD. Its presence was associated with worse respiratory quality of life, as well as a greater frequency of acute respiratory events.
Pulmonary hypertension (PH) frequently complicates COPD and its presence is often seen in early disease. To measure pulmonary artery (PA) enlargement is used as a surrogate for PH. A pulmonary artery to ascending aorta (AA) radio > 1 is an independent factor of exacerbation of COPD. PH in COPD is associated with vascular pruning in the peripheral regions. In patients with severe emphysema vascular alteration measured from the cross-sectional area of small pulmonary vessels correlates with the magnitude of PH.
Take Home Points: QCT analysis of emphysema extent and severity of functional small airway disease and CT measurements of airway dimensions may provide better understanding of pathophysiology of COPD and better phenotyping of COPD patients.
They contribute to improve stratification of patients in clinical trials and to predict outcomes following intervention.
They may be used to assess progression of disease during follow-up according to a strict control of variation sources.
Standardization is necessary for multicenter studies.

Imaging of complications in COPD

N. Sverzellati; Parma/IT

Body: Chronic obstructive pulmonary disease (COPD) patients have multiple coexistent diseases. Although some of these comorbidities share risk factors with COPD, tobacco smoking, and aging do not fully explain the strength of the associations. Indeed, there is growing evidence that inflammatory phenomena in one organ (e.g., the lung) could spill to the systemic circulation and affect other systems. In particular, other diseases could be present selectively among a unique subgroup of COPD (e.g. phenotypes). There is a gradient with worsening spirometry severity being associated with greater odds of cardiovascular disease and higher mortality. Computed tomography (CT) may suggest subclinical or overt pulmonary vascular disease. Relative pulmonary artery (PA) enlargement, defined as a PA to ascending aorta (A) diameter ratio greater than one (PA:A >1) identifies patients at increased risk for exacerbations. A ratio >1 on CT scan outperforms echocardiography for diagnosing pulmonary hypertension in patients with severe COPD. Furthermore, COPD is also a risk factor for lung cancer. Quantitative CT measures of COPD-related abnormalities may provide additional information for the identification of high-risk groups who might benefit the most from lung cancer screening. CT signs of lung fibrosis may also be observed in COPD, and their clinical relevance is yet to be determined.
Take Home Points: Both chest radiography and CT may be helpful in the differential diagnosis of acute complications such as acute exacerbations and pneumothorax
CT is a pivotal investigation for the diagnosis of cardio-vascular complications in COPD
COPD is an independent risk factor for lung cancer development

The role of CT in current guidelines?

C. S. White; Baltimore, MD/US

Body: The remarkable advancement in CT technology has resulted in ongoing evolution of guidelines for coronary/cardiac CT angiography (CCTA) in comparison with the more traditional functional approach exemplified by stress testing. CCTA had already received a strong recommendation based on the American College of Cardiology Foundation and American Heart Association (ACCF/AHA) guidelines most recently revised in 2013, although it was not viewed as advantageous compared to stress testing. However, since then a number of important studies, notably the PROMISE trial and SCOT-HEART trial have been added to the literature. The PROMISE trial showed non-inferiority for major adverse cardiac events (MACE) for CCTA versus standard of care approaches. The SCOT-HEART trial showed an advantage for CCTA with respect to a reduced number of MACE versus a standard of care approach.
The results of these and other trials have led to the recently revised 2016 National Institute for Health and Care Excellence (NICE) guidelines recommending coronary CT angiography (CCTA) as a primary test in outpatients presenting with chest pain (1). This is due to evidence of a higher sensitivity of CCTA for significant coronary artery disease (CAD) with similar specificity as compared to stress testing.
Moreover, the prognostic value of testing may depend on the subgroup of patients being evaluated. For example, CCTA may have greater benefit in younger patients with relatively fewer risk factors whereas stress testing may provide an advantage in individuals with prior cardiac events. In addition, CT is evolving and becoming a more versatile technique, as results from several of the CT FFR trials show. Thus, CCTA guidelines are likely to evolve further.
Bibliography:
1) Wolk MJ, Bailey SR, Doherty JU et al. ACCF/AHA/ASE/ASNC/HFSA/HRS/SCAI/SCCT/SCMR/STS 2013 multimodality appropriate use criteria for the detection and risk assessment of stable ischemic heart disease. J Am Coll Cardiol 2014;63:380-406.
2) National Institute for Health and Care Excellence Guideline CG95. Chest pain of recent onset. https://www.nice.org.uk/guidance/cg95
Take Home Points:
1) The 2013 ACCF/AHA guidelines described CCTA as appropriate but not necessarily the first line test compared to functional imaging.
2) The more recent 2016 NICE guidelines recommend CCTA as a first line test for patients with typical or atypical angina and those with non-anginal pain and rest ECG changes. Stress evaluation is relegated to secondary testing.

CT in acute chest pain patients: What's the evidence

C. S. White; Baltimore, MD/US

Body:
1) To describe the stratification of patients who present to the emergency room with chest pain.
2) To review conventional imaging approaches to assessing chest pain including chest radiography and stress testing.
3) To discuss the potential utility of CTA in chest pain evaluation based on the existing literature.

The evaluation of acute chest pain is a critical challenge for ED physicians. Both serious causes such as acute coronary syndrome (ACS = transmural MI, nontransmural MI, unstable angina) and pulmonary embolism and minor causes must be evaluated.

Approximately 15% of patients presenting with chest pain have ACS whereas about 50% are admitted, many who ultimately are rule-out for serious disease, often after a lengthy work-up.
Conventional non-invasive techniques include myocardial perfusion imaging and stress echocardiography but these have substantial limitations. With the rapid advancement of cardiac CT and increasing proximity of the scanner to the ED, investigators have suggested its use to provide an accurate and rapid evaluation of acute chest pain using either a dedicated coronary CTA or more comprehensive thoracic assessment (triple rule-out). Four USA multi-center trials have shown an excellent negative predictive value for ED cardiac CT with the potential for rapid triage. Additional trials have been performed in Europe testing high sensitivity troponins.
Challenges that must be addressed include staffing issues, economic issues and minimization of radiation dose. It will be important to develop appropriate guidelines based on further studies in order for acute chest pain evaluation by CT to permit increased use compared to competing functional techniques.
Take Home Points:
1) CT for acute chest pain is making increased inroads in the ED.
2) USA studies show an advantage in early diagnosis and more frequent discharge compared with standard approaches.

How to provide high quality 24/7 service: Structured and standardised reporting

U. J. J. Schoepf; Charleston/US

Body: Cardiovascular Imaging has seen an expanded role and significance in daily clinical routine during recent years. While substantial efforts have helped develop different methods of standardization for the reporting of cardiovascular imaging results, financial and workflow inefficiencies remain present throughout patient management. Often times, the final study report is the only mode of communication between the radiologist and referring physician. Therefore, it is crucial to have a standardized end-product; one which contains the necessary information to maintain excellent patient care across departments and specialties. Accordingly, the production of consistent, high-quality reports has been an important goal for cardiovascular imagers to achieve optimal patient outcomes and overall cost efficiency.
The success of breast, liver, and prostate imagers in creating a common lexicon for reporting should represent a low-hanging fruit for the field of cardiovascular imaging. Indeed, a template-type document would require reporting physicians to proceed through examinations in a systematic manner; however, perhaps more importantly, it would help transform report findings into actionable recommendations. Such terminology-based recommendations would likely help clinicians better understand the clinical ramifications of report findings. As a promising first step, the Coronary Artery Disease - Reporting and Data System (CAD-RADS) has been developed, which summarizes findings on coronary CT angiography based on the severity of atherosclerosis and provides patient management recommendations for each risk category.
This presentation will discuss current methods of reporting, such as CAD-RADS, and provide future outlooks for standardized reporting in cardiovascular imaging.
Take Home Points:
1. Cardiovascular Imaging has seen an expanded role daily clinical routine
2. The final study report is the only mode of communication between the radiologist and referring physician
3. A template-type document would require reporting physicians to proceed through examinations in a systematic manner and would help transform report findings into actionable recommendations.
4. Terminology-based recommendations would likely help clinicians better understand the clinical ramifications of report findings
5. Coronary Artery Disease - Reporting and Data System (CAD-RADS), a promosing first step in that direction, summarizes findings on coronary CT angiography based on the severity of atherosclerosis and provides patient management recommendations for each risk category.

CT for ischemia detection

R. Vliegenthart; Groningen/NL

Body: In case of low-intermediate pre-test probability of coronary artery disease (CAD) in symptomatic patients, both anatomical and functional imaging can be considered for diagnosis (ESC guideline 2013). Computed tomography angiography (CTA) is a highly reliable anatomical technique to rule out CAD. However, the positive predictive value of CTA for hemodynamically relevant CAD is suboptimal. Many coronary stenoses of intermediate and sometimes even higher grade do not significantly reduce blood flow. Assessment and quantification of the "downstream" blood supply is essential. For this purpose, a second non-invasive, functional imaging technique is often performed. No established non-invasive modality can analyse CAD morphology and functional significance in a single test. CT holds great potential to change this in the near future due to the possibility to evaluate myocardial blood supply with state-of-the-art CT systems. There are two main CT techniques to image myocardial blood supply, single-phase static and dynamic imaging. The single-phase acquisition is a snapshot of iodine distribution across the myocardium at a single moment. Dual-energy CT, i.e. simultaneous acquisition of images at different photon energy levels, is an alternative single-phase

method. Dynamic CT imaging, involves the acquisition of images at multiple time points during first-pass of the bolus of contrast through the left ventricle. This technique allows analysis of myocardial perfusion, including true quantitative perfusion parameters such as myocardial blood flow. In recent years, numerous articles have reported the diagnostic accuracy of CT for assessment of myocardial blood supply. Clinical studies so far mostly consist of relatively small patient populations, with different reference standards (nuclear imaging, invasive angiography or MRI). The multicenter SPECIFIC (dynamic Stress PErfusion CT for detectIon oF Inducible myocardial ischemia) study that is currently in preparation aims to answer the question of the accuracy of dynamic perfusion CT compared to the reference standard, invasive angiography with fractional flow reserve measurement. Taking all available evidence together, all myocardial perfusion CT techniques show acceptable diagnostic accuracy for myocardial ischemia detection, with sensitivity ranging from 75-89%, and specificity from 78-95%. Combined assessment of CTA with a CT acquisition under adenosine stress for myocardial blood supply evaluation tends to have a better diagnostic performance for detection of catheter-based stenosis. Although still in the early clinical phase, CT assessment of myocardial ischemia constitutes a promising step toward complete evaluation of CAD.
Take Home Points: CTA-derived diameter stenosis frequently fails to determine the functional significance of a stenosis.
CT can evaluate coronary stenosis as well as presence of ischemia under adenosine stress.
There is increasing evidence for the strength of an integral CT protocol for evaluation of hemodynamically significant CAD.

Update in hypersensitivity pneumonitis

A. Devaraj; London/UK

Body: This presentation will review the uncertainties surrounding the role of imaging in the diagnosis of hypersensitivity pneumonitis. Specifically, the historical and recent literature on the CT features of hypersensitivity will be reviewed and scrutinized. The integration of imaging with clinical aspects of the disease, as well as the classification of hypersensitivity pneumonitis will be reviewed.
Take Home Points: CT features of hypersensitivity pneumonitis vary in their reliability and diagnostic accuracy.
There may be overlap between CT features of hypersensitivity pneumonitis and other fibrotic interstitial lung diseases.
Imaging features must be integrated with clinical aspects prior to finalizing the diagnosis.

Nodule management guidelines: an update

A. Bankier; Boston, MA/US

Body: This presentation will present and summarize two recent guidelines, one for the management of incidental lung nodules found on CT, and one for the measureement of lung nodules on CT examinations. The motivation for the updates will be explained and the new elements in the guidelines will be highlighted. Moreover, the background of the guidelines will be explained, and the caveats and limitations of the guidelines with regard to their clinical application will be provided.
Take Home Points: The presented updated guidelines are aimed to standardize the measurement and management approach to pulmonary nodules. Their use and implementation requires clinical judgment and common sense.

Screening in Europe - What are we all doing?

S. Diederich; Düsseldorf/DE

Body: A single large prospective, randomized controlled trial (NLST) has demonstrated a 20% reduction in lung cancer mortality in a cohort of smokers or (maximum 15 years) ex-smokers aged 55 to 74 years with a minimum of 30 pack years.
Other smaller trials have either not yet published figures on mortality or have shown no mortality reduction.
Nevertheless, many societies, organisations and other bodies have issued recommendations for screening with annual low-dose CT in asymptomatic smokers at risk provided that inclusion criteria and conduct of the programme are identical to the NLST settings.
As smoking prevention and/or cessation are superior to screening/early detection with CT to prevent mortality from lung cancer recommendations include access to smoking cessation programmes for current smokers.
Due to marked differences in access to low-dose CT screening programmes, reimbursement, medicolegal and radiation protection aspects there is no common European strategy for lung cancer screening.
Currently, lung cancer screening in asymptomatic smokers is available only to a small proportion of individuals fulfilling the NLST inclusion criteria in Europe in different small trials or programmes.
Further research is warranted into refinement of inclusion criteria, conduct, quality assurance and cost effectiveness of screening programmes for the general population.

asymptomatic CT-detected NSCLC T1b, N0

asymptomatic CT-detected NSCLC T1a, N0

Take Home Points:

1. Lung cancer screening with annual low-dose CT can save lives
2. Quality assurance is required for every individual step from identification of screenees, informed consent, examination technique, radiation dose, analysis of images, recommendations for management of positive findings, further diagnostic procedures and therapy
3. Smoking cessation should be offered to current smokers who wish to join a screening/early detection programme
3. Many societies and bodies throughout Europe recommend lung cancer screening/early detection with annual low-dose CT
4. Access, reimbursement and medicolegal issues differ markedly between European countries

Quality Assurance (QA) in Lung Cancer Screening- Lessons from Breast Screening

M. Michell; London/UK

Purpose/Objectives

The United Kingdom (UK) National Screening Breast Screening Programme (NHS BSP) was implemented in 1989 following publication of the Forrest report which considered the available evidence for screening. Three yearly mammography screening is offered to asymptomatic women aged 50 to 70 years by 90 screening and assessment centre across the UK. Over two million women are screened per annum, and more than 17,000 cancers diagnosed. The effectiveness and development of the programme have been underpinned by robust quality assurance, specialist training, research and a multidisciplinary team approach.

Methods and Materials

- Quality Assurance
  · National Quality Assurance Guidelines and Standards for all professional groups
  · Local, Regional and National QA structure
  · Programme of regular QA visits and peer review
- Training
  · Four specialist National Training Centres established
  · Specialist training for all professional groups
  · Reader training and performance monitoring (PERFORMS)
- Research
  · Evaluation of new technology
  · Critical evaluation of evidence before programme development

Results

This presentation will discuss the importance of a rigorous quality assurance programme in ensuring that in a cancer screening programme for asymptomatic individuals, the potential benefits of screening are maximised and the harmful effects are minimised.
Conclusion:

References

- Breast Cancer Screening. Report to the Health Ministers of England, Wales, Scotland & Northern Ireland. By a working group chaired by Professor Sir Patrick Forrest. Department of Health and Social Security. London Her Majesty's Stationery Office 1986.
- NHS Breast Screening Programme Clinical guidance for breast cancer screening assessment NHSBSP publication number 49 Fourth edition November 2016 Public Health England
- Quality Assurance Guidelines for Breast Cancer Screening Radiology Second edition NHSBSP Publication No 59 March 2011
- https://www.gov.uk/topic/population-screening-programmes

Detailed TAVI workflow

R. Salgado; Edegem/BE

Body: Aortic valve stenosis is the most common valvular heart disease in the Western World, effectively treated by surgical valve replacement. However, several studies have identified various subgroups of patients who have a significant elevated risk for operative complications and death. Recent developments in transcatheter-based therapies have provided an alternative therapeutic strategy for the non-surgical patient population, replacing the native aortic valve by a bioprosthetic valve brought in place using a non-surgical endovascular or trans-apical pathway. This procedure has been named transcatheter aortic valve replacement or implantation (TAVR, TAVI), or also percutaneous aortic valve replacement (PAVR). Nevertheless, several anatomic and technical criteria have to be fulfilled to safeguard procedural eligibility and success. Therefore, there is a crucial role for non-invasive imaging in both patient selection and subsequent matching to a specific transcatheter valve size, to ensure accurate prosthesis deployment and minimize peri- and post-procedural complications. In this lecture, a detailed workflow will be discussed regarding the evaluation with CT of TAVI-candidates. Both the scan protocol as well as all the necessary measurements and their implications will be discussed.

Take Home Points:
1. A high-quality pre-procedural CT is essential for procedural success.
2. CT can help in confirming the diagnosis of severe aortic valve stenosis in selected patients.
3. CT is the best image modality for evaluation of the aortic root and different access routes.

Imaging and management of typical complications

P. Monney; Lausanne/CH

Body: TAVI has become a major treatment option for patients with severe aortic stenosis (AS). The 2017 guidelines of the European Society of Cardiology for the management of valvular disease provide a IB recommendation for performing TAVI in patients not suitable for surgical aortic valve replacement or in patients at intermediate or high surgical risk after an inidividualized assessment by the Heart Team. The most recent randomized controlled trials including AS patient with an intermediate surgical risk (PARTNER 2 and SURTAVI studies) reported a low 30-days incidence of death or disabling stroke between 2.8 and 6.1% and a 1% incidence of myocardial infarction after the TAVI procedure.
Beside the major cardiovascular averse events, several specific procedural complications also may occur, including vascular access complications, bleeding requiring blood transfusion, atrio-ventricular conduction block requiring pace-maker implantation, prosthesis migration, pericardial tamponade resulting from cardiac perforation or annular rupture, coronary obstruction and para-valvular aortic regurgitation. Careful planning of the intervention using non-invasive imaging (mainly cardiac CT-angiography) is key for the selection of the optimal access site, the most suitable prosthesis type and the right prosthesis diameter, in order to minimize the risk of procedural complications.
During the TAVI intervention, procedural guidance is mainly performed with fluoroscopy. However, in case of acute hemodynamic instability, trans-oesophageal echocardiography is the imaging test of choice to identify the cause of instability and to guide its management in the cathlab.
Finally, imaging follow-up after TAVI, using echocardiography, cardiac CT and/or cardiac magnetic resonance, may also be of importance as complications can occur even after successful valve implantation. Typical late complications include persistent paravalvular aortic regurgitation, subclinical or obstructive leaflet thrombosis, and prosthesis-related endocarditis.
Take Home Points: TAVI is a major treatment option for severe aortic stenosis Cardiac CT is the imaging of choice for planning the intervention and selecting the appropriate prosthesis size Trans-oesophageal echocardiography is ideally suitable to assess the cause of hemodynamic instability during the TAVI procedure and to guide the treatment of complications

Ablation in lung cancer: Are there any contraindications

P. Dalal; London/UK

Body: Percutanoeus tumour ablation has gained increasing interest since the early 2000's when the proof of concept and early case series were published. Early interest was largely in liver tumour ablation with lung ablation coming more to fore recently.
It is well understood that a relatively small number of newly diagnosed lung cancers are amenable to curative surgery (even despite their early stage). In addition there is increasing interest in the use local therapies to augment systemic treatments for oligo- and multi-metastatic disease. Hence there is increasing interest in non-surgical techniques.
The three most common types of ablation used in the lung are radiofrequency, microwave and cryotherapy. Other techniques, including irreversible electroporesis and laser therapy, are less frequently utilised. There is increasing evidence for the use of percutaneous ablation for lung tumours, but there remain few published trials comparing the efficacy of the various ablative techniques and fewer still which directly compare ablation with surgery and local radiotherapy. Anecdotally also, there are widely

variant results in the published literature. This has hampered the widespread uptake of percutaneous ablation as a mainstream alternative to surgery or steortactic radiotherapy in the treatment of lung tumours.
This session will focus on the use of percutaneous ablative techniques in the treatment of primary lung cancer with occasional reference to thier use in metastatic lung tumours.
Take Home Points:
1) To understand the principles of percutaneous tumour ablation
2) To understand the strengths and weaknesses of the common types of tumour ablation used in the lung
3) To undertand when and when not to consider using this technique in primary lung cancer

Imaging in haemoptysis

S. Bhalla; St. Louis, MO/US

Body: Hemoptysis is a frequent cause of consultation in the hospital setting (10% of pulmonary medicine and 38% of thoracic surgery consults). It can be alarming on exam. No grading system exists but generally, < 30 ml in 24 hours is considered minimal and 300-1000 ml in 24 hours is considered massive. Massive hemoptysis only represents 10% of cases of hemoptysis but can be lethal, not from exsanguination but from asphyxiation. In the modern era, bronchial artery embolization with gelfoam has become the major treatment for massive hemoptysis. Although surgery may be potentially curative, the mortality if performed emergently, may increase from 10-40%.
The goal of imaging and of bronchoscopy is to identify the **site of bleeding** and the cause of bleeding. Bronchoscopy additionally allows for securing the airway. Although CT and bronchoscopy are both equally effective in showing the site of bleeding, CT is better at delineating the **cause of bleeding**. The main causes of massive hemoptysis include: Tuberculosis Bronchiectasis Lung cancer Infectious pneumonias
Bronchitis resulting in hemoptysis is usually better seen on bronchoscopy. Other less common causes of massive hemoptysis include ruptured aortic aneurysm, pulmonary artery pseudoaneurysm, vasculitis (notably Behcets and granulomatosis and polyangiitis, aortobronchial fistula and intralobar sequestration.
Occasionally (10-20% of cases of massive hemoptysis) hemoptysis may be cryptogenic without a diagnosis on CT or bronchoscopy. These patients are usually smokers and up to 6% may present with a lung cancer in the subsequent 3 years. There may be a role for CT screening in these patients.
Most cases of hemoptysis (90%) arise from bronchial arteries. When these vessels arise at the level of T5-6, they are known as orthotopic bronchial arteries. Vessels greater than 2mm are considered abnormal. Occasionally bronchial arteries may arise from elsewhere in the descending aorta or from systemic feeder arteries. These anomalous bronchial arteries may be better seen on MDCT. Anomalous systemic feeding (nonbronchial) arteries, pulmonary arteries and the aorta itself may also account for the hemoptysis and should be interrogated by CT or angiography in patients with massive hemoptysis, especially when no bronchial source is seen.
Some have suggested that the radiograph may be a good initial imaging tool in patients with hemoptysis. It is certainly fast and may be done portably. But in 50% of cases, it may be normal. In our practice CT is almost always done (usually before bronchoscopy but sometimes after the initial bronchoscopy) . Bolstered by numerous studies (which we will discuss in the talk), we have found that CT can help target therapy and shorten fluoroscopy times for embolization. In certain instances, CT may show that surgery may be warranted over embolization.
CT findings can be described as direct and indirect. Direct signs of a source of hemoptysis include: Blush or extravasation (rare) Culprit lesion Ground glass surrounding an aneurysm Irregular pulmonary artery Detection of a saccular aneurysm or pseudoaneurysm in consolidation Aortic irregularity
The presence of these findings allows for the confident diagnosis of a source of bleeding. Indirect findings may also be helpful as well in suggesting a source but do not allow for the same confidence. These include: Focal tree-in-bud Focal bronchial wall thickening Ground glass opacity and consolidation with subpleural sparing Enlarged/increased number of bronchial arteries Pulmonary necrosis Focal enhancing pleural thickening
If a source is identified or if the hemoptysis is massive, bronchial artery embolization is usually considered. Gelfoam particles are used because 5-45% of patients may recur and the goal is not to block future access as may happen with coils. Complications of embolization are rare (<5%) but care must be taken to confirm that the spinal artery does not arise from the bronchial artery considered for embolization.
References: Adbulmalak C, Cottenet J, Beltramo G. Hemoptysis in Adults; a 5 year study using the French nationwide hospital dataset. Eur Respir J 2015;46:503-511. Bruzzi JF, Remy-Jardin M, Dehaye D, et al. MDCT of hemoptysis. Radiographics 2006; 26:3-22. Fartoukh M, Khoshnood B, Parrot A, et al. Early prediction of in-hospital mortality of patients with hemoptysis: an approach to defining severe hemoptysis. Respiration 2017; 83:106-114. Gupta M, Srivastava DN, Seith A, et al. Clinical impact of multidetector row computed tomography before bronchial artery embolization in patients with hemoptysis: a prospective study. Can Assoc Radiol J. 2013 Feb;64(1):61-73 Hartmann IJ, Remy-Jardin M, Menchini L, Teisseire A, Khalil C, Remy J. Ectopic origin of bronchial arteries: assessment with multidetector helical CT angiography. Eur Radiol. 2007;17(8):1943-1953 Ketai LH, Mohammed TL, Kirsch J, Kanne JP, Chung JH, Donnelly EF, Ginsburg ME, Heitkamp DE, Henry TS, Kazerooni EA, Lorenz JM, McComb BL, Ravenel JG, Saleh AG, Shah RD, Steiner RM, Suh RD; Expert Panel on Thoracic Imaging. ACR appropriateness criteria® hemoptysis. JThorac

Imaging. 2014 May;29(3):W19-22 Khalil A, Fedida B, Parrot A et al. Severe hemoptysis: from diagnosis to embolization. Diagnostic and Interventional Imaging. 2015; 96:775-788. McCollun WB, Mattox KI, Guin LN, et al. Immediate operative treatment of massive hemoptysis. Chest 1975;67:152-5. Lee YJ, Lee SM, Park JS, et al. The clinical implications of bronchoscopy in hemoptysis patients with no explainable lesions in computed tomography. Respir Med. 2012;106(3):413-419. Millar AB, Boothroyd AE, Edwards D et al. The role of CT in unexplained hemoptysis.Respir Me 1992; 86:39-44. Noe GD, Jaffe SM, Molan MP. CT and CTA in massive hemoptysis with emphasis on pre-embolization assessment. Clin Rad. 2011; 66: 869-875. Radchenko C, Alraiyes A, Shojaee S. A systematic approach to the management of massive hemoptysis. J Thorac Dis 2017;9:S1069-1086. Remy-Jardin M, Bouaziz N, Dumont P et al. Bronchial and nonbronchial systemic arteries at MDCT:comparison with conventional angiography. Radiology 2004; 233:741-9. Revel MP, Fournier LS, Hennebique LS, et al. Can CT replace bronchoscopy in the detection of the site and cause of bleeding in patients with large or massive hemoptysis? AJR 2002; 179: 1217-24. Set PA, Flower CD, Smith IE, et al. Hemoptysis. Comparative study of the role of CT and fiberoptic bronchoscopy. Radiology 1993;189;677-80. Shigemura N, Wan IY, Yu SC, et al. Multidisciplinary management of life-threatening hemoptysis. Ann Thorac Surg 2009; 127:2113-18. Thirumaran M, Sundar R, Sutcliffe IM, Currie DC. Is investigation of patients with haemoptysis and normal chest radiograph justified? Thorax. 2009;64(10):854-856. Yoon W, Kim JK, Kim TH, et al. Bronchial and nonbronchial systemic artery embolization for life-threatening hemoptysis: a comprehensive review. RadioGraphics 2022; 22:1395-1409

Take Home Points:

1. Massive hemoptysis can be lethal from exsanguination.
2. Frequent causes of hemoptysis include: Tuberculosis Bronchiectasis Lung cancer Infectious pneumonias
3. CT should be performed in patients with massive hemoptysis and should be considered in others.
4. The goal of CT is to delineate the site of bleeding and the cause of bleeding.
5. Embolization is a safe and effective treatment strategy as emergent surgery has a high mortality.

Aorta

C. Loewe; Vienna/AT

Body: Aortic diseases represent a relevant factor in overall morbidity and mortality showing an increased incidence with age. During the last years, exciting new treatment options have been established into the clinical routine by endovascular means, allowing for minimal invasive treatment of even complex anatomical situation in severely ill patients. However, such new minimal invasive treatment options require exact pre-therapeutic planning, since the devices used for treatment in complex anatomical situations are customized for every individual patient. Furthermore, careful treatment follow-up is requested to early detect secondary problems after endovascular therapy. Consequently, questions asked to imaging have changed, and a shift from setting up the diagnosis only to provide all information's needed to plan the treatment could be observed. CT angiography has been established as the method of choice for the diagnosis, treatment planning and follow up due to the high spatial and temporal resolution. In special circumstances, MR angiography is an important additional tool to set up the final diagnosis or to answer remaining questions after treatment.
In this presentation, state-of-the-art imaging techniques for CT and MR angiography will be introduced, and the possible advantages and disadvantages of both modalities for the management of patients suffering from aortic diseases will be discussed. Recent innovations for optimized imaging strategy including functional assessment and detailed analysis prior and after endovascular treatment will be discussed. Treatment indications should be explained based on clinical cases in the view of newly established treatment guidelines to further underline the outstanding role of appropriate imaging for optimized treatment in aortic diseases.
Take Home Points: CT angiography is the method of first choice for the diagnosis of and treatment planning in aortic diseases Questions to be answered by imaging in aortic diseases expanded from establishing the diagnosis only to provide all treatment relevant information's

Renal arteries

C. Catalano; Rome/IT

Body: Non-invasive diagnostic imaging plays a crucial role in the identification and management of pathological conditions affecting renal arteries.
Computed Tomography Angiography (CTA) and Magnetic Resonance Angiography (MRA) imaging - often preceded by Color-Doppler Ultrasound are robust and well established techniques and may characterize the entire spectrum of abnormalities including congenital (eg. artero-venous malformation), acute (dissection or traumatic injuries), atherosclerotic (stenosis or aneurysm) conditions or fibromuscular dysplasia.
In particular, thanks to their high sensitivity and specificity, MRA or CTA may detect renal arteries stenosis even when Doppler US is negative or nondiagnostic.
New imaging techniques, such as the Contrast-enhanced US, Dynamic MR-Angiography or Functional MRI, may offer additional

information that integrate the anatomical data and enable a more comprehensive assessment of the renal arteries.
The evaluation of renal arteries stenosis or microvascular damage, or the assessment after transplantation could benefit from a combined anatomical-functional approach warranted by these new techniques.
This lecture will review the various diseases affecting renal arteries, demonstrate typical imaging features enabling the diagnosis and discuss management options.
Learning Objectives:
1. To understand the different types of renal arteries diseases.
2. To learn about imaging findings and management options of the most common disease affecting renal arteries.
3. To appreciate the role of MR and CEUS for functional evaluation of renovascular disease

Lower Limb

T. Leiner; Utrecht/NL

Body: Imaging of lower limb vasculature demands high spatial resolution as well as high temporal resolution to optimally depict the features of interest for referring clinicians.
CT angiography
Proper CT angiography can be performed on any CT scanner with 64 or more detector rows. The vascular tree is typically covered from the infrarenal aorta down to and including the feet. To ensure adequate opacification of the vascular tree the concept of iodine delivery rate (IDR) is important (iodine concentration in mg/mL multiplied by injection rate in mL/s). IDR typically ranges between 1.4-2.1 g/s for CTA of the lower extremities. Acquired slice thickness should be set to the lowest possible value but for displaying the data slice thickness can be increased to 1.0-2.0 mm. Stenosis measurements should always be made using double oblique measurements perpedicular to the center lumen line on the source images.
MR Angiography
MR angiography can be performed on any state of the art MR system equipped with parallel imaging capable body surface coils. In contrast to CT, low contrast volumes can be used to opacify the peripheral vascular tree, and there is ample evidence that MR angiography is capable of detecting more small distal vessels compared to intra-arterial DSA in patient with chronic critical ischemia. Another advantage of MR angiography is the capability to obtain time-resolved information, which can be especially valuable to evaluate the vascular status below the knee.
Take Home Points:
1) CTA and MRA both play important role in management of patients with suspected or known peripheral arterial disease.
2) CTA and MRA are not needed to make the diagnosis, this is done by other means such as the typical history and ankle brachial index measurements
3) Both CTA and MRA are highly accurate for depicting location and extent of both atherosclerotic and non-atherosclerotic peripheral arterial disease.

Subsolid nodules

J. M. Goo; Seoul/KR

Body: When persistent, the malignancy rate of a subsolid nodule was reported to be much higher than that of a solid nodule. Although many of subsolid nodules are malignant, their growth rate is very slow.
The nodule management is mainly determined by the size and nodule classification. The problem is that there can be considerable observer variability for classification of nodules. One study showed that pair-wise inter- and intra-observer agreement was just moderate and 2/3 of discrepant readings result in different nodule management. To decrease this variability it is necessary to specify window settings in classifying and measuring nodules. When lung and mediastinal windows were compared, both settings showed similar interobserver agreement in identifying and measuring solid component. But when pathology measurement was used as a reference, lung window was better in terms of accuracy. Therefore, many guidelines including the Fleischner Society statements, Lung-RADS, and coding T-categories for subsolid nodules recommend to use lung windows in the assessment of subsolid nodules. Semi-automatic measurement can improve diagnostic accuracy and inter-observer agreement.
Now we have better understanding about the natural history of subsolid nodules based on larger clinical cohorts. NESON trial showed that there was no progression into malignancy among non-resected subsolid nodules. I-ELCAP study also showed that all resected nonsolid nodules were stage I adenocarcinoma with a survival rate of 100%. With accumulation of data, it is known that more indolent diseases can be detected with screening which may lead to overdiagnosis and overtreatment. In NLST data the estimated overdiagnosis was 18.5%. When patients hear the word cancer, most assume they would die. And therefore some researchers suggest that we need to change the term from cancer to IDLE, indolent lesion of epithelial origin in describing this kind of lesion. For the management of pure GGN, follow up would be enough without surgical intervention or biopsy until the appearance of solid component and pure GGN may not be called as cancers.
Take Home Points: Persistent subsolid nodules are likely malignant but show indolent nature. There can be considerable observer variability for classification of nodules and lung window is recommended in assessing subsolid nodules. Pure GGNs can be managed conservatively.

Mediastinal tumours

J. W. Song; Seoul/KR

Body: Like all the other body part, mediastinum also has many categories of disease entities. And a wide variety of lesions can manifest as a localized tumor or mass in the mediastinum. Just the tumor itself contains a long list of neoplastic diseases.
For the case-based study of mediastinal tumors, I want to introduce the best website and smartphone application 'KSTR weekly chest cases'.
Mediastinum, especially anterior mediastinum is surrounded by soft lung and this lung parenchyma can be easily displaced by the mediastinal space-occupying lesions. Therefore, many of the mediastinal lesions have no specific symptoms until the mass grow large enough to make a mass effect. It is emphasized on many journals that we can see many mediastinal lines, stripes, and interfaces on chest radiographs. Many of the mediastinal lesions are overlapped with sternum, vertebral bodies, and cardiovascular structures. So, it is not so easy task to detect the mediastinal lesions on chest PA radiographs. I want to emphasize and recommend checking the anterior, retrosternal clear space on lateral view.
Once we have detected some mediastinal lesions, then the next step is differential diagnosis. The most important factor for the differential diagnosis of the mediastinal tumor is location. Sometimes, especially for the huge tumor cases, it may be difficult to tell whether the tumor is in mediastinum, pleura, or even lung. The age and sex of the patients are also important. There may be some characteristic imaging findings such as cystic nature, fat component, calcification, enhancement pattern, and so on.
There have been many suggestions for the mediastinal compartments and mapping systems. Recently, the ITMIG (International Thymic Malignancy Interest Group) suggests new methods using CT images. Anterior mediastinum, prevascular compartment, is anterior to pericardium and it wraps around in curvilinear fashion and the major contents include the thymus, fat, lymph nodes. Middle mediastinum, visceral compartment is anterior to the vertical line 1 cm posterior to the anterior margin of thoracic vertebral bodies. And this vertical line is the border between middle and posterior mediastinum. The major contents of the visceral compartment are heart, pericardium, and great vessels including thoracic duct, trachea and esophagus, several lymph nodes. Posterior mediastinum, also called paravertebral compartment, has paravertebral soft tissue including dorsal root ganglia and neurons.
Almost half of the mediastinal tumors develop in the anterior mediastinum. Thymic lesions are the most common, with almost 45%, followed by lymphoma, germ cell tumor, and thyroid tumors. Among anterior mediastinal tumors, thymoma is the majority for the above 40 years of age, but for those who are below 30 years old, lymphoma including HD, and teratoma are more common.
Cystic tumors comprise about 15-20% of all mediasinal masses. Bronchogenic cyst, thymic cyst, pericardial cyst, cystic teratoma are relatively common entities. Occasionally, cystic degeneration of these solid tumors, mediastinal abscess or pancreatic pseudocyst can be presented as cystic mediastinal masses.
Bronchogenic cyst is the most common type of foregut cyst, with almost 60%, usually covered with respiratory epithelium. Sometimes, hemorrhage or gelatinous mucin component of the cyst can be presented as a high density on CT. Most common locations are near carina and around the central airway. But occasionally, we can see this bronchogenic cyst at lung parenchyme, pleura, or within diaphragm.
Thymic cyst can be categorized as either congenital or acquired. Congenital one is usually uni-locular pure cyst, usually detected at young age. Acquired cyst can be either unilocular or multilocular, showing various density, and sometimes calcification.
Mature cystic teratoma including dermoid cyst are usually found at anterior mediastinum and developed at young adult. 15% are pure cysts. Multi-locular cystic mass is much more common than unilocular one. Usually have discrete septation and encapsulated with well-defined wall, and there may be calcification. Occasionally, pancreatic tissue or intestinal mucosa within the tumor can secrete digestive enzyme and make the cyst rupture into lung, bronchi, pleura, or pericardial spaces.

References

Whitten CR, Khan S, Munneke GJ, Grubnic S. A diagnostic approach to mediastinal abnormalities. Radiographics 2007;27:657-671.
Carter BW, Tomiyama N, Bhora FY, et al. A modern definition of mediastinal compartments. J Thorac Oncol 2014;9:S97-S101.
Duwe BV, Sterman DH, Musani AI. Tumors of the mediastinum. Chest 2005;128:893-2909.
Jeung MY, Gasser B, Gangi A, et al. Imaging of cystic masses of the mediastinum. Radiographics 2002;22:S79-S93.

Take Home Points:

1. For the case-based study of mediastinal tumors, I want to introduce the best website and smartphone application 'KSTR weekly chest cases'.
2. I want to emphasize and recommend checking the anterior, retrosternal clear space on lateral view for the detection of anterior mediastinal tumor.
3. Cystic tumors comprise about 15-20% of all mediasinal masses. Bronchogenic cyst, thymic cyst, pericardial cyst, cystic teratoma are relatively common entities.

The forgotten structure: Revisiting the pericardium

A. Nchimi Longang; Liege/BE

Body: Pericardial diseases encompass a broad spectrum for which imaging is often necessary. Imaging aims at evaluating pericardial fluid collections, calcifications, thickening, hyperemia, masses and constriction. In addition, recent evidence suggest that epicardial adipose tissue play an active role in various vascular diseases, placing demands on standardized and reproducible methods for quantitative and qualitative assessment of epicardial adipose.
Learning objectives:
This presentation aims at describing
- The normal anatomy and function of the pericardium
- CT and MRI findings in pericardial diseases
- The involvement of the epicardial adipose in vascular diseases

Belgian Waffles and French Fries: Non-invasive cardiovascular risk assessment in the 21st century

R. Salgado; Edegem/BE

Body: Non-invasive imaging of the coronary arteries using CT has in the past decade reached worldwide clinical implementation. This is the consequence of both technical advances of CT imaging, as well as the validation of this technique in multiple clinical trials and randomised studies. One of the main strengths of non-invasive coronary artery imaging is the ability to exclude obstructive disease, as such eliminating the need for further invasive examinations. Furthermore, the quantification of coronary calcium provides a quantitative measure of the degree of arteriosclerosis, further helping in the risk stratification of patients. During this lecture, we will review the scientific evidence regarding the use CT-angiography of the coronary arteries in different populations, their impact on actual clinical management and their significance for short, mid- and long-term prognosis.
Take Home Points:
1. Cardiac-CT can help in the safe discharge of selected patients with acute chest pain in the emergency department
2. In patients with stable chest pain, cardiac-CT results provides prognostic information additional to functional testing.
3. Ca-score is a powerful prognostic tool in asymptomatic patients.

Pulmonary perfusion

M. Remy-Jardin; Lille Cedex/FR

Body: After more than one decade of clinical availability, dual-energy CT has reached a level of maturity that permits its use on a daily basis. In addition to the possibility of generating high-quality morphological images, dual-energy CT (DECT) can generate perfusion images from the same data set. These images are mostly considered as a diagnostic tool, completing the diagnostic information not easily detected on tradional cross-sectional imaging. Its second utility is to represent a new prognostic tool in all situations where detailed analysis of distal pulmonary vessels is clinically relevant. Among the various clinical situations requiring concurrent analysis of morphology and function, three main targets have been investigated over the last decade. The most important clinical application for DECT lung perfusion concerns pulmonary vascular diseases, with special mention for acute pulmonary embolism. More recently, a great deal of interest has been directed towards DECT lung perfusion in pulmonary hypertension (PH), in particular in the diagnostic approach of PH in competition with perfusion scintigraphy. The second target can be found in the context of tobacco-related diseases with the additional possibility of evaluating mismatch between ventilation & perfusion. Lung perfusion in oncology represents the third major clinical application, mostly directed toward prognostic implications.
Take Home Points:
- DECT lung perfusion is readily available from dual-energy CT data sets.
- High-quality lung perfusion images can be easily obtained using standardized acquisition & injection protocols.
- Lung perfusion analysis represents a powerful diagnostic tool for disorders mostly or predominantly involving distal pulmonary vessels.
- Lung perfusion can be visually assessed but it is also possibly to quantify perfusion abnormalities.

Spectral CT

T. Leiner; Utrecht/NL

Body: Dual-layer spectral detector CT is an exciting new technology that provides spectral information and thus the ability to perform material decomposition imaging (MDI) in all patients. All spectral information is contained in the spectral base image (SBI) datafile and apart from the minimum kVp, there is no need for a priori specification of desired spectral reconstructions or spectral contrasts. An important point to emphasize is that due to simultaneous collection of low- and high-energy CT projection data, spectral reconstructions can be made with constant, low noise levels, enabling high signal-to-noise ratio from 40-200 keV virtual monoenergetic (monoE) reconstructions.
Spectral CT will add exciting new capabilities in the field of cardiovascular CT. Some applications are listed below:

1) ability to map iodine distribution in the imaged body region, enabling quantitative estimates of end-organ perfusion. Multiple groups have demonstrated high accuracy for iodine quantification across a broad range of iodine concentrations because of the anti-correlated noise iterative model based reconstruction (AC-IMR). This feature also enables generation of virtual non-contrast images from a contrast-enhanced dataset.
2) ability to reduce contrast agent dose. As can be seen in figure 1, the iodine mass attenuation coefficient has an inverse, near linear dependency on X-ray energy in diagnostic CT range. In other words, low virtual monoE spectral reconstructions will increase iodine attenuation, leading to brighter iodine ‚signal' in the vessels compared to conventional CT imaging. This phenomenon allows for similar degree of vascular enhancement with the use of less iodine. Conversely, first-pass CTA-like contrast can be obtained from datasets acquired outside of the arterial phase.
3) ability to better visualize areas with hyper- or hypoperfusion such as myocardial perfusion defect or endoleaks. For the latter application, there is an additional clear benefit because of the potential for substantial radiation-dose savings due to the ability to omit both the non-contrast enhanced as well as the arterial phase scan. Conventional CT techniques rely on a multi-phasic approach for endoleak detection with a non-contrast acquisition followed by arterial-phase and late-phase imaging. Despite this extensive protocol, detection of endoleaks can still be cumbersome, especially when there is slow flow. In the context of endoleak imaging, features 1 and 2 as discussed above can be combined to obviate the need for the non-contrast scan, and potentially, the arterial phase images. An added advantage is better depiction of stent integrity at high virtual monoE levels.
4) ability to reduce blooming artefacts, enabling more accurate assessment of the degree of stenosis in the presence of (partially) calcified atherosclerotic plaques. Not only will this lead to improved stenosis grading, but it will also enable more accurate estimation of pressure gradients across coronary stenoses in virtual FFR applications, which heavily depends on high-fidelity segmentation of the coronary lumen. I will discuss the ongoing CLARITY study that will investigate the ability of spectral CT to improve specificity of coronary artery disease evaluation.
5) ability to use other contrast agents. Currently, iodine is the most widely used CT contrast agent but spectral and dual energy CT potentially allows for the use of other contrast agents as well. Particularly promising is the use of gadolinium at concentrations currently used for MR imaging. Dual-layer detector CT is also capable of highly accurate gadolinium quantification at concentrations typically seen in the body after injection of 0.1-0.2 mmol/kg body weight.

Take Home Points:

1) Spectral CT is a novel, vendor-specific way of acquiring dual energy CT data where energy separation is achieved at the detector level, as opposed to the source.
2) With spectral CT dual energy information can be routinely obtained in every patient without a priori specification of the desired reconstruction type.
3) Spectral CT, just like other dual-energy CT techniques, is capable of quantitatively mapping iodine distribution, reducing the amount of iodine needed for examinations, reducing the number of dynamic phases in examinations and is capable of reducing calcium blooming artefacts.

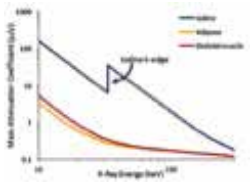

Iodine mass attenuation coefficient as a function of X-ray energy

Multi-Disciplinary (Clinical, Radiological, and Pathological)Discussion for the Diagnosis of Idiopathic Interstitial Pneumonias

Y. Inoue; Osaka/JP

Body: Idiopathic interstitial pneumonias (IIPs) are a group of acute and chronic diffuse parenchymal lung diseases of unknown origin. The international multidisciplinary classification of IIPs was updated in 2013. IIPs were classified to 6 major IIPs with 3 categories { 2 chronic fibrosing IIPs: Idiopathic pulmonary fibrosis (IPF) and idiopathic nonspecific interstitial pneumonia (INSIP), 2 smoking-related IIPs: Respiratory bronchiolitis-interstitial lung disease (RB-ILD) and desquamative interstitial pneumonia (DIP), 2 acute/subacute IIPs: Cryptogenic organizing pneumonia (COP) and acute interstitial pneumonia (AIP)}, 2 rare IIPs {Idiopathic lymphoid interstitial pneumonia (ILIP) and Idiopathic pleuroparenchymal fibroelastosis (IPPFE)}, and unclassifiable idiopathic interstitial pneumonia (Am J Respir Crit Care Med, 2013; 188: 733).

The increasing knowledges of imaging features on high resolution computed tomography (HRCT), including the clinical, radiological, and pathological (surgical lung biopsy) correlations, help radiologists in definite or suspected diagnosis of IIPs. However, because of low kappa value of the diagnostic agreements between radiologists or pathologists, multi-disciplinary discussion (MDD) with clinicians, radiologists, and pathologists has been emphasized for the diagnosis of IIPs as a gold standard. Except definite UIP pattern, most of IIPs require surgical lung biopsy, and cases of inappropriate information or without surgical lung biopsy should be called unclassifiable IIPs which require disease behabiour (Am J Respir Crit Care 2004; 170: 904, Am J Respir Crit Care Med, 2013; 188: 733).
IPF is associated with the histopathologic and/or radiologic pattern of Usual Interstitial Pneumonia (UIP) and is the most important progressive disease with poorer prognosis. IPF occurs 50-60% of IIPs. IPF is frequently associated with acute exacerbation or lung cancer, which make prognosis worse. Recent approval of anti-fibrotic drugs (nintedanib, pirfenidone) offered hope to IPF patients and their physicians. In addition, INPULSIS trial (nintedanib) provided important evidences that a confident diagnosis of IPF without biopsy is made in patients with clinical context of IPF and with CT pattern of typical or possible UIP pulse traction bronchiectasis, or probable UIP (Am J Respir Crit Care Med. 2017; 195; 78, Lancet Respir Med. 2018;6:138).
Although non-invasive diagnostic approach is preferable, pathological findings by surgical lung biopsy and MDD are necessary for most of cases. However surgical lung biopsy and MDD are not widely performed in the real world settings. Current diagnosis of IPF is based on the official international guideline (Am J Respir Crit Care Med. 2011; 183; 788), but Fleischner Society published IPF white paper and the current international guideline is required to be updated.
This lecture will be presented by me (pulmonary physician) from clinical and radiological standpoints, and Dr. Kitaichi (pathologist) from pathological standpoint.

Take Home Points:

- Idiopathic interstitial pneumonias (IIPs) are a group of acute and chronic diffuse parenchymal lung diseases of unknown origin.
- Except definite UIP pattern, most of IIPs require surgical lung biopsy, and cases of inappropriate information or without surgical lung biopsy should be called unclassifiable IIPs which require disease behabiour.
- Idiopathic Pulmonary Fibrosis (IPF) is associated with the histopathologic and/or radiologic pattern of Usual Interstitial Pneumonia (UIP) and is the most important progressive disease with poorer prognosis.
- IPF is frequently associated with acute exacerbation or lung cancer, which make prognosis worse.
- Confident diagnosis of IPF without biopsy is made in patients with clinical context of IPF and with CT pattern of typical or possible UIP pulse traction bronchiectasis, or probable UIP.
- Although non-invasive diagnostic approach is preferable, pathological findings by surgical lung biopsy and MDD are necessary for most of cases. However surgical lung biopsy and MDD are not widely performed in the real world settings.

Interstitial Lung Disease (ILD): Pathologic diagnosis of ILD as a part of multidisciplinary diagnosis in relation to prognosis

M. Kitaichi; Tanabe City/JP

Body: Interstitial Lung Disease (ILD): Pathologic diagnosis of ILD as a part of multidisciplinary diagnosis in relation to prognosis
Masanori Kitaichi, MD, PhD.
Department of Pathology, National Hospital Organization Minami Wakayama Medical Center, Tanabe City, Wakayama Prefecture, Japan.ÐE-mail: <kitaichi@mwn.hosp.go.jp>

<1> Introduction
Interstitial lung disease (ILD) is a relatively new terminology that has been used from the era of 1980's and a general term covering of diffuse infiltrative lung diseases of non-infectious etiology. During the study of ILD, we should remember that pulmonary emphysema and bronchial asthma are common bilateral lung diseases. This hand out is a summary of the background for the ILD session during the European Society of Thoracic Imaging (ESTI)/European Society of Cardiovascular Radiology(ESCR) Joint Meeting during May 24-26, 2018, in Geneva, Switzerland. During the session, a couple of cases of ILD will be shown from the view point of multidisciplinary diagnosis (MDD) in relation to prognosis.
Interstitial pneumonias were called as Hamman-Rich syndrome[1,2]. David M Spain reported in 1950 that there were five patterns of pulmonary fibrosis: bronchial, interstitial, parenchymal (intra-alveolar), pleural and vascular. He pointed out that these patterns may often co-exist and the different patterns will to great extent determine the functional disability. He studied 100 necropsied cases of cor pulmonare[3].
Averil Abraham Liebow pointed out that there are five types of interstitial pneumonia between 1967 and 1975[4-7]. Pathologic understanding of interstitial pneumonias was based upon the description by AA Liebow[8-49]. Idiopathic interstitial pneumonia (IIP) or interstitial pneumonia of unknown etiology was used as a clinical term[19]. In 1983, cryptogenic organizing pneumonitis (COP) was reported from the United Kingdom. The major differential diagnosis was infectious lung diseases11). In 1985, fifty cases of bronchiolitis obliterans organizing pneumonia (BOOP) was reported in the New Engl J Med[12]. With a question what is disease of BOOP, surgical lung biopsy (SLB) was resumed for the patients with diffuse infiltrative bilateral lung diseases using open thoracotomy method in 1985[13,15-19]. After an experience of 199 SLB cases in Japan, the writer (MK) was given a chance to study of approximately 2,000 SLB cases in North American and European countries from April 1986. MK returned home in October 1986

feeling some similarities and differences between the western countries and Japan[8-12]. On January 20, 1987, Tuesday, during the time of the review study of 7 autopsy cases who died in the clinical setting of adult respiratory distress syndrome at the Kyoto National Hospital, MK reached to recognize that the diffuse alveolar damage (DAD) to form hyaline membranes is different lung disorder from the usual interstitial pneumonia (UIP) that can develop honeycomb lung conditions19). This recognition made the question: what kind of meaning of UIP and DAD is there in the whole spectrum of diffuse bilateral lung diseases[19,23]. From the era of 1990'ies, endoscopic surgery has spread. From around 1995, video-assisted thoracoscopic surgery (VATS) has spread to perform surgical lung biopsy for the patients with diffuse infiltrative lung diseases. Open thoracotomy for surgical lung biopsy required the intractable pain to the patients and required a two-week hospitalization. VATS biopsy of the lung caused less degree of chest pain and required about 3-day hospitalization. The spread of VATS lung biopsy did not bring a conclusion in the field of diffuse lung diseases but expanded the questions. One of the widened spectra was the field of NSIP[28,31]. The pulmonary lesions of NSIP were called as unclassified interstitial pneumonia (Unclass IP) around the time of 1990[19,20].
During 1995-2005, the disease spectrum of chronic hypersensitivity pneumonitis (chronic HP) expanded and patients with chronic HP were underwent with a similar frequency as that of idiopathic pulmonary fibrosis (IPF). These situations have been continued[41].
During 2007 and 2015, lung diseases closely related to a connective tissue disease have been pointed out and currently have been included in the spectrum of idiopathic interstitial pneumonias (IIPs)[44].
From 2005, questions regarding combination disease state of chronic fibrosing interstitial pneumonia with respiratory airspace enlargement including bullae and pulmonary emphysema was raised using a label of combined pulmonary fibrosis and emphysema (CPFE)[46]. In the background of these trends, there is a fact that several drugs have become to be able to be administered for the patients with pulmonary hypertension.
Since around 2004, the term of pleuroparenchymal fibroelastosis (PPFE) has become to be useful when discussing the patients with upper lung field dominant pulmonary fibrosis[39,46].
Through these changes and expansion in and around the fields of idiopathic interstitial pneumonias (IIPs), the 2000 American Thoracic Society (ATS) document on idiopathic pulmonary fibrosis (IPF) stated the agreements that IPF as an American term and CFA(cryptogenic fibrosig alveolitis) as an British term should be used synonymously and that IPF should be used only for the patients with pathologic findings of usual interstitial pneumonia (UIP) in the clinical setting of idiopathic interstitial pneumonia (IIP)[33].
Based upon the works between 1998 and 2002, the International Multidisciplinary Consensus Classification of the IIPs was issued from the American Thoracic Society (ATS) and the European Respiratory Society (ERS) in 2002. The framework (the skeleton) of the 2002 document was the establishment of the concept of IPF/UIP in the general spectrum of IIP[34]. Because of the common understanding of IPF/UIP as having the intractable and progressive disease condition, clinical trials of drugs by pharmaceutical companies started and the field of anti-fibrosis drugs has been developed[42,43]. Due to take new turns of these clinical trials and drug therapies, the pathologic diagnosis of usual interstitial pneumonia (UIP) by a surgical lung biopsy and the question whether a UIP pattern is consistent with a disease condition of IPF/UIP have become to be strict[34,38,39].
In the central part of the way of thinking in the area of diffuse infiltrative lung diseases, idiopathic interstitial pneumonias (IIP) exists[19,33,3438,39]. The accuracy and consistency of taking histopathologic findings and pathologic diagnosis of idiopathic interstitial pneumonias (IIPs), especially idiopathic pulmonary fibrosis (IPF/UIP), are questioned again for the individual cases[49].

1) Handling the lung tissues

Inflation fixation is important for the lung tissues obtained by a transbronchial lung biopsy, a surgical lung biopsy, a lung surgery such as lobectomy and a postmortem examination. When the lung tissue is not well inflated as in the state of deep inspiration at the time of fixation, analytical assessment of interstitial lung disease or fibrotic lung disease is often impossible even if an elastic tissue is added. (Table 1)

2) Reading the histopathologic features of lung tissues:

The level of diagnostic pathology for diffuse infiltrative lung diseases is increasing according to the decade of 1980's 1990's, 2000's and 2010's. It was not rare that several days passed without any progress or results when MK observed a single slide stained with hematoxylin and eosin. To break and solve this kind of situation, the quantitative diagnostic method of interstitial pneumonia was invented in 2006 (Kitaichi M et al. Pathology and Clinical Medicine, 24:828-834, 2006, in Japanese).
When observing each specimen of the lung tissue stained with hematoxylin and eosin stain and Weigert's elatic tissue stain, the size of lung tissue, alveolar aeration ratio (AAR), normal alveolar wall ratio (AAR), fibrosis-ratio (F-ratio), and emphysema-ratio are noted. Using the objective lens of x2, x4, x10 and x40, the size of fibrocystic lesions and the number of lymphoid follicles, fibroblast focus (FF), abrupt changes from the fibrosis and the normal alveolar walls, smooth muscle proliferation and the number of eosinophils are noted. The lung tissue should read according to the airways system, vascular systems, alveolar walls, terminal air spaces, interlobular septa and the visceral pleura. For the recognition of granulomas, reticulin fiber formations in and around the granuloma are useful (Table 2).

<2> Idiopathic interstitial pneumonias (IIP) and idiopathic pulmonary fibrosis (IPF)

The term of idiopathic interstitial pneumonia (IIP) is a clinical term for the conditions as below and was coined when only the steroid hormone was used for the treatment for the patients of IIP until 1990's[19].

1) The main feature is an exertional dyspnea with bilateral pulmonary infiltrates on chest x-rays. Pulmonary function tests show a restrictive dysfunction with reduced lung volumes. The arterial blood gas analysis shows hypoxemia which tends to get worse after exercise. The etiology is not known, even after careful investigation of the past medical history and the environmental

history during life. The disease that possibly is complicated by a systemic disease such as the connective tissue disease, is excluded considering the present illness and the follow-up study.

2) The clinical course may be classified into acute, subacute and chronic type. In the chronic type, an aggravated acute problems occur sometimes with poor prognosis.

3) For treatment, steroid hormones are not effective in most cases, although these drugs have been effective in a small number of cases.

Idiopathic interstitial pneumonia has several types in relation to clinical features, radiologic and pathologic findings and prognosis [19,34,39] (Table 3).

(1) idiopathic pulmonary fibrosis/usual interstitial pneumonia (IPF/UIP)

Idiopathic pulmonary fibrosis (IPF) was a disease name in the U.S.A. while cryptogenic fibrosing alveolitis (CFA) was a disease name in the United Kingdom. An international document was published in 2000 to report that a consensus that IPF and CFA will be used synonymous. Because of the consensus document, clinical research could be able to have progresses in the field of IIPs[19,33,34,38,39,42,43].

In the U.S.A, the term of IPF was used to include various types of IIPs. Until the time around 1980, IPF was thought to include UIP and DIP. At this time, DIP and UIP were believed to be observed with similar frequency and that DIP is a relatively early stage of IPF while UIP is an advanced stage of IPF[8]. In around 1990, IPF was only understandable when the pulmonary histology was summarized to be usual interstitial pneumonia (UIP). Therefore, we used the terminology of IPF(UIP) in around 1990[19].

A consecutive study of 106 surgical lung biopsy for the patients with diffuse bilateral pulmonary diseases assessed that 52 cases had idiopathic interstitial pneumonia (IIP). Among them, 42 cases were assessed as IPF(UIP), 7 cases as BOOP, 1 case as LIP, 2 cases as unclassified IP and none as DIP. The diagnosis of these 106 cases were confirmed by Dr. Richard A DeRemee (Department of Respiratory Medicine) and Dr. Thomas V. Colby (Department of Diagnostic Pathology) from the Mayo Clinic, Rochester, U.S.A.[19].

From these data, the disease name of IPF has become to be used only for the IIP patients whose pulmonary histology was confirmed to have UIP. DIP became to be excluded from IPF. The expression of the disease name of idiopathic pulmonary fibrosis/ usual interstitial pneumonia (IPF/UIP) became to be generalized[33,34,38,39,47].

(2) Pathologic features of types of idiopathic interstitial pneumonias (IIPs)

1) Usual interstitial pneumonia (UIP):

UIP was recognized from the postmortem autopsy studies of cases that showed honeycombing during 1967 and 1975[5-7]. Fibroblast focus (FF) was recognized in 1986 as the young connective tissue (YCT) formation19). It was recognized in January of 1987 that the diffuse alveolar damage (DAD) that forms hyaline membranes along alveolar ducts occurred in the agonal terminal stage of cases of UIP19). During 1990 and 1994, nonspecific interstitial pneumonia (NSIP) was separated. Strict diagnosis was required for UIP from the view points of patchy distribution and temporal heterogeneity of fibrotic lesions[19,25,27,31]. UIP is a bilateral fibrotic diffuse lung disease and has a highest frequency and a poor prognosis[19,27,31]. Due to these facts, clinical trials of anti-fibrosis drugs were done in collaboration with pharmaceutical companies from the time when the 2002 ATS/ ERS documents on IIP classification was issued[34,42,43]. Because of the commencement of drug therapy of anti-fibrosis drugs, histologic diagnosis of UIP pattern in IPF has become to be required to be sure and the greater importance has become to be attached to the histologic findings of honeycombing when we read the documents in 2002, 2011 and 2013[34,38,39].

Currently, histologic findings of UIP in cases of IPF/UIP are summarized as below[38,47]. The validity of the way of thinking should be examined through the diagnostic works and discussions of real cases n relation to prognosis.

(A-1) Dense fibrosis causing architecture remodeling with frequent honeycombing

(A-2) Patchy lung involvement by fibrosis

(A-3) subpleural or paraseptal distribution, or both

(A-4) fibroblast foci at the edge of dense scars

(A-4) Absence of features against a diagnosis of UIP suggesting an alternate diagnosis: Hyaline membranes, Organizing pneumonia, Granulomas, Marked interstitial inflammatory cell infiltrates away from honeycombing, Prominent airway centered changes, Other features suggestive of an alternate diagnosis.

patients with features of other fibrotic disorders – eg, fibrotic hypersensitivity pneumonitis: fibrotic non-specific interstitial pneumonia; fibrosing organizing pneumonia; pleuroparenchymal fibroelastosis; pulmonary Langerhans cell histiocytosis, or smoking-related interstitial fibrosis.

UIP pattern with ancillary features strongly suggesting an alternative diagnosis: eg, prominent diffuse alveolar damage or organizing pneumonia (consider acute exacerbation of UIP), granulomas, (consider hypersensitivity pneumonitis; sarcoid; infection), marked interstitial inflammatory cell infiltrates away from areas of UIP (consider hypersensitivity pneumonitis)

2) Idiopathic non-specific interstitial pneumonia (I-NSIP)

NSIP has been described into two types , cellular and fibrosing patterns, without temporal heterogeneity as seen in UIP : Fibrosing NSIP is frequent compared to cellular NSIP. Cases of I-NSIP may show tissue eosinophilia. However, a histologic diagnosis of eosinophilic pneumonia requires the confirmation that there are no places of fibrosis with loss of normal alveolar structure (Table 4).

3) Respiratory bronchiolitis-interstitial lung disease (RB-ILD)

RB-ILD has bilateral lung diseases. The involved lung tissues shows accumulation of macrophages with brown-hued cytoplasm

in the centriacinar terminal air spaces and fibrotic changes of alveolar walls. When the patients have subjective symptoms, a diagnosis of RB-ILD is made[34,39].

4) Desquamative interstitial pneumonia (DIP)

DIP has bilateral lung disease. The involved lung tissues show diffuse accumulation of macrophages with brown-hued cytoplasm in the terminal air spaces and diffuse fibrotic thickening of alveolar walls[4,10,19,34,39].

5) Cryptogenic organizing pneumonia (COP)

Key histologic features are organizing pneumonia: intraluminal organizing fibrosis in distal airspaces (bronchioles, alveolar ducts, and alveoli), patchy distribution, preservation of lung architecture, uniform temporal appearance and mild interstitial chronic inflammation. Major differential diagnosis included infections and eosinophilic pneumonia. Fibrosing organzing pneumonia (FOP) was coined in 2013 and require the further study (Table 4, Table 5).

6) Acute interstitial pneumonia (AIP)

AIP is a bilateral lung disease and shows diffuse alveolar damage of unknown etiology. Involved areas shows diffuse and temporally homogeneous changes with loss of normal alveolar walls. Hyaline membrane formation is characteristic while hyaline membranes may not be so conspicuous in surgical lung biopsy cases. Major differential diagnosis is infections including viral infections[9,19,34,39].

7) Idiopathic lymphocytic interstitial pneumonia (I-LIP)

I-LIP is a chronic interstitial pneumonia and a bilateral lung disease. LIP shows diffuse and marked interstitial infiltration of lymphoid cells mainly in the alveolar walls[19,34,39].

When infiltration of lymphoid cells is dominant in the visceral pleura and in the interlobular septa, a diagnosis of lymphoma should be considered.

When marked dilation and tortuosity of lymphatic vessels are observed in the visceral pleura, interlobular septa and in the bronchiolovascular sheath, a diagnosis of disturbances of lymphatic flow should be considered rather than LIP as a chronic interstitial pneumonia.

8) Idiopathic pleuroparenchymal fibroelastosis (I-PPFE)

I-PPFE caused band-like subpleural fibrosis with cohesion and reinforcement of elastic fibers of alveolar frameworks. In the parenchymal fibroelastosis near the pleura, the remnant air space decreased and the amount of fibrosis increased. Fibrotic thickening of visceral pleura covering the parenchymal fibrosis is often observed[39,45].

PPFE is not a pathologic interstitial pneumonia which essentially involves the alveolar walls. However, PPFE is often observed in the upper part of lungs while the lower part of the lungs showed chronic fibrosing interstitial pneumonia, mainly IPF/UIP, in the same patients. PPFE was observed in 12 cases (5.9%) among the 205 consecutive surgical lung biopsy cases with diffuse infiltrative lung diseases between 2004 and 2012 at the Kinki-Chuo Chest Medical Center. Among the 12 patients, seven patients were alive (four of whom required home oxygen therapy) and 5 patients died from respiratory failure due to disease progression (median survival time from the SLB: 838 days)[45].

9) Acute fibrinous organizing pneumonia (AFOP)

AFOP is a bilateral lung disease and develop progressive exertional dyspnea and bilateral patchy pulmonary infiltrates during several weeks. Histologically, organizing pneumonia with marked fibrination is observed in a patchy distribution in the alveolar regions. AFOP is a rare disease and has a debate whether AFOP is a spectrum of DAD or not[39].

10) Bronchiolocenric patterns of interstitial pneumonia

Idiopathic bronchiolocentric interstitial pneumonia (BrIP)(n=10)(Yousem 2002), airway-centered interstitial fibrosis (ACIF) (n=12) (Churg,2004) and peribronchiolar metaplasia interstitial lung disease (PBM-ILD)(n=15)(Fukuoka, 2005) were reported. While the death was reported among BrIP patients (30%)(follow-up 48.2 months) and ACIF patients (33%), patients with PBM-ILD showed a good prognosis (no death during a follow-up of 2.37 years)[39].

(3) Interstitial pneumonias with autoimmune features (IPAF): Idiopathic interstitial lung disease closely related to a connective tissue disease

Patients with idiopathic interstitial lung disease closely related to a connective tissue disease (CTD) were pointed out by Kinder (2007), Fisher (2010), Vij (2011) and Corte (2012). When surgical lung biopsy specimens were observed microscopically, one tended to suggest a presence of defined CTD or future development of defined CTD because of presence of histologic features such as lymphoid follicles and marked infiltration of lymphoid cells in the lung tissues[44].

This group of patients were labelled as "interstitial pneumonia with autoimmune features (IPAF)" in an official ERS/ATS research statement in 2015[44].

The histopathologic features included within the morphologic domain criteria for IPAF are the primary pattern of NSIP, OP and LIP and the secondary features of interstitial lymphoid aggregates with germinal centers and diffuse lymphoplasmacytic infiltration with or without lymphoid follicles.

Patients with a histopathologic UIP pattern are not excluded from the IPAF definition. To be considered as having IPAF, a patient with a UIP pattern on histopathology also requires a least one feature from other two domains (a clinical feature or a serologic feature), or another morphologic feature.

Currently, IPAF is included in the spectrum of IIPs because these patients could not classified into a defined connective tissue disease (CTD)[44].

<3> Differential diagnosis and how to use the pattern recognitions of IIPs

(1) Differential diagnoses of idiopathic interstitial pneumonias (IIPs)

1) Connective tissue disease(CTD)-associated lung disease
If the lung tissue is divided into the four compartments of the alveolar walls, airway walls, vascular walls and visceral pleura/ interlobular septa, two or more compartments were tended to be involved in CTD. Fibrotic changes of UIP pattern in rheumatoid arthritis tended to show many lymphoid follicles with germinal centers and infiltration of many lymphoid cells. NSIP pattern is frequent in CTD than in IIPs patients[35)].
2) Hypersensitivity pneumonitis (HP), including chronic/fibrotic hypersensitivity pneumonitis (chronic HP)
In 1970's and 1980's, subacute HP was major among HP patients. From about 1995, chronic HP has been increased in frequency[41,47,50-64)]. For about half of the patients for whom the surgical lung biopsy histologic findings are consistent with chronic HP, antigens are not determined even after careful clinical and laboratory examinations[62)].
3) Pneumoconiosis
Airway-centered inflammatory and fibrotic lesions were observed in cases of pneumoconiosis including the early lesions of asbestosis. For the differential diagnosis of pneumoconiosis, microscopic observation using the birefringence lens is necessary.
4) Respiratory airspace enlargement disease
Patients with smoking history of more than 20 years and marked centriacinar emphysema (CAE) may show centriacinar loose fibrotic lesions with fibroelastosis mechanism with or without calcification[64-67)].
(2) How to use the pattern recognition of idiopathic interstitial pneumonias (IIPs).
Pathologic diagnosis of interstitial pneumonia has used the classification of IIPs as the fundamental form. Under the recognition that each type of interstitial pneumonias shows different histopathologic features according to the disease condition, classification of IIPs has been used in lung disease condition such as connective tissue diseases and chronic HP. Among the patients with bird fancier disease, a type of chronic HP, a relationship between the patterns of fibrotic lesions and prognosis was reported and a UIP pattern showed worse prognosis[55)].
UIP pattern shows secondary histopathologic features according to the disease conditions as below[50-93)].
1) Connective tissue disease: lymphoplasmacytic aggregates with germinal centers, remarkable lymphoplasmacytic infiltration in the fibrotic lesions and lesions of airways are observed[35)].
2) Chronic HP: Epithelioid cell granulomas measuring up to 100-300 microns in size, aggregates of multinucleated giant cells in the fibrotic lesions, centriacinar fibrotic lesions with loss of normal alveolar structures and/or centriacinar interstitial infiltration of lymhoplasmacytic cells are observed. The fibrotic lesion of the UIP pattern in chronic HP is more crowded with lymphoid cells compared to the fibrotic lesion in IPF/UIP[62)].
3) Asbestosis: Centriacinar fibrotic lesions and asbestos bodies in the fibrotic lesions are observed.
4) Hermansky-Pudlak syndrome: Iron-negative yellow-brown pigments (ceroid pigments) and foamy cells on the alveolar walls are observed[40)].
5) Pulmonary alveolar proteinosis (PAP): PAP may be associated with UIP pattern and revealed worse prognosis[85,90,93)] (Table 6).

<4> Summary
Pathologic diagnosis of diffuse infiltrative lung disease underwent remarkable changes and progression[1-93)]. It is now outdated if one makes only a histopathologic diagnosis of UIP pattern, NSIP pattern etc using the 2002 ATS/ERS international multidisciplinary consensus classification. The pattern recognition described in the 2002 ATS/ERS classification should be used from the view points to know the disease condition in each patient[34,35,39,47,62)]. Each patient is not known whether the patient belongs to the category of IIP, interstitial pneumonia with autoimmune features (IPAF), connective tissue disease or chronic HP. Histopathologic diagnosis in the field of interstitial lung disease is requested to make a diagnosis not only the pattern recognition of fibrosis but also adequate suggestion of disease condition in relation to prognosis.

Acknowledgement: This study was partially supported by the grants from the Japanese Ministry of Health, Labour, and Welfare (Pulmonary alveolar proteinosis, 17930161,H26-Nanchitoo(Nan)-ippann-076) and the National Hospital Organization Respiratory Diseases Network (H26-NHO(Kokyu)-01).

References:
<A> Idiopathic interstitial pneumonia (IIP) and idiopathic pulmonary fibrosis (IPF) Hamman L and Rich AR. Fulminating diffuse interstitial fibrosis of the lungs. Trans Am Clin & Climatol Asson 51: 154-163, 1935. Hamman L and Rich AR. Acute diffuse interstitial fibrosis. Bull Johns Hopkins Hosp, 74:177-212,1944. Spain DM. Patterns of pulmonary fibrosis as related to pulmonary function. Ann Intern Med 33: 1150-1163, 1950. Liebow AA, Steer A, Bilingsley JG. Desquamative interstitial pneumonia. Am J Med 39:369-404, 1965. Liebow AA. New concepts and entities in pulmonary disease. In: The Lung, Ed. By Liebow AA, Williams and Wilkins, Baltimore, 1967, pp.332-365.Ð Liebow AA, Carrignton CB. The interstitial pneumonias.In: Simon M, Pochen EJ, LeMay L (eds). Frontiers of Pulmonary Radiology . Pathophysiologic, Roentgenographic and Isotopic Considerations. Grune & Stratton, New York, 1968, p.102-141. Liebow AA. Definition and classification of interstitial pneumonias in human pathology. (Alveolar Interstitium of the Lung, Int. Symp., Paris 1974), Prog Resp Res 8: 1-33, Karger, Basel, 1975. Crystal RG, Fulmer JD, Roberts WC, et al. NIH Conference. Idiopathic pulmonary fibrosis. Clinical, histologic, radiographic, physiologic, scintigraphic, cytologic, and biochemical aspects. Ann Intern Med 85: 769-788, 1976. Katzenstein A-LA, Bloor CM, Liebow AA. Diffuse alveolar damage – the role of oxygen, shock, and related factors. Am J Pathol 85: 210-228, 1976. Carrington CB, Gaensler EA, Coutu RE, et al. Natural history and treated course of usual and desquamative interstitial pneumonia. New Engl J Med 298: 801-809, 1978. Davison AG, Heard BE, McAllister WAC,

Turner-Warwick MEH. Cryptogenic organising pneumonitis. Q J Med 207: 382-394, 1983. Epler GR, Colby TV, McLoud TC, Carrington CB, Gaensler EA. Bronchiolitis obliterans organizing pneumonia. New Engl J Med 312: 152-158, 1985. Kubo Y, Murayama T, Amitani R, Kurasawa T, Kuze F, Chihara J, Kitaichi M. Two cases of bronchiolitis obliterans organzing neumonia (BOOP). Nihon Kyobu Rinsho (Jpn J Chest Dis) 45:1062-1071, 1986 (in Japanese with English abstract). Konishi H. A case of bronchiolitis obliterans organizing pneumonia in a patients with long-term administration of antibiotics and bone graft. Nihon Kyobu Shikkan Gakkai Zassi (Jpn J Thoracc Dis) 26: 1005-1009, 1988 (in Japanese with English abstract and figure legends). Imai H, Kitaichi M. A case of bronchiolitis obliterans rganzing pneumonia (BOOP) showing spontaneous regression after an ope lung biopsy. Nihon Kyobu Shikkan Gakkai Zassi (Jpn J Thoracic Dis) 27: 829-836, 1989 (in Japanese with English abstract and figure legends). Kitaichi M. Alveolar septal inflammation: A comparative pathological study of IPF and BOOP. In: Harasawa M, Fukuchi Y, Morinari H (eds). Interstitial Pneumonia of Unknown Etiology, University of Tokyo Press, Tokyo, 1989, p.189-199. Izumi T, Nagai S, Nishimura K, Kitaichi M et al. BALF cell findings in patients with BOOP, particularly in comparison with patients with UIP. Nihon Kyobu Shikkan Gakkai Zassi (Jpn J Thoracic Dis) 27:474-480, 1989 (in Japanese with English abstract and figure and table legends). Yamamoto M, Ina Y, Kitaichi M, Harasawa M, Tamura M. Bronchiolitis obliteraans organzing pneumonia (BOOP) in Japan. Nihon Kyobu Shikkan Gakkai Zasshi (Jpn J Thoracc Dis) 28: 1164-1173, 1990 (in Japanese with English abstract and figure legends). Kitaichi M. Pathologic features and classification of interstitial pneumonia of unknown etiology. Bull Chest Dis Res Inst, Kyoto Univ 23: 1-18, 1990. Colby TV, Lombard C, Yousem SA, Kitaichi M. Atlas of Pulmonary Surgical Pathology. W.B. Sounders Co., Philadelphia, pp.380, 1991. Yamamoto M, Ina Y, Kitaichi M, Harasawa M, Tamura M. Clinical features of BOOP in Japan. Chest 102: 21S-25S, 1992. Colby TV. Pathologic aspects of bronchiolitis obliterans organizing pneumonia. Chest 102: 38S-43S, 1992. Kitaichi M.ÐDifferential diagnosis of bronchiolitis obliterans organizing pneumonia. ChestÐ102: 44S-49S, 1992. Izumi T, Kitaichi M, Nishimura K, Nagai S. Bronchiolitis obliterans organizing pneumonia. Clinical features and differential diagnosis. Chest 102: 715-719, 1992. Nishimura K, Kitaichi M, Izumi T, Nagai S, Kanaoka M, Ith H. Usual interstitial pneumonia: Histologic correlation with high-resolution CT. Radiology 182: 337-342, 1992. Nishimura K, Izumi T, Kitaichi M, Nagai S, Itoh H. The diagnostic accuracy of high-resolution computed tomography in diffuse infiltrative lung diseases. Chest 104: 1149-1155, 1993. Kanematsu T, Kitaichi M, Nishimura K, Nagai S, Izumi T. Clubbing of the fingers and smooth-muscle proliferation in fibrotic changes in the lung in patients with idiopathic pulmonaru fibrosis. Chest 105: 339-342, 1994. Katzenstein A, Fiorelli RF. Nonspecfic interstitial pneumonia/fibrosis. Histologic features and clinical significance Am J Sur Pathol 18: 136-147, 1994. Kitaichi M. Bronchiolitis obliterasn organizing pneumonia (BOOP). In: Basic and Clinical Aspects of Pulmonary Fibrosis, Edited by Takishima, Yamauchi K, Shimura S. CRC Press, Boca Raton, 1994, p.463-488. Kitaichi M. Editorial: Desquamative interstitial pneumonia : an idiopathic interstitial pneumonia with a possibility of spontaneous regression.Internal Medicine 36: 672-673, 1997. Nagai S, Kitaichi M, Itoh H, Nishimura, Izumi T, Colby TV. Idiopathic nonspecific interstitial pneumonia/ fibrosis: comparison with idiopathic pulmonary fibrosis and BOOP. Eur Respir J 12: 1010-1019, 1998. Nishimura K, Itoh H, Kitaichi M, Nagai S, Izumi T. Computed tomographic findings I usual interstitial pneumonia:CT and pathologic correlation. Curr Topics in Radiology 1: 65-77, 1998. American Thoracic Society. Idiopathic pulmonary fibrosis: Diagnosis and treatment. International consensus statement. Am J Respir Crit Care Med 161: 646-664, 2000. American Thoracic Society. ATS/ERS international multidisciplinary consensus classification of the idiopathic interstitial pneumonias. Am J Respir Crit Care Med 165: 277-304, 2002. Kitaichi M, Nagai S, Ito I, Yanagi S. Pulmonary pathology in association with connective tissue disorders. Curr Diag Pathol 10: 291-303, 2004 Travis WD, Hunninghake G, King TE Jr et al. Idiopathic nonspecific interstitial pneumonia. Report of an American Thoracic Society project. Am J Respir Crit Care Med 177; 1338-1347, 2008. Akira M, Inoue Y, Kitaichi M, Yamamoto S, Arai T, Toyokawa K. Usual interstitial pneumonia and nonspecific interstitial pneumonia with and without concurrent emphysema: Thin-section CT findings. Radiology 251: 271-279, 2009. Raghu G, Collard HR, Egan JJ et al. An official ATS/ERS/JRS/ALAT statement: Idiopathic pulmonary fibrosis: evidence-based guidelines for diagnosis and management. Am J Respir Crit Care Med 183: 788-824, 2011. Travis WD, Costabel U, Hansell DM et al. An official ATS/ERS statement: update of the international multidisciplinary classification of the idiopathic interstitial pneumonias. Am J Respir Crit Care Med 188: 733-748, 2013. Kanazu M, Arai T, Sugimoto C, Kitaichi M, Akira M, Abe Y, Hozumi Y, Suzuki T, Inoue Y. An intractable case of Hermansky-Pudlak syndrome. Internal Med 53: 2629-2634, 2014. Morell F, Villar A, Montero M-A, et al. Chronic hypersensitivity pneumonitis in patients diagnosed with idiopathic pulmonary fibrosis: a prospective case-cohort study. Lancet Resp Med 1: 685-694, 2013. King TE Jr, Bradford WD, Castro-Bernardin S et al. A phase 3 trial of pirfenidone in patients with idiopathic pulmonary fibrosis. New Engl J Med 2014 (Doi 10.1056/ NEJMoal402582) Richeldi L, du Bois RM, Raghu G et al. Efficacy and safety of nintedanib in idiopathic pulmonary fibrosis. New Engl J Med 2014 (DOI: 10.1056/NEJMoa1402584). Fischer A, Antoniou KM, Brown KK, et al. An official ERS/ATS research statement: interstitial pneumonia with autoimmune features. Eur Resp J 2015 (DOI: 10.1183/13993033. 00150-2015) Nakatani T, Arai T, Kitaichi M et al. Pleuroparenchymal fibroelastosis from a consecutive data base: a rare disease entity? Eur Res J Feb 19, 2015 (doi: 10.1183/09031936. 00214714) Kohashi Y, Arai T, Sugimoto C, Tachibana K, Akira M, Kitaichi M, Hayashi S, Inoue Y. Clinical impact of emphysema evaluated high-resolution computed tomography on idiopathic pulmonary fibrosis diagnosed by surgical lung biopsy. Respiration 92: 220-228, 2016. Lynch DA, Sverzellat N, Travis WD, Brown K, Colby TV, Galvin JR, Goldin JG, Hansell DM, Inoue Y, Johkoh T, Nicholson AG, Knight SL, Roof S, Richeldi L, Reyerson CJ, Ryu JH, Wells A. Diagnostic criteria for idiopathic pulmonary fibrosis: a Fleischner Society White Paper. Lancet Respir Med 2017,p.1-16. (published online ,November 15, 2017). Kobayashi T, Kitaichi M, Tachibana K, Kishimoto Y, Inoue Y, Kagawa T, Maekura T, Sugimoto C, Arai T, Akira M, Inoue Y. A cryptogenic case of fulminant fibrosing organizing pneumonia. Intern Med 56: 1185-1191, 2017. Arai T, Tachibana K, Sugimoto C, Inoue Y, Tokura S, Okuma T, Aira M, Kitaichi M, Hayashi S, Inoue Y. High-dose prednislone after intravenous methylprednisolone improves prognosis of acute exacerbation in idiopathic interstitial pneumonias. Respirology 2017, doi: 10.1111/resp.13065.
<B> Hypersensitivity pneumonitis

50. Fujimura N, Kino T, Nagai S, Kitaichi M, Izumi T, Ohshima S, Ogawa S, Sato K. Hypersensitivity pneumonitis in a polyrethane aint sprayer. Nihon Kyobu Shikkan Gakkai Zassi (Jpn J Thoracc Dis) 22: 506-513, 1984 (in Japanese with English abstract and figure legends).
51. Ozasa K, Inui T, Sugano T, Fujita Y, Kitaichi M, Kino T et al. Familial hypersensitivity pneumonitis probably induced by Cladosporoum. Nihon Kyobu Rinsho (Jpn J Chest Dis) 43: 520-529, 1984 (in Japanese with English abstract).
52. Umegae Y, Matsui S, Irokawa M, Katakai S, Nakazawa T, Iizuka K, Miura S, Fueki R, Kobayashi S, Kitaichi M. A case of hypersensitivity pneumonitis related to Sericulture (Sericalturist's lung disease). Nihon Kyobu Shikkan Gakkai Zassi (Jpn J Thoracic Dis) 24: 804-809, 1984 (in Japanese with English abstract and figure legends).
53. Kitaichi M. Comparative pulmonary histopathology of sarcoidosis, chronic beryllium disease and hypersensitivity pneumonitis. Nihon Kyobu Shikkan Gakkai Zasshi (Jpn J Thoracic Dis) 22: 769-782, 1984 (in Japanese with English abstract and legends).
54. Chida K, Sato A, Honda K, Okano A, Taniguchi M, Akiyama J, Hayakawa H, Imai H, Kitaichi M. A case of chronic hypersensitivity pneumonitis induced by wheat flour. Nihon Kyobu Shikkan Gakkai Zasshi (Jpn J Thoracic Dis) 23:1472-1479, 1985 (in Japanese with English abstract and figure legends).
55. Ohtani Y, Saiki S, Kitaichi M et al. Chronic bird fancier's lung. Histopathlogical and clinical correlation. An application of the 2002 ATS/ERS consensus classification of the idiopathic interstitial pneumonias. Thorax 60: 665-671, 2005..
56. Takemura T et al. Pathology of hypersensitivity pneumonitis. Curr Opin ulm Medicine 2008: 14: 440-454.
57. Akashi T, Takemura T, Yoshizawa Y et al. Histopathologic analysis of sixteen autopsy cases of chronic hypersisitivity pneumonitis and comparison with idiopathic pulmonary fibrosis/usual interstitial pneumonia. Am J Clin Pathol 2009: 131:405-415.
58. Tateishi T, Ohtani Y , Takemura T, Yoshizawa Y et al. Serial high-resolution computed tomography findings of acute and chronic hypersensitivity pneumonis induced by avian antigen. J Comp Assist Tomogr. 2011; 35: 272-279.
59. Miyazaki Y, Tateishi T, Akashi T, et al.. Clinical predictors and histologic appearance of acute exacerbations in chronic hypersensitivity pneumonitis. Chest 2008; 134: 1265-1270.
60. Takemura T, Akashi T, Ogura T et al. Pathologic differentiation of chronic hypersensitivity pneumonitis from idiopathic pulmonary fibrosis/usual interstitial pneumonia. Histopathology 2012; 61: 1026-1035,
61. Kuromachi J, Inase N Miyazaki Takemura K, Yoshizawa Y et al. Lung cancer in chronic hypersensitivity neumonitis. Respiration 2011: 82: 263-267.
62. Kitaichi M, Shimizu S, Tamaya M, Takaki M, Inoue Y. Pathology of hypersensitivity pneumonitis. Sharma OP (ed), Clinical Focus Series: Hypersensitivity Pneumonitis, Jaypee Brothers Medical Publishers LTD, New Delhi,2013, p.22-32.
63. Minomo S, Tachibana K, Tsuyuguchi K, et al. A unique case of hot tub lung worsening during the winter. Intern Med 54: 491-495, 2015.
64. Chiba S, Miyazaki Y, Takemura T, Inase N et al.: Chronic hypersensitivity pneumonitis with a usual interstitial pneumonia-like pattern: correlation between histopathologic and clinical findings. Chest 2016: 149: 1473-1481.
<C> Other types of ILD and diffuse lung diseases
64. Reid L. The Pathology of Emphysema, Year Book Medical Publishers, Inc, Chicago, 1967, pp.372
65. Heard B. Pathology of Chronic Bronchitis and Emphysema, J.&A. Churchill LTD, London, 1969, pp.136
66. Thurlbeck WM. Chronic Airflow Obstrction in Lung Disease, W.B.Saunders Co, Philadelphia, 1976, pp.456.
67. Snider GL, Kleinerman J, Thurlbeck WM et al. The definition of emphysema. Report of a National Heart, Lung and Blood Institute, Division of Lung Disease Workshop. Am Rev Respir Dis 132: 182-185, 1985.
68. Longcope WT, Freiman DG. A study of sarcoidosis. Based on a combined investigation of 160 cases including 30 autopsies from the Jhons Hopkins Hospital and Massachusetts General Hospital. Medicine 31: 1-132, 1952.
69. Kitaichi M. Pathology of pulmonary sarcoidosis. Izumi T (ed),Sarcoidosis, Clinics in Dermatology 4(4): 108-115, 1986.
70. American Thoracic Society: Committee: Hunninghake GW, Costabel U, Ando M, Baughman R, Cordier JF, du Bois R, Eklund A, Kitaichi M, Lynch J, Rizzato G, Rose C, Selroos O, Semenzato G, Sharma OP. Statement on sarcoidosis. Am J Respir Crit Care Med 160: 736-755, 1999.
71. Kitaichi M. Pathology of diffuse panbronchiolitis from the view point of differential diagnosis. In: Sarcoidosis and other granulomatous disorders, Edited by Grassi C, Rizzato G, Oozzi E, p.741-746, 1988, Elsevier Science Publishers B.V. (Biomedical Division).
72. Rosen SH, Castleman B, Liebow AA. Pulmonary alveolar proteinosis. New Engl J Med 258: 1123-1158, 1958.
73. Kitaichi M, Nishimura K, Izumi T. Diffuse panbronchiolitis. In: Lung Disease in the Tropics, Edited by Sharma OP, Marcel Dekker, New York, 1990, p.479-509.
74. Iwata M. Colby TV, Kitaichi M. Diffuse panbronchiolitis: diagnosis and distinction from various pulmonary diseases with centrilobular interstitial foam cell accumulations. Hum Pathol 25: 357-363, 1994.
75. Asamoto H, Kitaichi M, Nishimura K, Itoh H, Izumi T. Primary pulmonary alveolar proteinosis – Clinical observation of 68 patients in Japan-. Nihon Kyobu Shikkan Gakkai Zassi (Jpn J Thoracic Dis) 33: 835-845, 1995.
76. Asamoto H, Kitaichi M, Nagai S, Nishmura K, Itoh H, Izumi T. Pulmonary eosinophilic granuloma –clinical analysis of 17 patients-. Nihon Kyobu Shikkan Gakkai Zassi (Jpn J Thoracic Dis)b 33: 1372-1381, 1995.
77. Kitaichi M, Nishimura K, Itoh H, Izumi. Pulmonary lympahngileiomyoatosis: A report of 46 patients including a clinicopathologic study of prognostic factors. Am J Resp Crit Care Med 151: 527-533, 1995.
78. Kitaichi M, Izumi T. Lympangioleiomyomatosis. Curr Opinion in Pulm Med 1: 417-424, 1995.
79. Kitaichi M. Eosinophilic lung diseases – Pathologic view. Korean J Allergy 17: 449-463, 1997 (Abstract: The 24th Annual Meeting

of the Korean Society of Allergology held on November 7, 1997, Cheju, Korea).
80. Kitaichi M, Nagai S, Nishimra K, Itoh H, Asamoto H, Izumi T, Dail DH. Pulmonary epithelioid haeangioendothelioma in 21 patients, including three with partial spontaneous regression. Eur Resp J 12: 89-96, 1998.
81. Muir TE, leslie KO, Popper H, Kitaichi M,Gagne E, Emelin JK, Vinters HV, Colby TV. Micronodular pneumocytes hyperplasia. Am J Surg Pathol 22: 465-472,1998.
82. Izumi T, Kitaichi M, Nagai S. Perspectives on lymphangioleiomyomatosis in Japan. In: LAM and Other Diseases Charactrized by Smooth Mucsle Proliferation, Marcel Dekker, Inc, New York, 1998, p.1-8.
83. Sugimoto M, Kitaichi M, Ikeda A, Nagai S, Izumi T. Chronic bronchioloalveolitis associated with human T-cell lymphotropic virus type Ðinfection. Curr Opinion Pul Med 4:98-102, 1998.
84. Tanigawa K, Sugiyama K, Matsuyama H, Nakao H, Khno K, Komuro Y, Iwanaga Y, Eguchi K, Kitaichi M, Takagi H. Meslazine-induced eosinophilc pneumonia. Respiration 66: 69-72, 1999.
85. Inoue Y, Trapnell BC, Tazawa R, Arai T, Sakatani M, Nakata K et al. Characteristics of a large cohort of patients with autoimmune pulmonary alveolar proteinosis in Japan. Am J Resp Crit Care Med 177: 752-756, 2008.
86. Takeuchi A, Arai T, Kitaichi M, Inoue Y.: A comorbid case of multicentric Castleman's disease and pulmonary hyalinizing granuloma successfully treated with tocilizumab and corticosteroid. BMC Case Rep 2013. Doi:10.1136.
87. Balmes JR, Abraham JL, Dweik RA, Fireman E, Fontenot AP, Maier LA, Muller-Qerrhaim J, Ostiguy G, Pepper LD, Saltini C, Schule CR, Takaro TK, Wambach PF. An official American Thoracic Society statement: Diagnosis and management of beryllium sensitivity and chronic beryllium disease. Am J Respir Crit Care Med 190: e34-259, 2014.
88. Arai T, Inoue Y, Akira M et al. Autoimmune pulmonary alveolar proteinosis following oulmonary aspergillosis. Intern Med 54: 3177-80, 2015.
89. Takeuchi N, Arai T, Tachibana K, Kitaichi M, Hayashi S, Inue Y. Organizing pneumonia combined with alveolar hemorrhage after radiotherapy for breast cancer, Journal of the Japan Society for Respiratory Endoscopy, 37: 183-190, 2015 (in Japanese with English abstract and legends)
90. Akira M, Inoue Y, Arai T et al. Pulmonary fibrosis on high resolution CT of patients with pulmonary alveolar proteinosis. AJR Am J Roentgenol 207: 544-51, 2016.
91. McCormick FX, Gupta N, Finlay GR, Inoue Y et al. Official ATS/JRS clinical practice guidelines: lymphangioleiomyomatosis diagnosis and management. Am J Resp Crit Care Med 194: 748-761, 2016.
92. Koba T, Arai T, Kitaichi M, Kasai T, Horose M, Tachibana K, Sugimoto C, Akira M, Hayashi S, Inoue Y. Efficacy and safety of transbronchial lung biopsy for the diagnosis of lymphangioleiomyomatosis: A report of 24 consecutive patients. Respirology 2017 Sep 28.
93. Kitaichi, Kasai, Teramoto T, Takaki M. Pathology of pulmonary alveolar proteinosis, Nihon Kyobu Rinsho 75: 1245-1253, 2016 (in Japanese with English abstract)

Table 1. Handling the lung tissue obtained by a surgical lung biopsy

General background: For the surgical procedure to obtain the lung biopsy tissue, video-assisted thoracoscopic surgery (VATS) has been used since the middle of 1990's in addition to open thoracotomy.

<1> Selection of the lung biopsy sites:

1) Consideration of the clinical situation including the findings of chest HRCT

2) Selection of two sites/lobes for the surgical diagnosis: In the chronic disease, moderately involved area of one lobe and mildly involved area of another lobe are to be selected considering the findings of chest CT. Markedly involved areas of honeycomb changes are to be avoided . Each side of the lung will be marked at the two sites/lobes for possible biopsy site(s). The lung to the contralateral patient's dominant hand will be selected for the surgical biopsy.

In acute/subacute disease, markedly involved area of lung should be biopsied considering the possibility of infections and neoplasm.

3) At the surgery, the surgeon looks at the lung and thoracic cavity regarding the presence or absence of pleural fluid and pleural thickening and adhesions. It is often to select the basal part of segment 2 or segment 3 of the upper lobe and the basal part of segment 8 or segment 9 of the lower lobe. It is not desirable for the patient's safety to select segment 6 of the lower lobe because the distance between the central bronchi and vasculature and the lateral side of the visceral pleura is relatively short.

4) Size of biopsied lung tissue: The lung tissue of 2x2x3 cm to 3x3x4 cm is adequate size for the each site of biopsy.

5) The biopsied lung tissues are to be transferred in the sterile condition to the pathology laboratory to avoid becoming dry in the physiological saline.

<2> After the fresh sterile lung tissue(s) was delivered at the pathology laboratory:

1) Macroscopic observation:

Biopsied lung tissues should be transferred from the operation room to the pathology laboratory in the sterile physiological saline or covered with gauze moistened by the sterile physiological saline.

2-8) The following procedures should be done in a Biohazard system measuring such as 1,045 mm wide, 770 mm deep and 1,920 mm high.

Gross findings of the lung tissue:

2) Measurement of the lung tissue(s).

3) Pleuritis/pleural thickening/ hobnail appearance: absent/present
4) Stapled line of the lung tissue should be taken out by a sterile scissor.
6) The staple line of the lung tissue should be submitted for microbiological examinations including cultures for bacteria and fungi and polymerase chain reaction for mycobacteria (M.tuberculosis-PCR, M.intracellular-PCR, M.avium-PCR) and culture for mycobacteria.
7) Using sharp knife, small lung specimens measuring 2x2x2 mm should be made for electron microscopy study and fixed with 2.5% glutaraldehyde in phosphate buffer.
8) Cut the biopsied lung tissue(s) for research purposes and stored in the freezed condition at -70
9-18) The following procedures can be done outside the Biohazard system.
9) The remnant lung tissue(s) (the majority of the biopsied lung tissue(s)) is be fixed by the inflation fixation method: 15% formalin neutral buffer solution (e.g. WAKO) containing 5.25% of formaldehyde and 1.5% methanol in neutral phosphate buffer (pH7.4) is used as the fixative. The fixative will be suck up into the 10 ml or 20 ml syringe using 18 G needle (1.2x38 mm needle). Then, biopsied lung tissue(s) will be infused gently with the 15% formalin neutral buffer solution through several places of the lung pleural/non-pleural surfaces using 25G (0.50x25 mm) needle or 26G needle (0.45x13 mm) for Mantoux's skin test up to near the level of total lung capacity. Then, the biopsied lung tissue will be fixed overnight (12-24 hours) in 50-100 ml of 15% formalin neutral buffer solution.
10) After the overnight fixation with 15% formalin neutral buffer solution, wash the lung tissue (s) with tap water:
11) Take photos of biopsied lung tissue(s);
12) Slice serially the biopsied lung tissue(s) with a thickness of 3 mm using a sharp knife (e.g. FEATHER Trimming Blade, No.130, Type (S)). The sliced lung tissues should have the visceral pleura at the one or two edge surface(s) to know the orientation of lung lesions/fibrosis (subleural/periacinar/centriacinar).
13) Take photos of the sliced lung tissues to know the presence/absence of honeycombing, mass/nodular lesions and pleural/subpleural lesions.
14) Make paraffin blocks for each biopsied lung slice(s),
15) Using a microtome (e.g. YAMATO, RETRATOME, REM-710), paraffin sections will be made with a thickness between 2 micrometers and 3 micrometers.
16) Staining the sequential paraffin sections with hematoxylin and eosin method and elastic tissue method (e.g., Mayer's hematoxylin and eosin method and Weigert's elastic van Gieson method).
17) Detection of refringent bodies by a hematoxylin and eosin stained glass slides using polarized filters
18) After the microscopic observation of histopathologic fndings of hematoxylin and eosin stained glass slides, additional stains and imunohistologic stains will be done using recutted paraffin sections.

Table 2. Histopathologic examinations to confirm the presence of granulomas and for the differential diagnoses

(1) Hematoxylin and eosin stain: Size and sites of granulomas, with or without necrosis, birefringent materials in relation to granulomas
(2) Elastic tissue stain (Weigert's method): Sites of granulomas in relation to vessels
When intra-alveolar dominant granulomatous inflammation was observed, an infectious etiology is strongly suggested.
Granulomas in relation to the structure of blood vessels.
(3) Reticulin stain: Perigranulomatous and intragranulomatous/pericellular reticulin fibers
(4) Grocott stain: detection of fungi including Pneumocystis jirovetti (needs positive control)
(5) Ziehl-Neelsen stain:Ddetection of acid-fast bacilli (needs positive control)
(6) Gram stain: detection of Gram-positive and negative bacilli (needs positive control)
(7) PAS stain: detection of fungi
Alveolar macrophages have positive intracytoplasmic granules; Epitehlioid cells do not have them.Đ Đ
(8) PAS-alcian blue stain: detection of fungi
(9) CD 68 stain: Alveolar macrophages, epithelioid cells and multinucleated giant cells are positive
(10) Keratin (AE1/AE3) stain: Alveolar macrophages, epithelioid cells and multinucleated giant cells are negative.
Notes: Granuloma is a focal, organized collection of mononuclear phagocyte system cells. The presence of granulomas can be confirmed by the histologic findings of HE, reticulin and CD68 stains.
Ref: 1) American Thoracic Society. Statement on sarcoidosis. Am J Respir Crit Care Med 160: 736-755, 1999.

Table 3. Revised ATS/ERS classification of idiopathic interstitial pneumonias: Multidisciplinary diagnosis

Major idiopathic interstitial pneumonias
- Idiopathic pulmonary fibrosis
- Idiopathic nonspecific interstitial pneumonia
- Respiratory bronchiolitis-interstitial lung disease
- Desquamative interstitial pneumonia
- Cryptogenic organizing pneumonia
- Acute Interstitial pneumonia

Rare idiopathic interstitial pneumonias
- Idiopathic lymphoid interstitial pneumonia
- Idiopathic pleuroparenchymal fibroelastosis

Unclassifiable idiopathic interstitial pneumonias
Ref: 1) Travis WD et al. Am J Respir Crit Care Med 188: 733-748, 2013.
2) American Thoracic Society. Am J Respir Crit Care Med 165: 277-304, 2002.

Table 4. Histopathologic diagnostic criteria for eosinophilic pneumonia
The pathologic diagnosis of eosinophilic pneumonia (EP) is based upon the confirmation of the following three items :
(1) Existence of significant infiltration of eosinophils in the lung tissue (The focal cellularity of eosinophils should exceed the level of eosinophils that can be noted in cases of IPF/UIP).
(2) No foci of fibrotic lesions with loss of normal alveolar structures in the lesion of eosinophilic pneumonia (EP). (Preceding incidental fibrotic lesions can be observed in cases of EP.)
(3) Exclusion of previously described diseases (e.g. infections, granulomatosis with polyangiitis (GPA)(Wegener's), neoplasm, lymphoma, leukemia)
Ref: 1) Kitaichi M. Korean J Allergy 17: 449-463, 1997.

Table 5. Histopathologic criteria for the diagnosis of fibrosing organizing pneumonia (FOP)
1) Intraluminal organizing fibrosis in distal air spaces (bronchioles, alveolar ducts, and alveoli)
2) Patchy distribution
3) Preservation of lung architecture without honeycombing, even in areas of extensive obliterative alveolar duct fibrosis
4) Uniform temporal appearance
5) Mild interstitial chronic inflammation
6) Obliterative alveolar duct fibrosis with adhesions of alveolar duct walls due to the presence of air-space granulation tissues
Ref: Kobayashi T, Kitaichi M et al. Internal Medicine 56: 1185-1191, 2017.

Table 6. Histologic features of pulmonary alveolar proteinosis (PAP)
<1> The patient has bilateral lung disease showing the key histologic features for PAP:
(1) Terminal air spaces are filled with weakly eosinophilic microgranular materials measuring 0.2 microns in association with more eosinophilic macrogranular materials measuring several decades microns and lipid clefts measuring several microns in width.
(2) Intralveolar microgranular materials are positive for PAS stain (purple red to red).
(3) Intraalvelar microgranular materials are positive for surfactant apoprotein A (SpA) by an immunostain
<2> Possible histologic associations with PAP:
(1) Intralveolar aggregation of large foamy cells that may show cytoplasmic degeneration
(2) Interstitial infiltration of lymphoid cells: minimal to mild
(3) Interstitial fibrosis: May be present in the chronic stage
<3> Pertinent negative findings for PAP:
(1) Neoplastic lesion, (2) Granulomatous lesion, (3) Infiltration of neutrophils and eosinophils, (4) Necrosis, (5) Congestion of alveolar walls, (6) Fibrination, (7) Deposition of carbon pigments and birefringent materials
Note: For the histopathologic diagnosis of PAP, the finding of <1>(1) is most important.
Ref: 1) Kitaichi M et al. Jpn J Chest Dis 75: 1245-1253, 2017 (in Japanese with English abstract)

Take Home Points: Interstitial Lung Disease (ILD): Pathologic diagnosis of ILD as a part of multidisciplinary diagnosis in relation to prognosis

Masanori Kitaichi, MD, PhD.
Department of Pathology, National Hospital Organization Minami Wakayama Medical Center, Tanabe City, Wakayama Prefecture, Japan. E-mail: <kitaichi@mwn.hosp.go.jp>

Pathologic diagnosis of diffuse infiltrative lung disease underwent remarkable changes and progression1-93). It is now outdated if one makes only a histopathologic diagnosis of UIP pattern, NSIP pattern etc using the 2002 ATS/ERS international multidisciplinary consensus classification. The pattern recognition described in the 2002 ATS/ERS classification should be used from the view points to know the disease condition in each patient34,35,39,47,62). Each patient is not known whether the patient belongs to the category of IIP, interstitial pneumonia with autoimmune features (IPAF), connective tissue disease or chronic HP. Histopathologic diagnosis in the field of interstitial lung disease is requested to make a diagnosis not only the pattern recognition of fibrosis but also adequate suggestion of disease condition in relation to prognosis.

Lung Cancer

J. M. Goo; Seoul/KR

Body: There is a close relationship between pathology, CT, and prognosis of lung adenocarcinoma manifesting as subsolid nodules. Increase of GGO on CT correlates with the increase of lepidic component on histology and these lesions show excellent prognosis. In comparison, the increase of solid component means the increase of solid component on histology and these lesions have worse prognosis. The presence of GGO typically represent AAH, AIS, minimally invasive adenocarcinoma or lepidic predominant adenocarcinoma. In the 8th edition of TNM staging, T descriptor is determined by the size of invasive component histologically, and likewise clinical T stage should be determined by the solid component size in subsolid nodules.
Visceral pleural invasion (VPI) is an adverse prognostic factor in patients with NSCLC and the pleural involvement is probably associated with a greater risk of dissemination due to subpleural lymphatics. When peripheral pulmonary adenocarcinomas manifesting as subsolid nodules were evaluated, pleural contact, pleural thickening, solid proportion greater than 50%, and nodule size greater than 20 mm were significant predictive CT features. The pleural tag, especially when there are one or more linear pleural tag with soft tissue component at the pleural end, can be a sign of VPI.
The presence of EGFR mutation is an important prognostic factor for predicting the response to EGFR tyrosine kinase inhibitors. Presence and proportion of GGO in lung adenocarcinomas is significantly related with EGFR mutations.
Take Home Points: Solid component of subsolid nodules and invasive component of adenocarcinoma have a close relationship. Potential of VPI in lung adenocarcinoma should be assessed based on CT features. GGO in subsolid nodule has a close relationship with lepidic component and EGFR mutations in lung adenocarcinoma.

Utility of cardiac MRI for Cardiac Sarcoidosis in comparison with PET

N. Oyama-Manabe; Sapporo/JP

Body: Sarcoidosis is a multisystem granulomatous disease of uncertain etiology. Since cardiac sarcoidosis (CS) may cause sudden cardiac death and be a potentially life-threatening disease, the accurate diagnosis is important in patients with sarcoidosis. The Japanese Ministry of Health and Welfare criteria is the most commonly used and the Heart Rhythm Society ,s Expert Consensus Statement is recently published for the diagnosis of CS.
I will review MR and PET/CT image characteristics of CS, with regard to quantitative aspects of disease severity. MRI and FDG PET/CT fulfill the important role on of the non-invasive diagnosing methods.
Cardiac MRI with late gadolinium enhancement (LGE-MRI) is a useful diagnostic tool to detect myocardial involvement. In contrast to FDG PET/CT, MRI does not require special preparation. LGE-MRI enables to estimate the extent of CS quantitatively.
FDG PET/CT also plays an important role in the detection of active inflammatory lesions. However, physiological FDG uptake due to inappropriate pretest preparations such as a shorter fasting period, carbohydrate intake prior the scan or individual metabolic status could disturb an accurate imaging interpretation. For the precise evaluation of the extent and severity of CS, recent studies have focused on reducing physiological myocardial FDG uptake as a preparation before examination. Not only the visual analysis but also the quantification of the intensity and volume of FDG uptake are helpful to predict the clinical outcomes and evaluate the efficiency of steroid treatment.
The quantitative assessment of extent and severity with FDG PET/CT and LGE-MRI has significant implications for disease progression and monitoring treatment response in CS.
Take Home Points: Review specific image findings and distribution of cardiac sarcoidosis (CS) with cardiac MRI and PET/CT. Describe the role of cardiac MRI and PET/CT in evaluation of suspected CS for initial diagnosis and during follow-up after treatment.

Value of T1 mapping in DCM - Con

J. I. Jung; Seoul/KR

Body: Myocardial T1 mapping is emerging tool for myocardial tissue characterization. Native T1 and myocardial ECV have been validated as robust biomarkers in numerous cardiac pathologies including dilated cardiomyopathy (DCMP).
Recently there are several reports that myocardial T1 mapping is useful for cardiomyopathy; T1 value has prognostic significance in non-ischemic cardiomyopathy [1] and myocardial T1 in DCMP correlates well with myocardial fibrosis on histopathology [2].
Myocardial T1 mapping seems to be the right way to explore myocardial interstitial fibrosis and remodeling in cardiomyopathy. However, T1 mapping has numerous MRI-dependent and methodological factors that can influence the final T1 values [3]. The field strength and sequence were two of these factors. More research towards understanding the effect on accuracy, precision, and reproducibility of T1 mapping is needed [4, 5].
This presentation includes several limitations and potential pitfalls of myocardial T1 mapping to apply clinical practice and uncertainties to be resolved through ongoing researches.

References
1. Puntmann VO, Carr-White G, Jabbour A, Yu C-Y, Gebker R, Kelle S, et al. T1-Mapping and Outcome in Nonischemic Cardiomyopathy: All-Cause Mortality and Heart Failure. JACC: Cardiovascular Imaging. 2016;9(1):40-50.
2. Nakamori S, Dohi K, Ishida M, Goto Y, Imanaka Yoshida K, Omori T, et al. Native T1 Mapping and Extracellular Volume Mapping for the Assessment of Diffuse Myocardial Fibrosis in Dilated Cardiomyopathy. JACC Cardiovascular Imaging. 2018;11(1):48-59.
3. Piechnik SK, Jerosch-Herold M. Myocardial T1 mapping and extracellular volume quantification: an overview of technical and biological confounders. The International Journal of Cardiovascular Imaging. 2018;34(1):3-14.
4. van den Boomen M, Slart R, Hulleman EV, Dierckx R, Velthuis BK, van der Harst P, et al. Native T1 reference values for nonischemic cardiomyopathies and populations with increased cardiovascular risk: A systematic review and meta-analysis. J Magn Reson Imaging. 2017.
5. Kellman P, Hansen MS. T1-mapping in the heart: accuracy and precision. Journal of Cardiovascular Magnetic Resonance. 2014;16(1):2.

Take Home Points: Understand the technical aspects of T1-mapping methods and image protocols Understand the limitation of T1-mapping methods to apply the clinical practice

Is hyperpolarized Xenon the future of pulmonary imaging?

F. Gleeson; Oxford/UK

Body: Magnetic resonance imaging using hyperpolarised xenon gas (HP ^{129}Xe-MRI) provides a unique strategy for evaluating regional lung function by permitting direct visualisation of the lung airspaces. The inherent properties of xenon gas (^{129}Xe) may be exploited to regionally quantify ventilation and diffusion within the lung and provide comprehensive in vivo assessment of lung function.

The pioneering techniques developed to characterise global lung function using hyperpolarised ^{3}He MRI (HP ^{3}He-MRI) have been translated to HP ^{129}Xe-MRI. Ventilation imaging with HP ^{3}He-MRI has shown utility in detection of functional abnormalities in a range of obstructive lung pathologies e.g. chronic obstructive pulmonary disease (COPD), cystic fibrosis (CF), asthma and bronchiolitis obliterans.

High resolution imaging of pulmonary ventilation is also possible with HP ^{129}Xe-MRI. With wider availability and lower cost than ^{3}He, ^{129}Xe- MRI is a more clinically viable alternative and studies have compared ventilation image quality for the two gases. HP ^{129}Xe-MR diffusion-weighted imaging has also shown utility in the assessment of lung microstructure, with elevated whole lung mean apparent diffusion co-efficient (ADC) values present in COPD subjects corresponding to emphysematous tissue destruction.

Accurate lobar quantification of HP ^{129}Xe-MRI is particularly relevant to the field of respiratory medicine with emerging regional treatments not adequately assessed by standard whole lung methods. These HP ^{129}Xe-MRI lobar analyses offer the potential for improved description of COPD regional functional heterogeneity and assessment for regional treatments such as LVRS or endobronchial valve placement. HP ^{129}Xe-MRI exposes the patient to no radiation in comparison to CT, and may also be performed repeatedly, potentially immediately after an intervention to determine its efficacy. This may allow early treatment modifications or allow clinicians to inform patients of the likely success of their intervention.

Time-resolved breath-hold HP ^{129}Xe-MR ventilation imaging may also be used to demonstrate and quantify delayed ventilation in patients being assessed for Lung Volume Reduction Therapies.

HPX spectroscopy techniques have been reported to be capable of capturing the gas exchange dynamics between the alveolar air spaces, pulmonary tissues and capillaries separately and simultaneously due to the solubility and chemical shift of ^{129}Xe in the lung. The dynamics of ^{129}Xe gas signal (i.e. T2*) in the alveolae has been shown to be significantly different from the dissolved phase ^{129}Xe signal in the pulmonary tissue and plasma (PTP), and the red blood cell (RBC) compartments of the lungs, thus allowing all three signals to be both simultaneously detected and separately distinguished, and has also been reported to be capable of capturing the gas exchange dynamics between the alveolar air spaces, pulmonary tissues and capillaries separately and simultaneously due to the solubility and chemical shift of ^{129}Xe in the lung.

This presentation will discuss the current use and potential uses of HP ^{129}Xe-MR imaging.

Take Home Points:

- HP ^{129}Xe-MR is a new and potentially valuable imaging technique
- HP ^{129}Xe-MR does not involve ionising radiation, and appears safe and repeatable
- HP ^{129}Xe-MR may demonstrate lung structure and function at a whole lung and lobar level

Practical application to guide therapy and predict outcome

J. Bremerich; Basel/CH

Body: Purpose: Parametric tissue characterisation is a unique feature of cardiac MRI. Today, a variety of quantification sequences are available as clinical tools. This presentation shall illustrate clinical applications of T1- and T2-mapping.
Methods and Results: Late Gadolinium enhanced MRI (LGE-MRI) opened the door towards scar imaging. Meanwhile, more refined tools such as T1- and T2-mapping became available. The combination of pre- and postcontrast T1-mapping might even be used to calculate extracellular volume (ECV), when hematocrit is measured from blood samples. Contrast enhanced T1-mapping enables assessment of structural changes such as in mild inflammation. ECV enables detection and quantification of fibrosis such as in treatment with cardiotoxic medication or infiltrative diseases such as amyloidosis. It should be emphasized, however, that normal T1-values may vary among sequences and magnets. This explains the requirement to establish normal values for every hardware and sequence system. Moreover, T1-times at 3 Tesla are typically longer than at 1.5 Tesla. T2-mapping helps to identify tissue edema as an unspecific imaging marker of myocardial injury. Moreover, T2*-mapping is used to measure iron overload of the heart in hemosiderosis or hematologic diseases.
Conclusion: Parametric myocardial tissue mapping has matured to a robust clinical tool to guide therapy and predict outcome.
Take Home Points: Parametric tissue mapping has matured to clinical tool.
Normal values for T1 need to be definded for every scanner and sequence.

ORAL CHEST

Contrast agent accumulation patterns in fibrosing lung disease using 5D MRI

M. T. A. Wetscherek[1], A. Wetscherek[2], C. P. Heussel[2], M. Kreuter[2], J. Dinkel[3]; [1]Cambridge/UK, [2]Heidelberg/DE, [3]Munich/DE

Purpose/Objectives: We aim to analyze contrast agent accumulation patterns of fibrotic lesions in interstitial lung disease at different severity levels using a radial gradient echo sequence in free-breathing.
Methods and Materials: 24 consecutive patients with pulmonary fibrosis were prospectively included in the study and underwent thoracic thin-section CT and 1.5T MRI of the lung. The final analysis comprised 20 cases (mean age: 71 years; male:female, 13:7) with a diagnosis of idiopathic pulmonary fibrosis (IPF), n=12, and non-IPF, n=8. Contrast agent was administered to assess lung perfusion. Two minutes after contrast agent administration, a 3D encoded spoiled gradient echo sequence with radial stack-of-stars sampling and golden angle spacing was acquired during 5 minutes of free breathing. Self-gating based on the k-space center magnitude was used to assign data into respiratory bins and the motion compensated-HDTV algorithm was applied to reconstruct images at different time points from the highly undersampled raw data. Reference images and regions of interest (ROI) were defined and classified at thin-section CT and on MRI perfusion maps as showing severe or non-severe disease. A total of 200 ROI measurements were performed on the radial-VIBE reconstructions, including 10 ROI from each patient. The contrast agent accumulation for each specific fibrotic lesion was described by evaluating the intensity change at different time steps.
Results: In severe, as well as in non-severe disease, there is later peak enhancement and higher accumulation rate in IPF compared to non-IPF, $p<0.01$. In non-IPF, fibrotic lesions have fast time to peak and slow accumulation rate; however, the more severe lesions had longer time to peak and slower washout rate as compared to non-severe ones, $p<0.05$. In IPF, fibrotic lesions have late peak enhancement and slow accumulation rate, at both severity levels. Continuous contrast agent accumulation, without wash-out, was found only in patients with IPF. 22% of the lesions demonstrated plateau signal intensity, with a rate of signal intensity change between [-0.6 – (0.8)] %/minute.
Conclusion: The timing of contrast agent accumulation is influenced by the type and severity of fibrosis. The results might prove useful for a more thorough characterization of lung fibrosis burden, of special interest being the regional blood flow in the context of new antifibrotic treatment available and possible relationship with drugs' pharmacokinetics. Nevertheless, this may be achieved using a non-invasive, non-irradiating, free-breathing method.

Multicentre Standardisation of Chest MRI as Radiation-Free Outcome Measure of Lung Disease in Young Children with Cystic Fibrosis

M. O. Wielpütz[1], M. Stahl[1], L. Nährlich[2], M. V. Kopp[3], M. Buchholz[3], B. Tümmler[4], J. Vogel-Claussen4, H.-U. Kauczor[1], M. Mall[1]; [1]Heidelberg/DE, [2]Gießen/DE, [3]Lübeck/DE, [4]Hanover/DE

Purpose/Objectives: A recent single-centre study demonstrated that MRI is sensitive to detect early abnormalities in the lung and response to therapy in infants and preschool children with cystic fibrosis (CF) supporting MRI as an outcome measure of early CF lung disease. However, the feasibility of multicentre standardisation remains unknown. The objective was to determine the feasibility of multicentre standardisation of chest MRI in infants and preschool children with CF.
Methods and Materials: A standardised chest 1.5T MRI protocol was implemented across four specialised CF centres. Following training and initiation visits, 43 infants and preschool children (mean age 3.1±1.5y, range 0-6y) with CF underwent MRI. Image quality and lung abnormalities were assessed using a standardised questionnaire and an established CF MRI score.
Results: MRI was successfully performed with diagnostic quality in all patients (100%). Incomplete lung coverage was observed in 6% and artefacts also in 6% of sequence acquisitions, but these were compensated by remaining sequences in all patients. The range of the MRI score in CF patients was similar across centres with a mean global MRI score of 13.4±5.7.
Conclusion: Our results demonstrate that multicentre standardisation of chest MRI is feasible and support its use as radiation-free outcome measure of lung disease in infants and preschool children with CF.

Comparison of RECIST, iRECIST and PERCIST for evaluation of response to PD1-blockage therapy in patients with non-small lung cancer

L. Beer, M. Hochmair, T. Füreder, A. Haug, D. Kifjak, B. K. Schwabel, C. J. Herold, H. Prosch; Vienna/AT

Purpose/Objectives: The aim of this study was to compare the Response Evaluation Criteria in Solid Tumor (RECIST) 1.1, the immune RECIST (iRECIST) criteria and the Positron Emission Tomography Response Criteria in Solid Tumors (PERCIST) 1.0 for the assessment of response evaluation in patients with advanced non-small cell lung cancer (NSCLC) treated with PD-1 inhibitors.
Methods and Materials: This single center prospective study of 52 patients treated with a PD-1 inhibitor was approved by our institutional review board. All patients gave written informed consent. ^{18}F-FDG PET/CT was used to assess tumor burden dynamics before and after treatment initiation. Immunotherapeutic responses were evaluated according to the RECIST 1.1, iRECIST and PERCIST 1.0. Cohen's κ coefficient and Wilcoxon´s signed-rank test were used to evaluate concordance among these criteria. Progression-free survival (PFS) and overall survival (OS) was assessed using the Kaplan-Meier test.

Results: Thirty-two patients (mean age 60 years; range 38-81 years) had at least one follow-up examination. RECIST 1.1 and PERCIST 1.0 response classification were discordant in 18 patients (56.2%; κ= 0.199). RECIST 1.1 and iRECIST were discordant in only two patients who evidenced a pseudoprogression after treatment initiation that was classified as progressive disease (PD) or immune unconfirmed PD, respectively followed by a partial response (PR). According to PERCIST 1.0, both patients had a stable metabolic disease (SMD). Patients with a partial remission according to RECIST 1.1 had a significantly longer PFS (p=0.02) than patients with PD but not significantly longer than patients with stable disease (Fig. 1A). In contrast, patients with a partial metabolic response (PMR) according to PERCIST 1.0 had a significantly longer PFS than patients with SMD and progressive metabolic disease (PDM) (Fig. 1B). OS was significantly longer in patients with PR or PMR compared to PD or PMD, respectively (p<0.05) (Fig 1C, D).

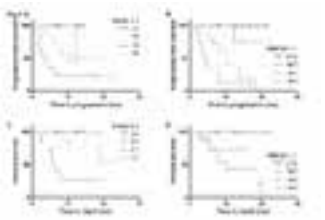

Figure 1

Conclusion: PERCIST 1.0 criteria are more sensitive than RECIST 1.1 or iRECIST for the detection of treatment response to checkpoint inhibitors in patients with advanced NSCLC. In the rare cases of pseudoprogression metabolic tumor activity may help to correctly classify treatment response.

Capability of 3D Computer-Aided Volumetry (CADv) with Pulmonary Nodule Component Evaluation for Quantitative Prediction of Malignancy on Thin-Section CT

Y. Ohno[1], A. Yaguchi[2], K. Aoyagi[3], S. Kaminaga[3], Y. Kishida[1], S. Seki[1], T. Yoshikawa[1]; [1]Kobe/JP, [2]Kawasaki/JP, [3]Otawara/JP

Purpose/Objectives: To evaluate the quantitative capability of newly developed 3D computer-aided volumetry (CADv) with pulmonary nodule component assessment for predicting malignancy and postoperative recurrence on thin-section CT.
Methods and Materials: 59 consecutive patients with 101 pulmonary nodulesÐunderwent repeated thin-section CT at 320-detector row CT scanner (Aquilion ONE, Canon Medical Systems Corporation, Otawara, Japan), pathological examination, surgical resection and/ or follow-up examination. Then, all nodules were divided into malignant (n=64) and benign (n=37) nodule groups. In addition, all patients with operated as malignancy were also divided into postoperative recurrence (n=12) and non-recurrence (n=53) groups. In this study, CADv automatically assessed solid, ground-glass opacity, cavity and total nodule volumes from two serial CT data. Then, total volume change per day (TV/day), solid to total volume change ratio per day (S/T ratio/day) and doubling time (DT) were determined. Student's t-test was performed to compare all indexes between malignant and benign groups, and between recurrence and non-recurrence groups. Then, ROC analyses were performed to compare differentiation capabilities of indexes as having significant differences between malignant and benign groups, and between recurrence and non-recurrence groups. Finally, each diagnostic performance was compared by McNemar's test.
Results: TV/day and DT had significant differences between malignant and benign nodule groups (p<0.05), although TV/day and S/T ratio/day had significant difference between recurrence and non-recurrence groups (p<0.05). On distinguishing malignant from benign groups, area under the curves (Azs) of TV/day (Az=0.94) was significantly larger than that of DT (Az=0.62, p<0.001). In addition, specificity (SP) and accuracy (AC) of TV/day were significantly higher than those of DT (p<0.001). For distinguishing recurrence from non-recurrence groups, Az of S/T ratio/day (Az=0.92) was significantly larger than that of TV/day (Az=0.68, p=0.006). Moreover, SP and AC of S/T ratio/day were significantly higher than those of TV/day (p<0.001).
Conclusion: Newly developed 3D CADv system has quantitative capability for prediction of malignancy and postoperative recurrence on thin-section CT.

Increasing the conspicuity of breast cancer by using dual-energy spectral computed tomography: Initial experience

Y. Metin[1], N. O. Metin[1], O. Ozdemir[1], S. Kul[2]; [1]Rize/TR, [2]Trebizond/TR

Purpose/Objectives: To determine the feasibility of dual-energy spectral computed tomography (DESCT) in breast cancer imaging and to find out the optimal virtual monochromatic energy level for improving the conspicuity of breast cancer.
Methods and Materials: A total of 29 patients (mean age 53; age ranged from 30 to 83 years) with pathologically proven 39 malignant breast lesions were recruited to undergo monophasic (delayed phase) contrast-enhanced DESCT imaging for investigating the presence of metastasis to lung. The conventional polychromatic and virtual monochromatic image (VMI) sets at photon energies from 40 to 140 keV along with iodine-based material-decomposition images were reconstructed for analysis. The iodine enhancement (in HU) and iodine content (in mg/ml) of malignant breast lesions, normal fibroglanduler tissue and pectoral muscle were measured on VMI and the iodine-based material-decomposition images. Two independent readers qualitatively scored lesion conspicuity at energy levels of 40, 60, 80, 100 keV. Contrast-to-noise ratios (CNR) were also calculated for comparison.
Results: Mean tumor size was 20.2±10.0 mm (ranged from 8 mm to 53 mm). The qualitative score of the lesion conspicuity was peaked at 40-keV series for both readers and significantly higher than those at other energy levels (all p<0.05). Compared with other energy levels, lesion iodine enhancement was highest for 40-keV VMI reconstructions (p<0.05). The highest contrast-to-noise ratio value was obtained at 60 keV, which was superior to 40-, 80- and 100 keV series (all p<0.05). The iodine content of malignant breast lesions was significantly higher than those of normal fibroglanduler tissue and pectoral muscle (p<0.05).

Conclusion: The conspicuity of breast cancers increases in monochromatic images of DESCT taken at low energy levels. Quantitative iodine enhancement and content measurements may be used to differentiate breast cancers from normal fibroglanduler tissue.

A computed tomography study of in-vivo growth behaviour in 60 non-screen detected lung cancers

O. Mets[1], K. Chung[2], P. Zanen[1], E. Scholten[2], W. B. Veldhuis[1], B. van Ginneken[2], M. M. Prokop[2], C. M. Schaefer-Prokop[3], P. A. de Jong[1]; [1]Utrecht/NL, [2]Nijmegen/NL, [3]Amersfoort/NL

Purpose/Objectives: Pulmonary nodules are a frequent finding on chest imaging, and the use of CT increased tremendously over the last decades; it is estimated that in about 1.5 million US adults a nodule is identified each year. Recommendations for follow-up have been developed to uniform management for lesions that may represent lung cancer. Current management guidelines are based on nodule volume doubling time (VDT), which assumes exponential growth behavior. However, in-vivo growth in lung cancers has been investigated only in a few lung cancer screening-based studies, yielding contrary results. Moreover, the theory has never been validated in the guidelines target population of routine-care patients. Therefore, this study evaluates growth patterns of untreated solid and subsolid lung cancers of various histology in a non-screening setting.
Methods and Materials: All subjects >40 years of age that underwent CT of the chest between 2004 and 2012 in two university centers were retrospectively collected. No selection based on imaging indication or in-/outpatient status was made. We selected pathology proven lung cancers that were imaged at least three times before diagnosis (N=60). Growth behaviour was analysed using dedicated lung nodule software. Random intercept random slope mixed models analysis was applied to test which growth behaviour most accurately described lung cancer growth, testing both exponential and various other growth patterns. Individual growth curves were plotted per pathology subgroup and nodule type.
Results: Our study confirms that in-vivo growth in lung cancers is best explained by an exponential model and is uniform between subsolid and solid lesions. We further showed that subsolid lesions are generally larger than solid lesions at baseline, but progress slower over time. Baseline lesion volume was not related to growth, indicating that smaller lesions do not growth slower compared to larger ones.
Conclusion: By showing that lung cancer conforms to exponential growth we provide the first experimental basis in routine-care setting. This supports the assumption made in the generally used volume doubling time analysis.

Evaluation, comparison and optimization of the effects of manual versus software automated protocols on radiation dose and image quality in paediatric chest computed tomography

G. Argentieri[1], C. Soldati[1], C. Puligheddu[2], L. Bellesi[2], M. Merli[1], S. Presilla[2], F. Del Grande[1]; [1]Lugano/CH, [2]Bellinzona/CH

Purpose/Objectives: The aim of this study was to retrospectively compare the effects of switching from automated to manual acquisition parameters on image quality and radiation dose in a small paediatric cohort of patients and in several simulated paediatric chest CT scans utilizing a phantom.
Methods and Materials: The study took place in a non-paediatric medical center from Jan. 2016 to Dec. 2017 and included seven paediatric patients (mean age 6 y.o., range 4-11y.o.) who underwent CT scans of the thorax.
To obtain the lowest possible dose-length-product (DLP) value while maintaining an adequate image quality, the scans were performed by manually reducing the dose below the lowest dose value proposed by automated software prior to the exam. The images obtained were found to be diagnostic.
A CATPHAN phantom underwent multiple simulated paediatric chest CT acquisitions with the same 128 slice scanner (Siemens Somatom Definition FLASH) in both standard and high pitch modes. CARE Dose4D and CARE kV algorithms were also adjusted.
Both automated and manual CT acquisitions were obtained with protocols utilizing various values for kV, mAs and pitch.
SAFIRE iterative reconstruction was always unchanged and fixed on level 3 (max 5).
Qualitative and quantitative image characteristics obtained from the phantom study were evaluated independently by three experienced thoracic radiologists.
Computed tomography dose index (CTDIvol) and DLP values were collected and analysed with dedicated software.
Equivalent dose to organ at risk (OAR) was assessed with the Montecarlo system using a digital phantom simulating a six year old paediatric patient.

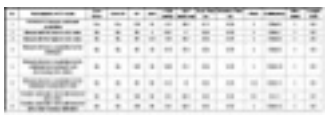

Details about CT acquisitions.

Results: Dose to OAR, CTDIvol and DLP were significantly lower (90%,58% and 32% respectively) by using manual settings, while maintaining a good perceived image quality as assessed by visual scoring test.
Linearity and resolution remained quite constant while image noise (mean -6.4, standard deviation 10.1) and uniformity (mean -6.4, standard deviation 10.1) varied between scans as observed by visual score analysis (VSA).

Dose to organs of interest (mSv).

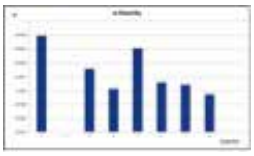

Linearity of the CT numbers: linked to the response of the tomograph with respect to the „density" of the objects, made up of various materials, in the phantom. Acquisition 2 can't be evaluated by the software.

Noise values.

Conclusion: In both real and simulated paediatric chest CT studies manual acquisition settings generated the best results in terms of optimal dose-image quality ratio compared to automated parameters.

Radiomics allows classification of lung nodules as benign or malignant (adenocarcinoma and squamous cell carcinoma). A study based on the NLST data set

S. P. Martin, J. Hofmeister, S. Burgermeister, J. Gariani, G. Feutry, W. Karenovics, P. Gasche-Soccal, C. D. Becker, X. Montet; Geneva/CH

Purpose/Objectives: To investigate the added value of radiomics applied on the National Lung Screening Trial (NLST) dataset in predicting solitary pulmonary nodule etiology (benign – adenocarcinoma – squamous cell carcinoma).
Methods and Materials: Lung adenocarcinoma (n=227) and squamous cell carcinoma (n=94) with a long axis greater than 8 mm obtained from the NLST dataset were included and matched with benign lung nodules (n=299). Feature extraction (n=124671) was performed using an open-source python package after semi-automatic segmentation of the 620 lung nodules from low-dose unenhanced computer tomography (CT) scans. Nodule classification based on radiomics and clinical data was achieved via feature selection, dimension reduction (using principal component analysis), and classification (using a support vector machine classifier). As a secondary endpoint the demographic data was also evaluated solely according to the PanCan model. The diagnostic performance of the 3-subtype classification was compared on the basis of their area under the receiver operating characteristic curve (AUC).
Results: Radiomics model (benign vs malignant): AUC: 0.983. PanCan model (benign vs malignant): AUC: 0.797. Radiomics model (adenocarcinoma vs squamous cell carcinoma): AUC: 0.686.
Conclusion: Artificial intelligence and data mining in chest CT raise the diagnostic confidence higher than any other model in the field of non-invasive lung nodule characterization.

Comparison of image quality in high pitch free breathing versus standard pitch breath-holding CTPA

K. O. Ombati, S. Vinayak, K. Were; Nairobi/KE

Purpose/Objectives: To compare image quality when using high pitch free breathing versus standard pitch breath-holding Computed Tomographic Pulmonary Angiography (CTPA) using a dual source scanner.
Methods and Materials: This was a randomised control trial whereby patients referred for CTPA were randomly selected into two arms: Arm A imaged using a pitch of 1.2 with breath-holding instructions while those in arm B underwent the examination using a pitch of 3.2 with quiet free breathing. Both arms were imaged using the same dual source scanner (Somatom Definition Flash, Siemens Healthcare, Forchheim, Germany). Two blinded reviewers subjectively assessed the image quality while a single blinded reviewer recorded objective image parameters. The primary endpoint was to demonstrate non-inferiority of high pitch free breathing CTPA.
Excel 9.0 and statistical software (SPSS 22.0) were used for analysis. Continuous variables were expressed as mean ± SD. Categorical variables were expressed as frequency (percentage). Chi-square test was performed to assess statistically significant differences between categorical variables and t test for continuous variables. P-values of ±0.05 were considered statistically significant. The two-sided 95% CI of the mean outcome difference between the two groups, which was used for non-inferiority testing, was calculated from the study data. Agreement between the two readers was expressed in terms of kappa statistics and proportional agreement.
Results: A total of 112 patients were randomly selected into the two arms of the study. PE was present in 20/112 patient's (20%). The patients in the standard pitch group received a higher mean DLP compared to those in the high pitch group (P< 0.001). There was no statistically significant difference in the mean main pulmonary artery attenuation between the two groups (P=0.215). There was no significant difference in the qualitative analysis of the images in the two arms. Inter reader agreement for the subjective measurements ranged from moderate to almost perfect agreement between the 2 independent readers.
Conclusion: Main pulmonary artery contrast opacification in high pitch CTPA is non-inferior to standard pitch CTPA using a dual source scanner. The high pitch method can be used on all patients with no compromising in the image quality and ability to detect pulmonary emboli with an added advantage of reduction in the radiation dose.

Is there correlation between radiological and microbiological criteria to diagnose invasive pulmonary aspergillosis?

I. Pulzato, S. Mennella, G. Cittadini, E. Zoppolo, M. Mikulska; Genoa/IT

Purpose/Objectives: Evaluate the correlation between radiological findings and microbiological data in neutropenic patients with invasive pulmonary aspergillosis (IPA).
Methods and Materials: We retrospectively enrolled 127 patients which underwent hematopoietic stem cell transplantation (HSCT) between January 2010 and June 2017 at San Martino Hospital in Genoa. All these patients after HSCT had either clinical or laboratory serological suspicion of IPA and a CT scan within 48 hours. Early CT findings were reviewed by one radiologist blinded to the clinical and microbiological data. The radiologist classified patients according European Organization for Research and Treatment of Cancer and the Mycosis Study Group (EORTC-MSG) criteria for the diagnosis of IPA. We compared radiological results with the Bronchoalveolar lavage (BAL) galactomannan (GM) assay performed with an optical density (OD) index cut off of 0.5.
Results: 56 patients (44%) were classified as positive for IPA according to EORTC-MSG radiological criteria; among these 44 (79%) exhibited a GM-BAL positive assay result while 12 (21%) were negative. Among these 56 patients 39 (69%) were evaluated as meeting the criteria due to clinical conditions (fever and dyspnoea) while 17 (30%) were clinically negative. 30 (53%) patients were positive both on clinical and microbiological analysis. The group IPA positive according to the radiological criteria had more frequent positive GM-BAL tests and clinical evaluation with a significant statistical difference ($p<0.001$).
Conclusion: Although EORCT-MSG criteria are definitions of IPA to be used for clinical and epidemiological research, they contribute consistently to the nonculture-based diagnosis of IPA and could be used in daily clinical practice to start therapy.

Quantification of pleural plaques by computed tomography and correlations with pulmonary function: Preliminary study

J. S. Kim, Y. K. Cha; Goyang-si/KR

Purpose/Objectives: The aims of this study were to quantify pleural plaque volumes by computed tomography (CT) and investigate relations between pleural plaque volume and pulmonary function after excluding other factors that might affect pulmonary function.
Methods and Materials: Twenty-six subjects with pleural plaques and pulmonary function test (PFT) results among 1544 subjects that registered with the Korea Environment Corporation for asbestos damage relief from January 2011 to December 2015 were included. Subjects with CT evidence of lung diseases and/or previous surgery were excluded. Pleural plaque volumes (PPVs) were measured by tracing the outlines of all pleural plaques on CT images. Patients were allocated to three groups by PPV, as follows, < 10 ml, 10 ~ 20 ml, or ≥ 20 ml, and the PFT results of these groups were analyzed and compared. Simple linear regression analysis and multiple regression analysis were used to evaluate correlations between PPV and PFT variables.
Results: No significant relationship was found between total PPV and pulmonary function indices or between PPV groups and PFT results ($p > 0.05$). However, forced expiratory volume in 1 second (FEV1), forced vital capacity (FVC), and diffusing capacity of the lung for carbon monoxide (DLCO) values in the higher PPV group (≥ 20 ml) tended to be lower, indicating a restrictive pattern of pulmonary function.
Conclusion: We quantified pleural plaque volume on CT and found out higher pleural plaque volume tended to exhibit a restrictive pattern. However, pleural plaques alone were not found to be significantly associated with pulmonary function.

Clinical performance and confidence of ultra-low dose computed tomography compared to chest X-ray investigations for diagnosing pulmonary pathology

L. Kroft, L. van der Velden, I. Hernandez Giron, J. J. Roelofs, A. de Roos, J. Geleijns; Leiden/NL

Purpose/Objectives: Ultra-low dose CT (ULDCT) of the chest allows for 3D diagnostic imaging with a radiation exposure of the patient that is in the same range of a conventional 2D chest X-ray (CXR) examination. The purpose of the study was to assess the clinical diagnostic performance and confidence of ULDCT as compared to CXR examinations for diagnosing pulmonary pathology.
Methods and Materials: The study was approved by the Institutional Review Board and all patients gave written informed consent. 200 patients of 50 years of age or older were recruited. They were referred by outpatient clinics or general practitioners to the radiology department for a CXR examination and they underwent an additional ULDCT of the chest. A posteroanterior and lateral CXR examination was performed with a standard acquisition protocol (DelftDI, Triathlon DR, Oldelft-Benelux). An ULDCT examination was performed using a volumetric 320-detector row CT scanner (Aquilion ONE Genesis, Toshiba Medical Systems, Otawara, Japan), with CTDIvol=0.1mGy. Radiation dose was recorded for CXR (Dose-Area-Product) and ULDCT (Dose-Length-Product) and the effective dose was calculated. Images were transmitted to a PACS workstation for clinical evaluation. The radiological diagnosis and level of confidence for diagnosis was reported for each patient and each modality. Statistical analyses based on two-tailed t-tests were performed using SPSS for Windows (SPSS, Chicago, IL, USA).
Results: The effective dose was 0.040 ± 0.017 mSv for CXR and 0.071 ± 0.006 mSv for ULDCT. The clinical question was answered in 98% of the patients with CXR and in 100% with ULDCT ($p=0.045$). Relevant pathology was found in 33% of the patients with CXR and in 47% with ULDCT ($p<0.05$). Confidence for diagnosis was 88% ± 12% with CXR and 98% ± 2% with ULDCT ($p<0.05$).

Relevant diagnostic difference regarding presence of pathology was found in 69 out of 200 patients (35%, p<0.05), where ULDCT was reported as having higher confidence than CXR in 100% of the cases. There were no cases with CXR reported as having a higher confidence than ULDCT.
Conclusion: 3D chest imaging with ULDCT can be considered as a better alternative for 2D CXR imaging since ULDCT has better clinical performance and better diagnostic confidence than CXR whereas effective dose is comparable to CXR examination.

Digital Tomosynthesis and ground glass nodules: Optimization of acquisition protocol. A phantom study

E. Baratella, F. Arban, I. Campo, E. Serena, E. Quaia, M. A. Cova; Trieste/IT

Purpose/Objectives: To evaluate the capability of chest Digital Tomosynthesis (DTS) in detecting pulmonary ground glass nodules.
Methods and Materials: A male anthropomorphic chest phantom and simulated pulmonary ground glass nodules with different diameter (3-12 mm) were used. The nodules were positioned in 4 different areas (apex, hylum, marginocostal and paradiaphragm areas) then the phantom was scanned by DTS and MDCT; for each areas 7 different scans (n=35) were performed varying technical parameters: kV (105 – 125), mAs, Dose Rateo and copper filtration (0.2mm). The radiation dose were recorded and converted into effective dose.
Two radiologists were asked to evaluate in consensus both DTS and CT images and to provide a visual score: 4 for an unequivocal identifiable nodule; 3 for a good identifiable nodule; 2 for a poor identifiable nodule; 1 for no identifiable nodules.

Chest phantom N1 „LUNGMAN"

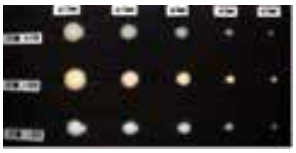

Fifteen synthetic nodules with spherical shape different in size and Hounsfield units (HU).

Results: Ground glass nodules located in the apex and in the basal region were better recognised (from score=2 to a score=3) with a Dose Rateo of 25. Ground glass nodules located in the hylar region were no visible even with an higher Dose Rateo. A progressive increasing in kVp (from 105 to 125) did not provides an increase in nodule visibility.

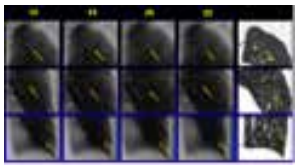

Pure ground glass nodules located in the apex and in the basal regions were better recognized (from a score 2 to a score 3) passing from a Dose Rateo of 10 to a Dose Rateo of 25

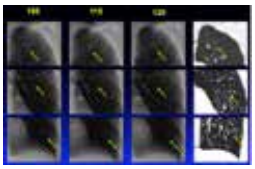

A progressive increase in kVp, from 105 to 125, did not show a significant difference in terms of pure ground glass nodule's conspicuity

Conclusion: DTS can identify pure ground glass nodules with a Dose Rateo of 25 and 105 kVp with a mean effective dose of 0,11-0,13 mSv.
Although CT has to be considered the gold standard to detect pure ground glass nodules, DTS can have a role in the follow-up in patients with known ground glass nodules, in particular for nodules with a diameter greater than 10 mm.

CT characteristics of lung adenocarcinomas with epidermal growth factor receptor mutation: A propensity score matching study

Y. J. Suh[1], H.-J. Lee[1], H. Kim[1], Y. T. Kim[1], Y. K. Jeon[1], Y. J. Kim[2], K.-G. Kim[2], E. S. Lee[1]; [1]Seoul/KR, [2]Incheon/KR

Purpose/Objectives: There have been controversies regarding the relationship between computed tomography (CT) imaging characteristics and epidermal growth factor receptor (EGFR) mutation in lung adenocarcinomas. We aimed to investigate correlation between CT characteristics and presence of EGFR mutation in a large Asian cohort who received surgical resection from invasive lung adenocarcinomas.
Methods and Materials: We retrospectively included 864 patients (524 with EGFR mutation and 340 with EGFR wild-type) who received surgical resections for invasive lung adenocarcinoma at our institution. After applying propensity score matching with covariates of sex, smoking and staging, 312 patients with EGFR mutation were matched with 312 patients with EGFR wild-type. CT characteristics were classified into four categories (pure ground-glass nodule [GGN], ground-glass opacity [GGO]-predominant part-solid nodule [PSN], solid-predominant PSN and pure solid nodule). For cases of PSN, computerized 3D segmentation of inner solid portion was performed using fuzzy C-means clustering algorithm, and volume and estimated diameter were calculated for total tumor and inner solid portion. CT characteristics, predominant histologic subtype, and CT measurement (volume and estimated diameter of total tumor and inner solid portion, and GGO proportion) were compared within matched pairs.
Results: After matching, tumors in EGFR mutation group showed higher proportion of pure GGN (4.1% vs 1.3%), GGO-predominant (23.7% vs 14.7%) and solid-predominant PSN (37.2% vs 31.7%) as CT characteristics than EGFR wild-type tumors, whereas EGFR wild-type tumors most predominantly presented as pure solid nodule (34.6% vs 52.2%, P<0.0001). EGFR mutation tumor had

more frequent lepidic predominant subtype than EGFR wild-type tumor (20.2% and 11.9%; P<0.0001). Based on CT measurements, EGFR mutation tumor showed smaller whole tumor size and solid portion than EGFR wild-type tumors (P<0.0001), and also higher proportion of GGO (P<0.0001). Among various types of EGFR mutation, exon 19 deletion and exon 21 missense had smaller tumor size and solid portion size with higher GGO proportion comparing with EGFR wild-type tumors (posthoc P<0.01) , whereas miscellaneous mutation did not show any significant difference compared with EGFR wild-type tumors (posthoc P>0.01).
Conclusion: Adenocarcinomas with EGFR mutation had higher GGO proportion than those with EGFR wild-type, both on visual interpretation of CT characteristics and quantitative CT image analysis, after matching of clinical variables. Especially, lesions with exon 21 mutation had higher GGO porportion than other types of mutation.

Discordance between radiological and clinical response in a cohort of patients treated with Nivolumab in second-line therapy

C. Moroni, D. Cozzi, M. Bartolucci, E. Cavigli, F. Giannelli, V. Scotti, M. Perna, V. Bonti, F. Mazzoni, V. Miele; Florence/IT

Purpose/Objectives: Nivolumab is a human IgG4 programmed cell death-1 immune check point inhibitor antibody that has been approved for second line treatment of stage IIIb/IV Non-Small Cell Lung Cancer (NSCLC). Patients which underwent Nivolumab treatment differ for gender, age, cancer histology and presence of mutations. Lesions treated with Nivolumab may show different radiological response during computed tomography (CT) follow up, sometimes inconsistent with the patient's clinical findings. The aim of this study is to evaluate the radiological response, based on iRECIST, and comparing it with patient's clinical response measured with Performance Status (PS) (ECOG criteria).
Methods and Materials: Between August 2015 and August 2017 we overall selected 75 patients with NSCLC stage IIIb/IV treated with Nivolumab. Their pre- and post-treatment CT scans were evaluated by two senior and two junior radiologists dedicated to thoracic imaging in order to define the radiological response; in case of discordant results, a definite response was obtained by general agreement. Clinical response was evaluated by radiotherapists and oncologists.
Results: 32 patients were excluded from this study because of the lack of inclusion criteria as absence of target lesions, relapsing lesions after radiotherapy, skeletal metastases. 43 patients were selected finally. Radiological response was defined as: complete response (CR), partial response (PR), stable disease (SD) and progression disease (PD) according to iRECIST criteria. We finally divided patients in Responders (CR+PR+SD) and Non-Responders (PD). Based upon clinical evaluation, patients with stable or increased PS score were considered Responders while patients with decreased PS score during follow up were defined Non-Responders. We found a statistically significant difference between radiological and clinical assessment in Responders and Non-Responders (p<0,001) at the first radiological and clinical evaluation after Nivolumab therapy.
Conclusion: Discrepancy between clinical benefit and radiological response was found at the first evaluation. This data is quite in accord with the majority of literature despite the different PS scores or the different CT parameters applied in order to assess clinical and radiological progression.

Effect of five-line signs in the prediction of staging, progression and prognosis of peripheral lung carcinoma – preliminary observation report

A. Yu, Q. Li, J. He, Y. Zhan; Haikou/CN

Purpose/Objectives: To observe the effect of five-line signs in staging, progression and prognosis of peripheral lung carcinoma. Methods and Materials: This study included 132 patients with peripheral lung carcinoma (93 males, 39 females) with an age range of 27 to 82 years, and a lung nodule range of 0.98 to 8.75 cm. Totally there were 133 nodules (masses)Ðmost of that were solid except 4 partial solid nodules. MIP (maximum intensity projection) was reconstructed based on 1.0 mm or 1.25 mm of thin-slice image in multi-slice spiral CT. Five-line signs between the margin of the nodule (mass) and pleura were observed. According to sharpness of five-line sign shown on MIP image, it was classified into grade 1 five-line signs completely disappeared, 55 cases grade 2 most of them disappeared, 58 cases grade 3 partial disappeared, 11 cases and grade 4 clear/relatively clear, 6 cases.
Results: The sharpness of the five-line sign was linearly correlated to T N and TNM staging of peripheral lung carcinoma (p=0.006 Ð0.001, 0.014) but no relation to M staging(p=0.749). The lower the sharpness of the five-line sign, the faster the progression of the tumor (p=0.001), the higher the mortality rate (p=0.003) and the lower the three-year survival (p=0.003). Particularly, following-up 3 cases coming from grade 3 (2 cases) and 4 (1 case) with small solid nodules (< 2.6cm) keeping survival for 4 (1 case, who not died of cancer) to 10 years (2 cases) without experiencing being resected surgically, the tumors showed character of indolent growth with a doubling time exceeding 800 days. On the other hand, 7 small nodules (≤2.0cm) falling into grade 1 (1 cases) and grade 2 (6 cases) were found invading visceral pleura on pathology, 4 of them occurred metastases after resection.

Fig.1 Adenocarcinoma. Axial MIP6.25mm thick image showed that the five-line sign at the edge of nodule was clear and regular (black arrow), that was thicker and denser than those of normal interlobular fissures (white arrowhead).

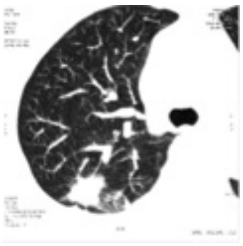

Fig.2-01 Lung cancer in the right upper lobe. On MIP 6.25mm thick rebuilding image five-line sign at the edge of the nodule was barely clear. CT scanning time was 2009-09-11. The nodule was found on July 7, 2007 on plain film.

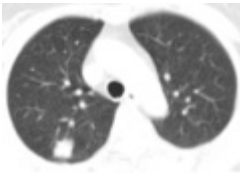

Fig.2-02 The same CT scanning time and same case as Fig.2-01. Conventional lung window 5mm thick axial image showed that the nodule in the right upper lobe was 18.1mm+14.5mm.

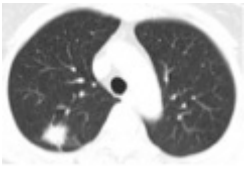

Fig.2-03 The same case as Fig.2-01. CT scanning time was 2012-09-25. On 5mm thick axial image the nodule in the right upper lobe was 28.1mm+12.6mm after 3 years follow-up. Doubling time of the tumor was 867 days.

Conclusion: The five line sign between nodule and pleura shown on MIP reconstruction image reflects the planar structure of thickened septa actually. Clear five-line sign imply that the plane was relatively smooth and regular. While destroyed five-line sign represented the plane rough and irregular. That reflected the damaging and invasion of the tumor to septa. Our observation imply that the sharpness of the five-line sign has certain effects in the prediction of invasion, progression and prognosis of lung carcinoma.

Incidence of pulmonary embolism and right heart dysfunction and impact on survival in patients with malignant melanoma

S. M. Rennebaum, C. Weiß, T. Henzler, S. O. Schönberg, H. Haubenreisser; Mannheim/DE

Purpose/Objectives: Incidental pulmonary emboli (PE) are seen with a prevalence of 4% in oncology patients, especially in patients with malignant melanoma (MM). Thus the aim of this study was to determine a representative incidence of PE in patients with MM. Additionally, the impact on the circulation of the patient in form of right heart strain and D-Dimer was evaluated.
Methods and Materials: 381 consecutive MM patients were retrospectively included. Medical reports of patients who underwent intravenous contrast medium enhanced computed tomography (ivCT) were examined. We evaluated the occurrence of PE in ivCT, elevated D-dimer, right heart and left heart diameter, date of first diagnosis of MM, the subtype of MM (according to American Joint Committee of Cancer 2009), TNM classification, mutation analysis, Clark level, Breslow level, tumor localization and time of death. The occurrence of PE was determined by a radiologist with at least 5 years' experience at time of scan. We differentiated between incidental PE detected by routine staging CT and symptomatic PE. Values exceeding 0.5mg/dl D-dimer were considered positive.
Results: 23 patients showed PE during disease (6.04%). Of these 23 PE, 17 (73.91%) were diagnosed incidentally during routine staging CT. The remaining 6 (26.08%) patients showed a symptomatic PE and received ivCT for this reason.
Significantly correlated to PE were D-Dimer (p= < 0.0001), tumor localization (47.8% on trunk, p= 0.0732) and RV/LV ratio (p=0.0425). Additionally a significant correlation existed between the D-dimer and RV/LV ratio (p=0.0330, r= 0.13051). The mortality in patients with PE compared to patients without PE was significantly higher (p= 0.0481).
Conclusion: Our study emphasizes the frequency and relevance of PE in oncologic patients (6.04%, 9.49% with right ventricular strain), especially in patients with MM. This has a not to be underestimated impact on disease and prognosis in MM patients with PE, showing a significantly higher mortality. (p=0.0481)

Course of CT features in chronic lung allograft dysfunction after double lung transplantation

P. Agarwal[1], A. Benazzo[2], P. Jaksch[2], A. Wielandner[2], H. Prosch[2]; [1]Freiburg/DE, [2]Vienna/AT

Purpose/Objectives: To describe the imaging correlates of the two main phenotypes of chronic lung allograft dysfunction (CLAD) on computed tomography.
Methods and Materials: This retrospective study analyzed the clinical data of 451 patients who underwent double lung transplantation from January 2008 to December 2012 at Vienna General Hospital. Patients with death in the immediate postoperative period, insufficient lung function data, insufficient CT- scans or insufficient clinical data were excluded. Patients with development of tumors in the follow-up period were similarly excluded.
The patients were divided into three groups based on the lung function: Stable (n= 111), Bronchiolitis obliterans syndrome (BOS, n=47) and restrictive allograft syndrome (RAS, n=18) based on FEV1 and TLC values.
CT scans before the decline of lung function, at the time of onset, after the time of onset and the last CT scan were scored by two thorax radiologists in consensus based on a previously described semi-quantitative scoring system by Verleden et. al.

Results: At the time of onset, there was a significant difference in the presence of peripheral consolidations (p=0.18), peripheral ground glass opacities (p=004), subpleural thickening (p=0.045), septal and non-septal lines (p=0.000), architectural distortion (p=0,000) and hilar retraction (p=0.030) in the BOS and RAS groups. The CT scores of peripheral and central consolidations, subpleural thickening, architectural distortion, septal and non-septal lines increased and remained significantly predominant in RAS group compared to BOS and stable patients in the last CT.
Both RAS and BOS patients developed apical caps during follow-up (p=0.379), however only RAS patients showed additional perilymphatic thickening/nodules (p=0.040) at the time of disease onset that progressed to subpleural consolidations in 7 patients.
Conclusion: During the follow up of double lung transplanted patients, computed tomography can play an important role in determining the onset and phenotype of chronic lung allograft dysfunction with significantly more peripheral consolidation, peripheral GGO, septal and non-septal lines, architectural distortion and hilar retraction in RAS patients compared to BOS patients. Development of perilymphatic thickening or nodules in addition to apical caps can be an additional feature to predict the RAS phenotype.

Predicting Non-Small Cell Lung Cancer Recurrence Risk: Radiomics Analysis of the Tumor and Peritumoral Lung Parenchyma on Computed Tomography

T. Akinci D'antonoli, A. Farchione, J. Lenkowicz, M. Chiappetta, V. Valentini, L. Bonomo, A. R. Larici, R. Manfredi; Rome/IT

Purpose/Objectives: To estimate recurrence risk after surgery in non-small cell lung cancer (NSCLC) patients by a predictive model including radiomics signature derived from tumour/peritumor and clinical parameters.
Methods and Materials: 124 NSCLC patients (stages I to IIIA) who received surgery (2008-2013) in in a single centre were retrospectively enrolled. Outcome defined as tumour recurrence (TR), the summation of local recurrence (LR) and distant metastasis (DM), on follow-up imaging. The region of interest (ROI) of the tumour (GTV), the peritumoral lung parenchyma (PTV) and the involved lobe (LB) were semiautomatically contoured on presurgical CT images (Figure 1). 91 features (15 morphological, 17 first order-statistical, 54 textural and 5 fractal-based) were extracted from each ROI with in-house developed software (Moddicom). Imaging datasets were created from the single (GTV, PTV, LB) or combined (GTV+PTV, GTV+LB, GTV+PTV+LB) ROIs. For each outcome, the radiomics score (RS) was computed from best performing ROI models (Cox regression model and AIC stepwise selection). Youden index used to distinguish high- and low-risk patients and Kaplan-Meier Curves were built accordingly. Finally, clinicopathological data were included, and the resulting predictive models were compared (Cox regression model and DeLong's test) alone (RS/clinicopathologic) or combined (RS+clinicopathologic). ROC curves and AUC values were used to evaluate models' performance. For each outcome, nomograms were created at 1-, 2-, 3-year end-point.

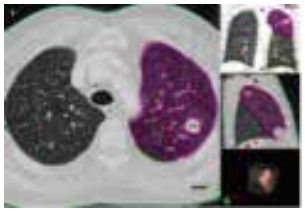

Figure 1. CT images show the 3D ROIs on axial, coronal, sagittal and volumetric views.

Results: 56 (45%) patients developed TR after surgery: 31 (25%) patients had DM and 25 (20%) patients had LR. Median time to tumour recurrence was 23 (IQR 11.5-32) months. For TR and DM outcomes GTV+PTV (AUC 0.750 for both), for LR outcome GTV (AUC 0.731) resulted as the best-performing ROI models. Through step-wise selection, the best clinicopathologic predictor turned out to be the tumour-node-metastasis stage (TNMS) with lower AIC values for each outcome (TR, LR, DM AICs;487, 221, 268, respectively). By adding TNMS, all models' performance was improved (TR: AUC 0.760; DM: AUC, 0.759; LR: AUC 0.750). A statistically significant difference was demonstrated when comparing the combined model to the TNMs alone (P<.05). All high-risk patients developed recurrence at each end-point. High-risk group recurrence risk was seven-fold higher than that of low-risk group during the follow-up (P<.0001).
Conclusion: The predictive model based on the radiomics signature of intratumoral and peritumoral features combined with TNMS from presurgery CT images in NSCLC outperforms TNMS alone in stratifying patients at different recurrence risk after surgery. Presurgical identification of NSCLC patients at high risk of recurrence allows to tailoring a personalised treatment.

Is it reliable to evaluate pulmonary nodule calcification on chest radiography?: Correlation with volumetric quantification by computed tomography

J. Sun, S. You, E. Y. Kim, K. J. Park; Suwon/KR

Purpose/Objectives: To determine the ability of digital chest radiography (CXR) to reveal calcification in solitary pulmonary nodules (SPNs), and to examine the correlation between a visual assessment and volumetric quantification of the calcification using MDCT.
Methods and Materials: This study was a retrospective review of 220 SPNs in 220 patients identified by both CXR and chest CT. Eleven observers who were blinded to CT calcification assessment results reviewed the CXR images and scored nodule calcification on a confidence scale of 1 to 5. The area under the receiver-operating characteristics (ROC) curve (AUC) was obtained to analyze the overall diagnostic performance. The Intraclass correlation coefficient (ICC) for inter-rater reliability was calculated. The AUC and ICC were calculated according to the following nodule diameter groups: group1 (<10 mm), group2 (≥10 mm and <20 mm), and group3 (≥20 mm).
Results: Of the 220 SPNs, 145 SPNs (65.6%) were identified as non-calcified and 75 (34.4%) as calcified in the CT evaluation. The average percentage of calcification volume in the SPN >160 HU (Vol160HU) among the 75 calcified nodules was 47.5%. The mean Vol160HU of the 68 SPNs classified as having definite benign calcification was 51.1%. The overall AUC was 0.71. The AUCs for group 1, 2, and 3 was 0.835, 0.639, and 0.620, respectively. The ICCs for group 1, 2, 3 was 0.65, 0.48, and 0.33, respectively.

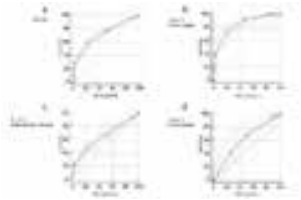

Figure 1. The AUC for all SPNs (a), SPNs <10 mm (b), SPNs ≥10 mm and <20 mm (c), and SPNs ≥20 mm (d).

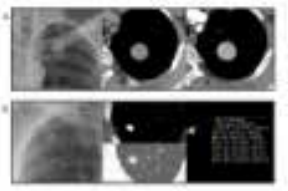

Figure 2. a) A 53-year-old man with hepatocellular carcinoma (HCC) b) A 47-year-old woman with calcified granuloma. An approximately 11 mm, ovoid SPN was seen in the right upper lung.

Table1. Volumetric quantification of calcification in 220 SPNs according to the diameter

Table2. AUC value in ROCs for all observers for prediction of pulmonary nodule calcification on chest radiographic images

Conclusion: The overall diagnostic performance of digital CXR to predict calcification in SPNs was moderately accurate and the diagnostic performance for predicting calcification in SPNs was significantly higher and interobserver reproducibility was good when the SPN < 10 mm compared with ≥10 mm in diameter.

Ultrasound guided cervical lymph node sampling in the staging and management of lung cancer

J. Baren, A. L. Johnstone, S. Karthik; Leeds/UK

Purpose/Objectives: Lung cancer is the leading cause of cancer related death worldwide and the majority of patients present with advanced disease. Pre-treatment tissue diagnosis is vital prior to commencing treatment as it helps guide the type of systemic treatment in advanced lung cancer. It is the guiding ethos in the multidisciplinary team (MDT) at our institution to confirm a pathological stage pre-treatment where feasible. Involved cervical or supraclavicular lymph nodes confirm stage IV disease and are accessible and safe for ultrasound guided cervical lymph node sampling (USGCLNS) by fine needle aspiration (FNA) or core biopsy. We aim to determine the outcomes following USGCLNS, including the proportion of sampling procedures that are sufficient for diagnosis, whether success rates vary between FNA and core biopsy, and the effect that lymph node size has on the rate of a successful diagnosis.
Methods and Materials: All patients with a newly diagnosed lung cancer discussed in the Lung MDT over a 30 month period between January 2014 and June 2016 were included. Data was retrospectively collected from the computerized hospital records and radiology information system, including patient demographics, details of the initial imaging and sampling procedure, lymph node size and the cytology/histopathology report.
Results: Of the 1400 newly diagnosed lung cancer patients (Median age 68, 50.4% male, 49.6% female), 142 (10.1%) patients were referred for USGCLNS following review in the diagnostic MDT. The procedure was performed in 123 (86.6%) patients and a confirmed pathological diagnosis was obtained in 115 of these (93.5%). Core biopsies were generally performed on larger lymph nodes (Median short axis 14mm for core biopsy compared with 11mm for FNA, Mann-Whitney U test, $p<0.05$), however the diagnostic sampling rates between core biopsy and FNA were not significantly different. For FNA, an adequate sample was obtained in 94.5% if the node was >10mm in short axis diameter and in 87.1% if the diameter was <10mm. 4 patients (3.3%) required a repeat sampling procedure and no complications were recorded.

Conclusion: USGCLNS is a safe, easily available and effective investigation in the staging and management of advanced lung cancer. A tissue diagnosis was made in nearly 94% when it was attempted, avoiding more invasive procedures such as transthoracic lung biopsy and endobronchial ultrasound guided sampling. There is an increasing demand for greater quantities of tissue to enable more complex histopathological analysis to be performed, and both core biopsy and FNA are effective in achieving this.

Can an annotation tool using standardized label segmentation improve TNM accuracy in NSCLC staging?

R. Sexauer, G. Sommer, K. S. Mader, T. J. Weikert, J. Bremerich, B. Stieltjes, A. W. Sauter; Basel/CH

Purpose/Objectives: FDG-PET/CT is the standard procedure for staging of NSCLC patients. Currently, many radiologists and nuclear medicine physicians create free-style reports that might not contain all staging-relevant information. This may lead to misstaging and consequently inaccurate treatment management. Therefore, we readout the TNM staging formula from previous PET/CT reports and compared these with a segmentation-based approach.
Methods and Materials: Patients were selected by screening the reports from 375 patients who underwent FDG-PET/CT for primary staging of NSCLC. From these reports, TNM (7th edition) stage was determined by an experienced radiology and nuclear medicine physician. For each patient the full PET-CT image dataset was downloaded from the PACS and transferred to a 3D-slicer-based annotation software that supports manual segmentation of tumors, lymph nodes and metastasis using a full set of labels including location information and morphological TNM features (see figure „visually structured reporting"). Both approaches including the median report dictation and annotation time were compared.

figure 1: visually structured reporting

Results: In a considerable number of patients, not enough information was provided by the report to extract an accurately defined TNM stage: T: 17.3% (65/375); N: 5.3% (20/375); M: 1.9% (7/375). TNM information could be extracted in all patients with the segmentation-based approach. This led to upstaging due to the annotations in 46 cases (T: n = 26, N: n = 13, M: n = 7) and downstaging due to the annotations in 59 cases (T: n = 50 ; N: n = 7; M: n = 2). Changes in UICC stage could be documented in 6 % (18/279; cases with incomplete TNM were excluded). The median report dictation time was 22.1 min, while the median for the annotation time was 19.1 min.
Conclusion: We could demonstrate that the TNM stage could not be derived from unstructured PET/CT reports in approx. 30% of the cases. This commonly affects the T-stage because of missing diameter measurements, but also N and M stage. Our approach with tumor labels allows for a clear definition of cancerous lesions in a standardized and reproducible manner. Additionally, the segmentated data can be utilized for further analysis such as machine-learning.

Radiological response of second-line Nivolumab therapy correlates with cancer stadium rather than patient's gender, histology and genetic mutations (EGFR, KRAS)

D. Cozzi, C. Moroni, A. Bindi, M. Bartolucci, F. Giannelli, V. Scotti, C. Muntoni, D. Lavacchi, F. Mazzoni, V. Miele; Florence/IT

Purpose/Objectives: Nivolumab is a human IgG4 programmed cell death-1 immune check point inhibitor antibody that has been approved for second line treatment of stage IIIb/IV non-small cell lung cancer (NSCLC). Patients which underwent Nivolumab treatment differ for gender, age, cancer histology and presence of mutations. The aim of this study is to evaluate the radiological response, based on iRECIST, and to correlate it with different parameters such as histology and stage of the neoplasm, patient's gender and presence of genetic mutations (EGFR, KRAS).
Methods and Materials: Between August 2015 and August 2017 we overall selected 75 patients with NSCLC stage IIIb/IV who received Nivolumab. Their pre- and post-treatment CT scans were evaluated by two senior and two junior radiologists dedicated to thoracic imaging in order to define the radiological response; in case of discordant results, a definite response was obtained by general agreement. Demographic data as well as genetic mutations and histology of the population were obtained.
Results: Radiological response was defined as: complete response (CR), partial response (PR), stable disease (SD) and progression disease (PD) according to iRECIST criteria. We finally divided patients in Responders (CR+PR+SD) and Non-Responders (PD). At baseline, male/female ratio was 33/10; stage of disease was IIIb (11 patients) and IV (32 patients); histology was adenocarcinoma in 21 patients (48,8%) and squamous cell carcinoma in 22 patients (51,2%). Genetic analysis demonstrates EGFR mutation in 10 patients (23%) and KRAS mutation in 4 patients (9,3%). PDL-1 mutation and quantification was studied in 7 patients only, therefore it was excluded from the study. Chi-square statistic was applied between two categorical variables: radiological Responders/ Non-Responders and patient's gender, cancer histology and stage, EGFR and KRAS mutation. We found statistically significant difference in radiological response only between different tumour stages (p-value <0,05). No significant difference in radiological response was found between patients of different gender and with different cancer histology.

Conclusion: A significant better radiological response to Nivolumab therapy is associated with stage IIIb neoplasm. Instead, patients with stage IV NSCLC have worst radiological trend. This result is concordant with the majority of literature and confirm the prognostic value of lung cancer stages classification. The lack of difference in Nivolumab radiological response found between different histology of NSLC concord with the more recent studies which expanded Nivolumab utilization not only to squamous cell carcinoma but also to adenocarcinoma.

A Bronx Tale: Establishing and developing a Lung Cancer Screening Program in an Urban, Diverse Multi-Ethnic community

A. Shmukler[1], H. Milch[2], M. Kaminetzky[2], R. Peng[3], E. Mardahaev[3], L. Haramati[3]; [1]Brooklyn/US, [2]New York/US, [3]Bronx/US

Purpose/Objectives: The results of the National Lung Cancer Screening Trial (NLST) have demonstated 20% reduction in lung cancer mortality in the high risk patients screened with CT as compared to CXR. Given the convincing evidence from the NLST that CT screening may yield a mortality benefit, we initiated a Lung Cancer Screening clinical program at Montefiore in 2012. The purpose of this abstract is to discuss the results, challenges and triumhs of establishing and developing a clinical lung cancer screening program in ethnically diverse, poor, predominantly overweight, and obese population, which differs dramatically from the National Lung Screening Trial population.
Methods and Materials: All patients had a physician referral forlow dose CT lung cancer screening and met National Lung Screening Trial eligibility criteria. A dedicated bilingual screening coordinator interviewed the patients to confirm eligibility. The coocrdinator also communicaticated with physicians, managed and updated the database, as well as contacted patients for follow up. Infrastructure developed for the program included a standardized results report. LDCT results were prospectively assigned a Lung-RADS or equivalent score during interpretation.
Results: The cohort comprised of 1591 patients with 2240 person-years of follow up as of December 2017. As of December 2016, Mean age 64 [SD16.2] years, 51% women, 23% white, 71% current smokers, 69% overweight or obese, multiple comorbidities. Lung cancer prevalence was 2.1%. Mortality was 37% in lung cancer patients versus 2.5% in the remaining cohort ($p<0.001$). 54% of patients were overdue for first annual exams. 84% (989) had follow-up via electronic records or personal contact and the remainder had vital status ascertained via National Death Index. Data from December 2016-December 2017 is being calculated and will be available by April 2018.
Conclusion: Lung Cancer LDCT screening is feasible in a diverse inner-city population with the support of a robust infrastructure. Major limitations and challenges of the present study are related to follow-up as over half the eligible cohort was overdue for annual LDCT. The program is limited by a single part-time coordinator scheduling and following-up patients.

Multivariate modeling for benign vs malignant diagnosis in CT guided trans-thoracic biopsies: How well can we predict diagnosis based on clinical and CT imaging information?

E. J. M. Barbosa Jr., N. Sachs, W. Lindsay, J. Wang, J. Gee; Philadelphia/US

Purpose/Objectives: CT guided trans-thoracic biopsy (CTTB) is an established, minimally invasive method for diagnostic evaluation of a variety of thoracic diseases. We utilized a large cohort of CTTB patients to assess how well multivariate models utilizing clinical and imaging variables can predict malignant versus benign pathology diagnosis.
Methods and Materials: 796 patients were retrospectively selected in our CTTB database, comprising biopsies performed at a large tertiary hospital in the USA (1/1/2013 to 7/1/2017). Our model included the following variables: age, race, sex, smoking history, smoking pack-years, history of prior cancer, immune status, nodule location, nodule size, nodule margin and nodule shape. These variables were extracted from radiology reports and electronic medical records. Ground-truth was CTTB pathology diagnosis, classified as benign (23.4%) vs malignant (74.1%), with 2.5% of indeterminate cases excluded. We compared the performance of random forest (RF), logistic regression (LR) and Decision Tree (DT) multivariate classifiers utilizing a 75%/25% training/validation ratio for the CTTB cohort and 10-fold cross validation for model tuning.
Results: The RF model produced AUC (area under the curve) of ROC (receiver operating characteristic) of 0.64 and accuracy of 0.72 (figure 1); the LR model produced AUC of ROC of 0.61 and accuracy of 0.75 (figure 2), whereas the DT model produced AUC of ROC of 0.62 and accuracy of 0.75 (figure 3).

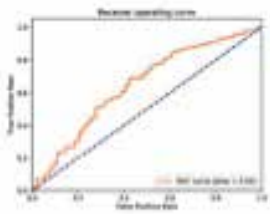

Random Forest model performance

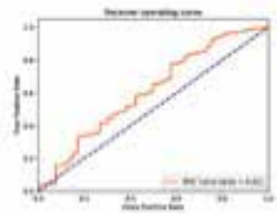

Logistic Regression model performance

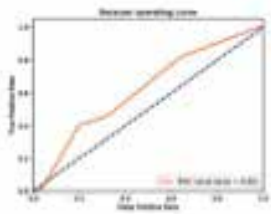

Decision Tree model performance

Conclusion: CTTB is a very accurate method for pathologic diagnosis of thoracic lesions, however, there are risks associated with the biopsy and some patients may be too sick to fully cooperate during the biopsy or may not be able to tolerate potential complications of the procedure. Therefore, predicting the diagnosis based on a combination of multiple non-invasive imaging and clinical variables may be useful for patient management, and our results suggest that the accuracy of our models may be high enough to be clinically useful. The best performing model was decision tree, with accuracy of 75%, similar to logistic regression, and slightly better than random forest. We intend to further investigate whether quantitative CT imaging features can improve diagnostic accuracy of these models in future research.

Accuracy, Performance Metrics and Complication Rates of CT guided thoracic biopsies: A large tertiary center 5-years' experience

E. J. M. Barbosa Jr., N. Sachs; Philadelphia/US

Purpose/Objectives: CT guided transthoracic biopsy (CTTB) is an established, minimally invasive method for diagnostic work up of a variety of thoracic diseases. Alternative options for pathological diagnosis include transbronchial and surgical biopsies. We assessed a large cohort of CTTB to assess how well this performs in terms of diagnostic accuracy and complication rates.
Methods and Materials: We retrospectively searched our electronic medical record for all CTTB performed at a large tertiary hospital in the USA between 1/1/2013 and 7/1/2017, and recorded characteristics of each lesion biopsied, type of biopsy, diagnostic yield, type of diagnosis and complication rates. Data management was performed with RedCap and statistical analysis with JMP (SAS).
Results: We identified 796 CTTBs (43% were fine needle aspirations, 5% were core biopsies, 52% both). Lung lesions comprised 81.8% of CTTBs (the rest were pleural 8.0%, mediastinal 6.7% and chest wall 3.5%). Diagnostic yield was 97.5%. In our cohort, 74.1% of lesions were malignant, 23.4% were benign and 2.5% were indeterminate or non-diagnostic. Most patients had no post-biopsy complications (86.3%). 11.8% had minor complications (no hospital admission or invasive procedure required), and 1.9% had major complications requiring hospital admission or invasive procedures. The most common complication was pneumothorax (13.1%), followed by bleeding (0.6%).
Conclusion: CTTB performed by expert thoracic radiologists in a tertiary center have a very high diagnostic yield (over 97%) with a very low clinically significant complication rate (less than 2%), making it an excellent modality for diagnostic evaluation of a large variety of thoracic diseases. While pneumothorax was the most common complication, it is rare that patients require chest tube placement or hospital admission to manage post procedural complications. Our overall performance (diagnostic accuracy and complication rates) in a large patient cohort surpasses published results of transbronchial biopsy cohorts, suggesting that CTTB performed at specialized centers should be considered a first line choice and may be preferable to transbronchial biopsies in most situations.

Differences in thrombotic load between symptomatic and unsuspected pulmonary embolism

J. Vassallo, G. Ritchie, N. Morley, K. Muir, E. J. R. van Beek, J. Murchison; Edinburgh/UK

Purpose/Objectives: With the ever-increasing use of CT, unsuspected pulmonary embolism (UPE) has become an increasing problem for the clinician. Although most clinicians would recommend treatment in symptomatic or unsuspected proximal PE irrespective of malignancy, there is less agreement regarding treatment of distal UPE, with recent guidelines suggesting that some of these patients should not be anticoagulated. In this study, we aim to identify whether there are any differences in the thrombotic load between symptomatic and unsuspected pulmonary embolism.
Methods and Materials: Using data previously obtained in this institution, we compared the thrombotic load using the modified miller score (MMS) in both symptomatic and UPE. For symptomatic pulmonary embolism (SPE), all reportedly positive CTPAs over a period of one year were reviewed and their MMS calculated. For UPE, unselected outpatient and inpatient scans over a period of six months were individually reviewed and their MMS also calculated. Poor or absent contrast enhanced CTs were excluded.

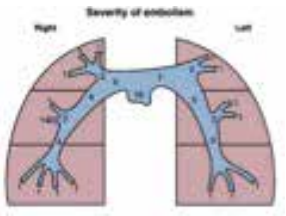

The Modified Miller Score: Each occluded or partially occluded segmental pulmonary artery is given a score of 1 (nine on the right and seven on the left) and any more proximal vessels score the number of segmental branches distal to that vessel

Results: Following exclusions, a total of 927 unselected inpatient and outpatient scans were reviewed (487 inpatients and 440 outpatients). 39 patients (25 inpatients and 14 outpatients) were found to have an UPE. 12 out of the 39 PEs (30.7%) were not initially reported and 6 of these were segmental and the other 6 were subsegmental. The indication for the majority of patients

who underwent CT of the chest was malignancy (77.7% in the outpatient population and 70.4% in the inpatient population). In the suspected group, 400 positive CTPAs were reviewed. Statistical analysis using a statistical software package showed a median MMS of 6 in the suspected group and 3 in the unsuspected group (P=0.005 using Mann-Whitney U test for Independent Samples). There was no statistical difference in gender (p=0.64, Fisher's exact test) or age (p=0.82, T-test for independent samples) between these groups. The bar chart below shows the spread of the MMS for UPE and SPE.

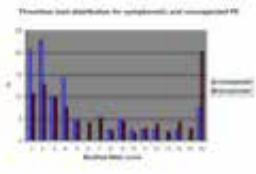

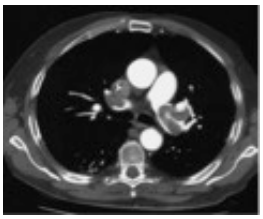

CTPA showing massive pulmonary emboli within the left and right main pulmonary arteries.

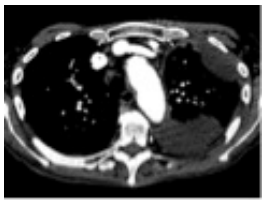

Unsuspected pulmonary embolism showing a filling defect within a right subsegmental pulmonary artery.

Conclusion: The association between UPE and a low MMS, irrespective of malignancy, seems to be consistent with the idea that UPE should be considered separately of SPE as they might be managed differently. This highlights the importance for the radiologist in giving an idea of the thrombotic load to the referring physician especially when reporting UPE where it might impact on patient management. The MMS can be a useful tool in determining the thrombotic load in these cases.

Malignant pleural effusion: Quantitative and qualitative diagnosis with Chest CT and PET-CT

M. S. Juárez-García, E. Pallisa, A. L. Sánchez, D. Varona Porres, O. Persiva Morenza, C. Aleman; Barcelona/ES

Purpose/Objectives: Contrast-enhanced thoracic CT has limitations in distinguishing malignant from benign pleural effusion. A recent meta-analysis concludes PET-CT has moderate accuracy and precludes its routine recommendation for discriminating malignant from benign pleural effusion. The role of PET-CT in a subgroup with high clinical suspicion of malignant pleural effusion needs to be determined.
Methods and Materials: A prospective study of a series of 42 patients with high clinical suspicion of malignant pleural effusion and negative cytological examination of the pleural fluid who underwent Chest CT and FDG-PET-CT previous to a pleural biopsy.
The thoracic CT and FDG-PET/CT features were evaluated by two independent radiologists blinded to the final diagnosis; one was a nuclear-medicine radiologist.
Both radiologists established a qualitative effusion pleural diagnosis as malignant, benign or inconclusive. Pleural effusion was categorised as malignant if malignant cells were detected after thoracoscopic pleural biopsy or follow-up.
Results: 18 effusions were malignant and 24 benign. Among the malignant, 8 were mesoteliomas (7 epithelioid, 1 sarcomatous) and 10 metastasics (1 Non Hodgkin lymphoma, 1 adenocarcinoma of unknown primary origin and 8 NSCLC).
Nodular pleural thickening, affected mediastinal pleura and also cardiofrenic lymph nodes on Chest CT correctly classified 85.4% of the patients (sensitivity 83%, specificity 87%). PPV was calculated at 83% and NPV calculated as 87% for the diagnosis of malignancy. FDG-PE/CT demonstrating pleural thickening and SUV > 5.64 combined with internal mammary lymph nodes with SUV > 6.34 correctly classified 95.2% of the patients (sensitivity 89%, specificity 100%). PPV was calculated at 100% and NPV at 92% for the diagnosis of malignancy.
After qualitative interpretation by Chest CT and FDG-PET/CT, 18 patients were diagnosed as malignant, 11 as benign and 13 as inconclusive in Chest CT group, with an accuracy diagnosis of 59.5%. In the FDG-PET/CT group, 16 patients were diagnosed as malignant, 24 as benign, and 2 as inconclusive, with an accuracy diagnosis of 88% of all patients.
Conclusion: Chest CT qualitative diagnosis has an important role in the diagnosis of pleural effusion, and the addition of qualitative interpretation FDG-PET/CT increased its accuracy between 60% to 88% in our case series.

A comparative study of CT findings and clinical conditions that predispose patients to lung infarction following PE

K. K. Šifer, J. Vidmar, I. Kocijancic; Ljubljana/SI

Purpose/Objectives: With this pilot study we try to identify imaging and clinical factors predisposing to lung infarction (LI) in patients with pulmonary embolism (PE) with a focus on individual variations in anatomy and comorbidity.
Methods and Materials: This retrospective study was conducted on patients admitted in November 2017 to the University Medical Centre Ljubljana, Slovenia, who underwent a CTA of pulmonary arteries based on a clinical suspicion of PE. We selected those with radiologically confirmed PE and determined if they were concurrently suffering from malignancy, left cardiac failure or COPD. We used the length and central/peripheral location of thrombi as a proxy for thrombotic burden. We located the LI, bronchial arteries and recorded the angles and widths of central pulmonary arteries.
Results: We included 68 patients, of which 12 (18%) had at least one area of LI. 8 of the patients with LI had central thrombi and two of them had comorbidities; the other 6 had peripheral thrombi and at least one comorbidity. The average length of the most

central thrombus and the width of pulmonary trunk did not differ significantly between the two groups. We found an average of 1.6 bronchial arteries on the left and 1.1 on the right in the group without LI; and an average of 2.0 bronchial arteries on the left and 1.2 on the right in the group with LI. The angle between both main pulmonary arteries and pulmonary trunk in the group without LI was 48° and 61° for LPA and RPA, respectively; and in the group with LI 45° and 66°, respectively.
Conclusion: Our preliminary results seem to oppose the notion that LI is most commonly caused by PE in combination with left cardiac failure, which falls in line with some of the recent studies on the field[1]. There also seems to be no clear connection of the occurrence of lung infarction and the central/peripheral distribution of thrombi. Our further work (to be presented at ESTI meeting), which we expect will include more than 200 subjects, will focus on the theory that in the absence of comorbidity it is the thrombotic closure of physiological anastomoses between the pulmonary and bronchial arteries that determines the occurrence of LI.
[1] Kirchner, J, Obermann, A, Stückradt, S, Tüshaus, C, Goltz, J, Liermann, D, Kickuth, R. Lung Infarction Following Pulmonary Embolism: A Comparative Study on Clinical Conditions and CT Findings to Identify Predisposing Factors. Fortschr Röntgenstr. 2015, 187: 440–444.

Bronchial and vascular alterations in patients with severe pulmonary hypertension: Role of quantitaive computed tomography

I. Benlala[1], F. Coste[1], G. Dournes[1], F. Baldacci[2], P. Berger[1], F. Laurent[3]; [1]Bordeaux/FR, [2]Talence/FR, [3]Pessac/FR

Purpose/Objectives: Little is known about in vivo alterations at bronchial and vascular levels in severe pulmonary hypertension (PH) of different etiologies. We thus hypothesized that, unlike other groups of PH, severity of PH secondary to COPD may be predicted in a non invasive manner by assessing both bronchial and vascular alterations.Therefore, we compared quantitative computed tomography (CT) data from three groups of severe precapillary PH patients: COPD, idiopathic pulmonary arterial hypertension (iPAH), and chronic thromboembolic PH (CTEPH).
Methods and Materials: This study was approved by the institutional review board. Severe PH patients (mean pulmonary arterial pressure, mPAP ≥ 35 mmHg) with COPD, iPAH or CTEPH (n= 24, 16 or 16, respectively) who underwent pulmonary function tests, unenhanced chest CT scan and right heart catheterisation (RHC) were included retrospectively between January 2008 and January 2017. Multivariate analysis of mPAP was performed in each severe PH group. Bronchial wall thickness (WT), cross-sectional area of vessels less than 5 mm2 (%CSA<5) were measured and compared using CT then combined to PaO2 to generate a "paw score" compared within the 3 groups using Krusskal-Wallis and its sensitivity using Fisher exact test.
Results: Bronchial wall thickness (WT) was higher and %CSA<5 lower in the COPD group compared to iPAH and CTEPH groups. The mPAP was positively correlated to %CSA<5 in the COPD group, and negatively or not correlated in iPAH or CTEPH groups, respectively. To predict mPAP variability, 2 models including either WT or %CSA<5 and PaO2 were significant in COPD and not significant in other groups at multivariate analysis. In the COPD group, "paw score" showed higher sensitivity than in other groups.
Conclusion: Unlike in severe iPAH and CTEPH, severe PH with COPD can be predicted by "paw score" reflecting bronchial and vascular morphological differential alterations.

What is a perifissural nodule? Low inter-observer agreement in NLST data

A. Schreuder[1], B. van Ginneken[1], E. Scholten[1], C. Jacobs[1], M. M. Prokop[1], N. Sverzellati[2], S. R. Desai[3], A. Devaraj[3], C. M. Schaefer-Prokop[4]; [1]Nijmegen/NL, [2]Parma/IT, [3]London/UK, [4]Amersfoort/NL

Purpose/Objectives: Pulmonary nodules on chest CT classified by radiologists as perifissural nodules (PFN) have been shown to have a negligible chance of malignancy. We studied the inter-observer variability for classifying nodules as PFNs in National Lung Screening Trial (NLST) data.
Methods and Materials: Out of a sample of 5819 low-dose CT scans of slice thickness ≠2mm from the NLST, we detected and annotated 3669 non-calcified solid nodules with diameters of 5 to 10mm. 359 nodules were selected for the observer study. With definitions provided, six radiologists independently classified these nodules as either "typical PFN," "atypical PFN," "non-PFN," or "not applicable." A "typical PFN" has a lentiform, triangular, or polygonal shape, is located on or within 10 mm of the visceral pleura or lung fissure, and has extending linear densities. An "atypical PFN" lacks one of the three key criteria defining a typical PFN. A "non-PFN" showed at least one of the following features: spiculation, irregular shape, un-sharp borders, and distortion of the pleura or fissure. Adherence to these definitions was not required. Opacities deemed to be subsolid, completely calcified, not nodular, or not visible were considered "not applicable"; when rated as such by at least three radiologists, these were excluded (n=43). This left 316 nodules for analysis using descriptive statistics, Mann-Whitney U tests, and Fleiss' kappa (Ð).
Results: Fifty-six of 316 nodules (17.7%) were classified by all six radiologists as either typical or atypical PFNs. More than four times the number, 229/316 nodules (72.5%), were classified by at least one radiologist as PFNs. Ð was 0.50; when distinguishing PFN subgroups, Ð decreased to 0.30. Only 7/316 nodules (2.2%) were unanimously classified as typical PFNs; none were atypical PFNs by unanimity. Compared to non-PFNs, nodules classified by at least three readers as either typical or atypical PFNs were smaller on average and were more often located in the lower lobes and attached to a fissure ($p<0.001$). Pleural attachment was not a good distinguishing factor between PFNs and non-PFNs ($p=0.54$).

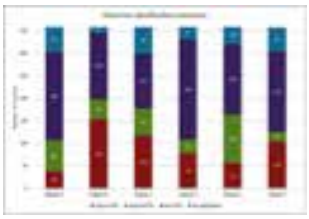

Classification outcomes of all six readers. Abbreviations: PFN, perifissural nodule.

Conclusion: There is only a fair to moderate inter-radiologist agreement when classifying pulmonary nodules as PFNs. More than two-thirds of all nodules in our sample were considered to be a PFN by at least one radiologist; less than one-fifth were PFNs by full consensus, and considerably less when distinguishing PFN subgroups. This suggests that better criteria for identifying PFNs need to be developed and adhered to.

A Deep Learning Algorithm for Classifying Fibrotic Lung Disease on High Resolution Computed Tomography

S. L. Walsh[1], L. Calandriello[2], M. Silva[3], N. Sverzellati[3]; [1]London/UK, [2]Rome/IT, [3]Parma/IT

Purpose/Objectives: We investigated the utility of a deep learning algorithm for providing automated classification of fibrotic lung disease on high-resolution computed tomography (HRCT) based on idiopathic pulmonary fibrosis (IPF) diagnostic guideline criteria. We benchmarked algorithm performance against a cohort of 91 thoracic radiologists.
Methods and Materials: A database of 1078 volumetric HRCT studies showing evidence of a diffuse fibrotic lung disease was generated from 2 institutions. Each HRCT was classified as meeting usual interstitial pneumonia (UIP), possible UIP or inconsistent with UIP criteria based on current IPF diagnostic guidelines. Using a combination of simple thresholding and contour approximation (using the Python computer vision library, OpenCV), the lungs from each HRCT were segmented. For each of these segmented HRCT studies, a maximum of 500 unique 4-slice combinations (1 slice per quarter thoracic length) were extracted and converted into montages (see Figure 1). The final training dataset for algorithm development was made up of 460,586 unique montages. The computer algorithm used to classify the images was a deep convoluted neural network (CNN) based on Google's InceptionV3 architecture. The optimisation algorithm used was Adam. Algorithm performance was tested on a cohort of 150 HRCTs with fibrotic lung disease against 91 subspecialist thoracic radiologists drawn from multiple international thoracic imaging societies. The ground truth label ('UIP', 'possible UIP', 'inconsistent with UIP') for each of the 150 cases was the majority vote of the 91 thoracic radiologists. Interobserver agreement between observers and the ground truth label was calculated using the Kappa coefficient and accuracy is reported as the percentage of HRCTs correctly classified based on the ground truth labels.

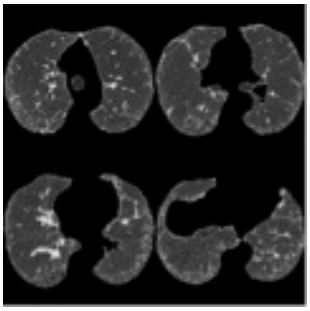

Example of a montage generated from four segmented HRCT axial images, used to train the deep neural network. The radiologic diagnosis in this patient was usual interstitial pneumonia. 460,586 unique montages were created from 1078 volumetric HRCTs.

Results: Median accuracy of the 91 thoracic radiologists was 70.7% (IQR 9.5). CNN accuracy was 76.3%, outperforming 51/91 thoracic radiologists. Median agreement between each thoracic radiologist and the ground truth label was 0.48 (IQR 0.13). Agreement between the CNN and the ground truth labels was 0.50, outperforming 59/91 thoracic radiologists.
Conclusion: Automated HRCT evaluation may provide reproducible, near-instantaneous classification of fibrotic lung disease on HRCT with human-level accuracy. These methods may be of benefit to centres where thoracic imaging expertise is limited as well as for stratification of patients in clinical trials.

Incidental Extrapulmonary Findings in Low -Dose CT of the Thorax: Just LOW or MORE?

Z. N. Tekin, A. Türk, S. Alzafer, O. Saygili; Istanbul/TR

Purpose/Objectives: The study aims to describe the prevalence of extrapulmonary findings in low-dose computed tomography (CT) imaging of the thorax.
Methods and Materials: The study was carried out on 102 consecutive patients (61 males; mean age: 54.5 years, age range: 25-90 years), who were underwent clinically indicated low-dose CT of the thorax to assess either a certain or a potential pulmonary disease. The patients were referred to the radiology department by the department of pulmonary medicine from June 2016 to January 2018 for a period of 18-month.
The CT was performed by using a 64-detector CT scanner including low-dose CT parameters standardized as 120 kVp and 20 mAs with 3mm axial, and coronal image reconstructions. Regardless of parenchymal findings, examinations were retrospectively reviewed according to organ system in the scan area by the same radiologist with five years experience in thoracic imaging.
Results: A total of 245 incidental extrapulmonary findings were detected in 87 (85.3%) out of 102 patients. Incidental extrapulmonary findings were classified into 8 groups including cardiac, vascular, mediastinal, abdominal, bone, thyroid, breast and soft tissue and muscular pathologies.Abdominal pathology was defined in 62 (60.8%) of the patients. Among the patients with the abdominal pathology, the most common findings were 38 hepatosteatosis (37.3%) and 12 sliding hiatal hernia (11.8%).
Conclusion: Lung Cancer is a life-threatening disease in which its incidence and mortality rate are increasing globally. Early detection of lung cancer through low-dose CT of the thorax becomes widespread, especially in pulmonary nodules management and follow-up. Due to the high rate of incidental extrapulmonary findings (85.3%) that can be even detected in low-dose CT of the thorax, it is essential to evaluate all the structures in the scan area to detect potential pathologies. In particular, this is necessary to prevent misdiagnosis and to avoid malpractices by radiologists, which is important medico-legally.

Unmasking COPD in patients excluded by the lower limit of normality

M. Occhipinti[1], M. Paoletti[1], C. Nardi[1], M. Palazzi[1], G. Camiciottoli[1], R. Inchingolo[2], S. Colagrande[1], A. R. Larici[2], M. Pistolesi[1]; [1]Florence/IT, [2]Rome/IT

Purpose/Objectives: The fixed ratio of FEV1/FVC was proposed by the GOLD to define airflow obstruction in chronic obstructive pulmonary disease (COPD).As this ratio may overdiagnose COPD in elderly patients the European Respiratory Society (ERS) proposed to use the lower limit of normal (LLN) of FEV1/FVC, considering the normal distribution of values in the reference population. Patients diagnosed with COPD by GOLD criteria may be excluded by using LLN. Thus, we aimed at investigating the presence of imaging findings indicative for COPD with both quantitative and qualitative analyses of computed tomography (CT) scans in those patients excluded by LLN criteria.
Methods and Materials: From January2012 to December2016 we recruited 216 consecutive eligible COPD patients (GOLD stages I-IV),after IRB approval. All patients underwent complete pulmonary function evaluation (static and dynamic lung volumes, single-breath diffusing capacity for carbon monoxide-DLco) and chest CT scan within 48 hours.LLN for FEV1/FVC was calculated by using prediction equations proposed by ERS. CT images were qualitatively analyzed in consensus by two radiologists,who classified COPD subtypes according to the Fleischner Society statement.CT images were quantitatively analyzed by coregistration analysis of paired inspiratory and expiratory scans (LDA® Imbio LLC,US).Relative volumes of normal lung, emphysema (persistent low density area,pLDA), and functional gas trapping (functional low density area,fLDA) were computed.
Results: 46/216 (21.3%) patients with COPD as defined by GOLD criteria were excluded by using the LLN criteria.Excluded patients were 71±7 years-old (52-84), mostly male (M:F=41:5), with an average FEV1/FVC of 64.3% (vs 51.4% GOLD) and DLco of 80.3% (vs 68.5% GOLD).Patients complained of cough (28/46, 61%),sputum (18/46, 39%),and wheezing (1/46, 2%),with an average modified Medical Research Council questionnaire of 2.At CT all 46 patients had findings of either emphysema or airway disease:2 advanced destructive emphysema,4 confluent centrilobular emphysema (CLE),6 moderate CLE,6 mild CLE,9 trace CLE,9 mild paraseptal emphysema (PSE),7 substantial PSE, and 3 airway disease.Overall CLE was present in 27/46 (58.7%) cases and PSE in 16/46 (34.8%) cases.At co-registration analysis the excluded patients had on average 7.5% of pLDA and 29% of fLDA.
Conclusion: One out of five patients with COPD as defined by GOLD criteria was excluded by LLN.Most excluded patients presented with cough and/or sputum,whereas all of them presented with findings of COPD at CT scan.CLE was the most common finding,followed by PSE,and airway disease.

Opportunistic Lung Cancer CT Screening in Outpatient Service in Germany: Frequency, Predictors and Quality

D. Schneider, B. Amler, O. von Stackelberg, H.-U. Kauczor, C. L. L. Schlett; Heidelberg/DE

Purpose/Objectives: While currently there is no organized CT screening for lung cancer in Germany, we aimed to capture and evaluate opportunistic lung cancer screening by CT in outpatient care.
Methods and Materials: IRB approval was obtained to study retrospectively the chest CT exams of two radiological outpatient centers within to large cities in Germany between 2011 and 2012. Data were combined from several sources including radiology information systems, DICOM headers and CT reports. Our results were compared with previously published results of the National Lung Screening Trial (NLST) in the US and the Lung Tumor Screening and Intervention Trial (LUSI) in Germany using 95% confidence intervals (CI).
Results: Of 3,853 performed chest CT scans, all cases with known malignancy or CT as part of follow-up were excluded, thus the final cohort consisted of 1,826 chest CT examinations (age 61±14 years, 56% male) (attached Figure 1). Based on the information given from the referring physician, 23 CT scans (1.26%) were unmistakably identified as part of opportunistic lung cancer screening. Screened patients were on average younger (53.91±8.61yrs, p=0.0003) and agreed to 57% with the recommended age-category in LUSI (50-69yrs), while they agreed only to 35% with the age-category in NLST (55-74yrs). Within patients undergoing opportunistic lung cancer screening (n=23), 4 CT scans were positive (17.39%, 95%CI: 4.95-38.78%), this rate did not vary significantly from NLST (95%CI: 26.80-27.88%) or LUSI (95%CI: 24.71-28.61%). In a multi-stage analysis of the clinical particulars we could identify a significant portion of examinations with a high probability of execution with the intention of screening, e.g. information suggested "rule-out of thoracic cancer" and history of smoking or information on symptoms missing (n=68) (attached Figure 2). Some disagreement (37.5%) was found between suggested follow-up time in the CT report and formal recommendation based on Fleischner criteria (attached Figure 3).

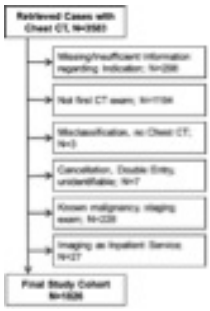

Visualization of the different criteria for the exclusion of examinations and definition of the final study cohort.

Analysis of the clinical particulars regarding the question for lung cancer screening, the implicit tumor rule out, the specification of clinical symptoms and their specificity and exposure to cigarette smoke.

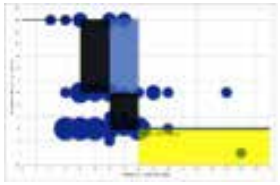

Comparison of follow up recommendations by the radiologist and according to Fleischner Guidelines. Bubbles represent the follow up recommendation, shadowing represents Fleischner recommendations. Bubble size represents frequency of pulmonary nodules.

Conclusion: The rate of opportunistic lung cancer screening is low, however a large number may remain unknown. A good agreement with published lung cancer screening trials has been observed while some disagreement existed regarding recommended follow-up time.

Perifissural nodule count as a biomarker for COPD GOLD stages and emphysema measurements?

A. Schreuder[1], C. M. Schaefer-Prokop[2], E. Scholten[1], D. Lynch[3], J.-P. Charbonnier[1], C. Jacobs1, M. M. Prokop[1], B. van Ginneken[1]; [1]Nijmegen/NL, [2]Amersfoort/NL, [3]Denver, CO/US

Purpose/Objectives: One of the main pathophysiological mechanisms of chronic obstructive pulmonary disease (COPD) is inflammation mediated by the immune system. Intrapulmonary lymph nodes have a distinctive computed tomography (CT) morphology as perifissural nodules (PFN). The purpose of this study was to evaluate the relation between the number of PFNs and **emphysema scores.**
Methods and Materials: CT scans, lung function performances, and clinical data were obtained from the COPDGene study. Forty participants were randomly selected per GOLD stages groups 0 through 4, (n=200). The baseline scans were screened for nodules by a trained medical researcher with support from computer-aided detection (CAD) software. Nodules which were considered solid, had sharp borders, lacked spiculation, and were not completely calcified were assessed independently by two experienced radiologists. The number of these nodules classified as PFNs was counted per scan and averaged per GOLD stage group, and normalized emphysema score (NormES-950)- and 10mm airway lumen perimeter (Pi10)-based groups divided by quartiles. Statistical analyses was done using descriptive statistics, one-way ANOVA, and Cohen's kappa.

Results: Three of 200 (1.5%) scans could not be processed by the CAD. Out of 175 scans, 584 CAD annotations were accepted and an additional 172 nodules were identified. 174 calcified, 20 ground glass, 8 subsolid, and 136 spiculated, unsharp, or irregularly shaped solid nodules were excluded by the trained medical researcher. The median diameter and volume of the remaining 418 nodules were 3.9mm (25th percentile (P25)=2.6mm, 75th percentile (P75)=5.6mm) and 18.4mm3 (P25=8.1mm3, P75=40.4mm3), respectively. Readers A and B independently classified 198/418 (47.4%) and 311/418 (74.4%) of the remaining nodules as PFNs, respectively. The interrater agreement was 0.34 (Cohen's kappa). The average number of PFNs found in GOLD groups 0 to 4 were, respectively, 0.90, 1.00, 0.98, 1.15, and 1.00 for Reader A (p=0.97), and 1.44, 1.55, 1.38, 1.70, and 1.83 for Reader B (p=0.84). The medians of the NormES and Pi10 were 7.24HU (P25=2.45HU, P75=19.17HU) and 2.35mm (P25=1.95mm, P75=2.80mm), respectively. ANOVA of the average number of PFNs between the NormES and Pi10 quartiles respectively resulted in p-values of <0.001 and 0.499 for Reader A, and 0.001 and 0.585 for Reader B.

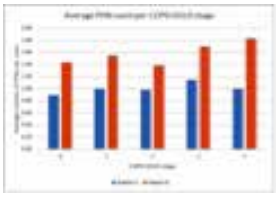

Average number of PFNs per scan across the COPD GOLD stages from two readers. Abbreviations: COPD, chronic obstructive pulmonary disease; GOLD, global initiative for obstructive lung disease; PFN, perifissural nodule.

Conclusion: Despite fair interreader agreement, higher NormES is associated with greater average numbers of PFNs. There are no statistically significant differences across GOLD stages and Pi10 quartiles. In practice, a scan may only contain whole numbers of PFNs; additionally, due to high variation, PFN count is not recommended for differentiating stages of COPD.

Preoperative CT guided wire localisation of lung nodules

S.-J. Choi, M. Darby, A. L. Johnstone, S. Karthik; Leeds/UK

Purpose/Objectives:
-To report local experience of preoperative CT guided wire localisation of the lung nodules
-To explain procedure method of CT guided wire localisation
Methods and Materials: A search was performed using our radiology information system between 1/1/2013 and 31/12/2017 for examination heading CSKMA (CT Guided skin marking). Once the data was collected, also using the hospital's electronic medical records system, data was collected on the nodule size, site, procedure related complications and pathology results.
Results: 22 patients were identified from the system of having CT guided wire localisation of lung nodule between the 5 year period. One patient had no procedure performed due to resolution of the proposed nodule on the day.
All wire localisation were performed using X-Reidy Breast lesion localisation needle (Cook Medical)
Out of the 21 patients, 10 (50%) were male and 11 (50%) female with age ranging 18-84 years and average age of 65 years. The size of the nodules for localisation ranged from 3 mm to 32 mm. 6 (27%) of the nodules were ground glass nodules.
5 of the nodules were located in left upper lobe, 4 in left lower lobe, 7 in right upper lobe, 4 in right lower lobe and 2 in right middle lobe.
7 patients had small asymptomatic pneumothorax and none of the patients required chest drain insertion.
All nodules were localised and resected subsequently with surgery. Histopathology of the nodules included lung adenocarcinoma, metastatic adenocarcinoma from bowel and breast, squamous cell carcinoma, anthracotic intrapulmonary lymph node, de-differentiated liposarcoma. One nodule had no evidence of malignancy but inflammatory changes only.
Conclusion: Our experience of CT guided wire localisation of lung nodules show that the procedure is an effective and safe method in localising pulmonary nodules for thoracoscopic resections.

Reasons for inadequate contrast in CT pulmonary angiography studies: Single-centre study in 225 consecutive patients

S. Sudarski[1], H. Haubenreisser[1], T. Henzler[1], S. O. Schönberg[1], A. Gutzeit[2]; [1]Mannheim/DE, [2]Zurich/CH

Purpose/Objectives: To retrospectively assess the incidence of and reasons for inadequate contrast enhancement in pulmonary CT angiography (CTPA) studies performed to rule out pulmonary embolism in our facility. Occurence of three reasons for inadequate contrast were assessed, namely incorrect bolus tracking, failure of i.v. contrast administration with extravasation and occurrence of the so-called TIC phenomenon (transient interruption of contrast).
Methods and Materials: In this retrospectively designed single-centre study, CTPA exams of 225 consecutive patients scanned within 4 months in our university hospital on our 16-slice single-source CT scanner system were analysed. The breathing command used in our facility for the CTPA exams is an inspirational breath-hold command. Exams were screened for non-adequate pulmonary artery contrast as follows: HU values in the thoracic aorta and in the pulmonary trunk were assessed in duplicate measurements and the aorto-pulmonary ratio was calculated. An aorto-pulmonary ratio > 1 was defined as inadequate

contrast. Three different reasons for inadequate contrast were differentiated: 1. due to incorrect bolus tracking 2. failure of i.v. contrast administration 3. in case of 1. and 2. not being present, inadequate contrast was defined to due presence of TIC (transient interruption of contrast). In case of inadequate contrast, the bolus-monitoring scan was looked at in the first place to exclude incorrect bolus tracking, and in the second place the medical report was screened for comments hinting at failure of i.v. contrast administration and in the third place the PACS system was checked for possible repetition of the whole scan.
Results: 225 patients (mean age: 65 ± 19 years, span: 18 to 99 years) were included in the analysis. In all patients the aorto-pulmonary ratio could be measured and in all patients with inadequate contrast, the reason for the latter could be retrospectively determined. In 3/225 patients (1.3%) bolus tracking was performed incorrectly. In 0/225 patients, i.v. contrast administration failed resulting in extravasation. 48/225 patients (21.3%) had an aorto-pulmonary ratio >1 and none of the other two reasons for inadequate contrast were present, being consequently classified as occurrence of TIC.
Conclusion: The most common reason for inadequate contrast in CTPA studies in our facility was occurrence of TIC in around 1/5 of the patients, followed by incorrect bolus tracking in around 1% of the patients.

Perceived quality measurement of low-dose lung CT after retrospective neural network image enhancement

Y. Nagaraj, L. B. van Den Oever, J. Guo, M. Oudkerk, P. M. van Ooijen; Groningen/NL

Purpose/Objectives: Image quality and reliability are critical for both diagnostic assessment and quantitative analysis of medical images. Emphysema screening or interstitial lung diseases are usually visually assessed using low dose CT (LDCT) and it is important for any enhancement technique to maintain the quality of the images. Most quantitative measures for image quality use 2D features, while for many diseases, 3D features are an important tool for assessment. The structural similarity index measurement (SSIM) will allow us to assess image quality without losing information added by using 3D images. Another advantage of SSIM is that it is a strong measurement tool for luminance and contrast. Aim of this work is to use SSIM to analyse the visual image quality of LDCT after an artificial neural network image enhancement technique
Methods and Materials: 24 LDCT were randomly selected from a population based lifeline cohort with different reconstruction kernel Br40 & QR59. All LDCT images are enhanced using artificial neural network technique (Pixelshine-AlgoMedica, Palo alto, California, USA). The image quality assessment between original LDCT and the enhanced LDCT consisted of three parts. First, the strong dependencies amongst pixels and its neighbouring pixels are measured both in 2D and 3D by using the SSIM. Next, we measure the error sensitivity with peak signal-to-noise-ratio (PSNR) and mean squared error (MSR) between the original and enhanced image with respect to each reconstruction kernel separately. Finally, the enhancement technique was applied multiple times and PSNR and SSIM measured between the images that are enhanced once and the ones that are enhanced twice.
Results: Mean values of the SSIM index were good in 2D and 3D between the original and processed images (0.9945 and 0.8845 respectively). Average of PSNRs measured between the original and post-processed images is good (77.41 dB) and the MSRs remained negligible. The SSIM between images once and double processed was 0.9982 for the 2D and 0.8699 for the 3D.
Conclusion: The SSIM and PSNR values measured between reference and enhanced image showed quality improvement with respect to the reference image. According to results, the artificial neural network image enhancement technique may improve the image quality without inducing noticeable changes to the original image. Furthermore, the enhancement technique can be reiterated for a greater effect. Clinical effect on the diagnostics of homogeneity and heterogeneity in emphysema has to be further explored.

Analysis of multi-parametric radiomics from low-dose CT scans for better discrimination be-tween non-emphysematous and emphysematous lung tissue

Y. Nagaraj, S. Zheng, M. Rook, Q. Li, G. J. Pelgrim, M. Oudkerk, P. M. van Ooijen; Groningen/NL

Purpose/Objectives: Chronic obstructive pulmonary disease (COPD) is one of the most common diseases worldwide, and its prevalence and mortality rates continue to rise. COPD comprises several diseases, including emphysema and chronic bronchitis. Emphysema is a heterogenous disease that can be detected by low-dose computed tomography (LDCT). In order to understand the distribution and heterogeneity of lung emphysema in CT, it is necessary to consider all clinical features that are quantifiable. In this study, we have analysed the radiomic features that can discriminate between emphysema and healthy lung tissue. This aids modelling early stages of the disease and establishing a differential diagnosis.
Methods and Materials: Our study considered 84 regions of interest (ROI) from 37 LDCT scans that were randomly selected from a large lung cancer screening trial. Experienced radiologists placed free form ROIs without overlapping between selected regions and avoiding pleural regions. Around 490 semantic and agnostic features were extracted using radiomics from each ROI. Statistical analysis was performed to check the variability between non-emphysema and emphysema patches using non-parametric Kolmogorov-Smirnov (KS) and Mann–Whitney post-hoc (MWph) tests.
Results: Among features extracted between two groups 159 features showed significant value ($p<0.05$) using MWph and KS test. This features included Gray-Level Co-Occurrence Matrix (GLCM), Gray-Level Run-length Matrix (GLRL), 1st order histogram features, shape descriptors and two image filters. In order to remove variables that were redundant, we cross-validated the results using generalised linear model with binomial regression. This resulted in 14 features: seven GLCM, four GLRL, two first-order features and cluster tendency showed higher variation coefficients between emphysema and non-emphysema patches.

Conclusion: In this study, we investigated the sensitivity of radiomics based quantitative descriptors of pulmonary low dose CT. A radiomics based multi-parametric method is feasible for discriminating between pulmonary tissue with and without emphysema. Potentially, it will become a valuable tool in early detection of emphysema. Further analyses are needed to achieve higher accuracy in discriminating emphysema from other pulmonary diseases.

ORAL CARDIOVASCULAR

Interobserver Agreement in Mapping Parameters compared to Lake Louise Criteria for the Assessment of Myocarditis by Inexperienced Observers

M. T. A. Wetscherek[1], W. Rutschke[2], C. Frank[3], M. Grothoff[2], P. Lurz[2], H. Thiele[2], M. Gutberlet[2], C. Lücke[2]; [1]Cambridge/UK, [2]Leipzig/DE, [3]Stuttgart/DE

Purpose/Objectives: To investigate the observer agreement of minimally trained readers for the assessment of myocarditis by using native T1 and T2 relaxation times, postcontrast T1 relaxation time and extracellular volume (ECV) fraction, in comparison to the well-established parameters within the Lake-Louise criteria: edema ratio (ER) and early gadolinium enhancement ratio (EGEr).
Methods and Materials: Data were collected retrospectively on 71 consecutive patients with clinically suspected myocarditis who underwent a complete diagnostic workup according to current guidelines. Cardiac MRI was performed using a 1.5 T equipment with a protocol including: cine imaging, short-tau inversion recovery, native T2 mapping, pre- and postcontrast T1-weighted turbo spin-echo and T1 mapping, and postcontrast short-axis phase sensitive inversion-recovery. To test for interobserver agreement, the determination of the myocardial native T1 and T2 relaxation times, postcontrast T1 relaxation time, ECV, ER and EGEr was done by two medical school graduates after a comprehensive training that included tutorials and case-by-case discussions. Bland-Altman analysis and intraclass correlation coefficients (ICCs) were assessed.
Results: The final analysis included 58 patients (mean age 47 ± 18 years; male:female, 33:25). 27 patients (47%) were diagnosed with chronic myocarditis, 21 subjects (36%) were diagnosed with dilated cardiomyopathy and/or hypertensive heart disease, while 10 patients (17%) showed unremarkable investigations and were included into the control group. The mean difference between the two readers was -0.3 ± 0.9 ms for T2 relaxation time, 2.4 ± 13.3 ms for native T1 relaxation time and 0.7 ± 6.9 ms for postcontrast T1 relaxation time. The interobserver mean difference for ECV values was -0.2 ± 1.3 ms. The ICCs were excellent between the two observers for all mapping parameters, ICC > 0.977, p < 0.001. Interobserver agreement was lower for ER (ICC = 0.841) and EGEr (ICC = 0.818). The mean difference for ER and EGEr between the two observers was -0.03 ± 0.13 and -0.3 ± 1.7, respectively.
Conclusion: Excellent levels of agreement can be obtained from minimally trained observers for the assessment of myocarditis by using native T1 and T2 relaxation times, postcontrast T1 relaxation time and ECV. Mapping parameters show better interobserver agreement than the Lake-Louise criteria. These results might prove useful to optimize the workflow in a busy clinical setting.

Biventricular intramural motion adaption correlates with electromechanical remodeling in repaired tetralogy of Fallot using tissue phase-mapping cardiac MR

M.-T. Wu[1], M.-C. Chang[2], K.-P. Weng[1], M.-Y. Su[3], H.-C. Huang[1], H.-H. Peng[2]; [1]Kaohsiung/TW, [2]Hsinchu/TW, [3]Taipei/TW

Purpose/Objectives: To investigate the intramural mechanism of right and left ventricular adaptive remodeling in patients with or without residual right ventricular outflow track (RVOT) obstruction after repairment of tetralogy of Fallot (rTOF).
Methods and Materials: We recruited 32 rTOF patients and 38 age- and gender-matched normal subjects for CMR. Catheterized pressure gradient between RV and pulmonary artery (PGRVPA) was performed in the patients, which were further divided by PGRVPA into rTOF-1, without residual RVOT obstruction (PGRVPA<15 mmHg, N=19) or rTOF-2, with RVOT obstruction (PGRVPAÐ15 mmHg, N=13).
Results: As compared to normal group, the rTOF patients presented decreased RV ejection fraction (EF) solely in rTOF-1 (P<0.05). As for intramural motion, rTOF-1 showed decreased systolic and diastolic Vz in both RV and LV, while rTOF-2 showed such change only in RV. Solely in rTOF-1, RVEF significantly correlated with RV systolic Vr (R=0.56, P<0.05) while LVEF correlated with LV systolic Vz (R=0.51, P=0.02). In addition, QRS prolong correlated with RV systolic Vr (R=-0.58, P<0.01) and LV diastolic Vr (R=0.81, P<0.001). None of abovementioned correlation existed in rTOF-2.
Conclusion: With the use of advanced CMR, we revealed the intramural mechanism of electromechanical ventricular remodeling in rTOF, which showed differential impact of longitudinal and radial motion in RV and LV remodeling respectively in rTOF-1. Avoidance of unfavorable functional interaction in both RV and LV in rTOF-2 suggested that a proper RVOT obstruction plays a protective effect in all aspects of the ventricular remodeling of rTOF.

Low contrast CT angiography prior to TAVI procedure: Feasibility, renal safety and diagnostic accuracy for coronary tree

A. D. Annoni, D. Andreini, G. Pontone, M. E. Mancini, A. Baggiano, A. Formenti, G. Muscogiuri, S. Mushtaq, E. Conte, M. Pepi; Milan/IT

Purpose/Objectives: To evaluate feasibility, image quality and accuracy of a reduced contrast volume protocol for pre-procedural CT imaging in transcatheter aortic valve implantation (TAVI) using a third generation wide array CT scanner
Methods and Materials: 115 consecutive patients (51F, mean age 82.5±6.2y, mean BMI 26.7±3.6) referred for TAVI were examined with wide-array CT scanner with a combined scan protocol: retrospective ECG-gated axial CTA of the heart and thoracic aorta

followed by a high-pitch spiral CTA for abdominal aorta and iliac-femoral arteries. A total amount of 50 ml contrast agent was used. Image quality was graded on a visual scale (4-1). Contrast attenuation values (HU) and contrast-to-noise ratio (CNR) were measured at the level of the aortic root, ascending/descending aorta, subrenal aorta and at the level of right and left common femoral arteries. Coronary tree was assessed. Aortic annulus measurements were compared with final procedural results. Patients creatinine was monitored at the baseline and 72h after procedure
Results: No exams were classified as not diagnostic. Mean quality score was > 3. Mean HU and CNR at the aortic root, ascending/descending aorta subrenal aorta and at the level of right and left common femoral arteries were: 578.4±55.5, 582.2±77.4, 553.1±83.4, 525.2±67.6, 510.7±93.4, 498.3±52.1 HU respectively and 14.8±2.3, 15.7±1.7, 14.9±3.1, 15.8±4.7, 20.3±9.9, 20.8±6.9 respectively. 113 out 115 pts underwent TAVI procedure. In 111 pts (95%) CT measurements were comparable to the size of the implanted valve prosthesis. Only 1 patient had severe paravalvular regurgitation. Mean creatinine before CT and 72h after procedure were 1.21±0.52 and 1.22±0.49 mg/dl. Mean DLP was 442.4±21.2 mGy/cm
Conclusion: CT with low contrast volume is feasible and clinically useful, allowing precise pre-procedural TAVI planning with accurate assessment of coronary tree, reducing the risk of contrast induced nephropathy and risks related to unnecessary coronary angiographies

Left atrial functional impairment in patients with cryptogenic stroke as quantified by cardiac magnetic resonance

W. Staab, A. Schuster, L. Wandelt, M. Steinmetz, G. Hasenfuß, C. Unterberg-Buchwald, R. Wachter, J. Lotz, J. T. Kowallick; Goettingen/DE

Purpose/Objectives: In 1/4 of patients with ischemic stroke, no etiologic factor can be identified. Asymptomatic paroxysmal atrial fibrillation (AF) is often suspected to be the cause of these cryptogenic strokes (CS). AF is frequently associated with left atrial (LA) structural and functional alterations. Accordingly, the aim of this study was to examine LA deformation in patients with CS using cardiovascular magnetic resonance myocardial feature tracking (CMR-FT).
Methods and Materials: 29 patients with the diagnosis of CS underwent CMR imaging. Based on the initial cranial computed tomography (cCT), the patient group was divided into patients with previous ischemic lesions (recurrent CS) and patients without (first-time CS). LA deformation was analyzed based on CMR-FT of standard cine 4- and 2-chamber views including LA reservoir function (peak total strain [e_s], peak positive SR [SRs]), LA conduit function (passive strain [e_e], peak early negative SR [SRe]) and LA booster pump function (active strain [e_a], late peak negative SR [SRa]). Moreover, the „time to e_s" and „time to SRs" were calculated and expressed as a percentage of the entire cardiac cycle (Figure 1).

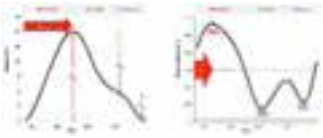

Results: Previous ischemic lesions were detected in 5 of 29 patients (17%). LA conduit strain was lower in patients with recurrent CS as compared to first-time CS (6.4 ± 1.1 % vs. 10.3 ± 3.3 %, respectively, p=0.005). Furthermore, „time to e s" and „time to SRs" were prolonged in patients with recurrent CS (47 ± 6 % vs. 57 ± 8%, p=0.007; and 19 ± 5% vs. 30 ± 7%, p=0.001, respectively). In multivariable regression models „time to e_s" and „time to SR" were independently associated with the presence of previous ischemic lesions (β=0.41, p=0.006 and β=0.51, p=0.015, respectively) after adjustment for traditional risk factors (age, gender, arterial hypertension, vascular disease and diabetes).
Conclusion: Prolonged time to peak LA reservoir strain and SR is associated with the presence of previous ischemic lesions in patients with CS. These findings propose advanced LA impairment as a distinct feature of CS which may be associated with unrecognized paroxysmal AF. Future research is warranted to confirm these findings alongside their prognostic implications in larger prospective clinical trials.

CT-Coronary Angiography in asymptomatic male patients with high atherosclerosis risk: Is it justified?

A. Hatzidakis, E. D. Savva, K. Perisinakis, N. Kosidekakis, A. Papadakis, M. Hamilos, G. Kochiadakis, A. Karantanas; Heraklion/GR

Purpose/Objectives: To study the necessity of coronary artery screening with CT-Coronary Angiography (CTCA) in asymptomatic male patients over 50 years with atherosclerotic risk factors.
Methods and Materials: 116 asymptomatic male patients aged over 50 years were included in this prospective study according to a clinical protocol approved by our hospital's ethical committee. All participants had at least 3 risk-factors for coronary atherosclerosis development. Risk factors for coronary disease development included smoking, diabetes mellitus, hypercholesterinaemia, hyperlipidaemia, arterial hypertension, stress, increased BMI, positive family history and lack of physical activities. All patients had previous normal non-invasive cardiologic tests and no contraindications for CTCA. All participants gave informed consent after being notified regarding contrast medium and radiation dose risks.

Results: Significant stenoses were found in 28 patients (24%). Out of them, 24 underwent invasive coronography. In 9 no lesions were found (37.5%). From the other 15 (62.5%), stent placement was performed in 7, by-pass surgery was proposed in 2 and in another 6 conservative treatment was suggested. The patients with positive CTCA had significant higher rate of risk-factors, especially diabetes (50% vs 18%), hyperlipidaemia (53% vs 13%) stress (65% vs 20%) and positive family history (65% vs 16.4).
Conclusion: CT-Coronography might be proposed for asymptomatic male patients over 50 years, especially in presence of positive family history, stress, hyperlipidaemia or diabetes.

Evaluation of the mitral valve anatomy, geometry and mobility in multiple cardiac phases by Multi-Slice Computed Tomography

L. Musayeva[1], S. Sündermann[2], N. Solowjowa[2], J. Kempfert[2], V. Falk[2]; [1]Baku/AZ, [2]Berlin/DE

Purpose/Objectives: Objective of this study was to assess the mitral valve anatomy, geometry and mobility of healthy subjects (control group) and of patients with FMR by multi-phase MSCT throughout the entire cardiac cycle in regards of optimization of the planning of transcatheter mitral valve procedures. Considering a great number of elderly and/or high-risk patients with FMR, new minimally invasive and catheter based therapies can be method of choice for them and image based planning of these procedures is crucial.
Methods and Materials: 24 healthy patients vs. 22 patients with varying degree of FMR who had undergone ECG-gated CTA were retrospectively evaluated. Mean age was 47 ± 11 vs. 63 ± 7 years (p<0,05), male gender 75 % vs. 68 % (ns), BMI 26 ± 2.8 kg/m^2 versus 26 ± 3.5 kg/m^2 (ns), LVEF 72 ± 6 % vs. 31 ± 9 % (p<0,05), LVEDD 55.3 ± 5.4 vs. 81 ± 11 mm(p<0,05). MV analysis was performed by 3mensio structural heart software (8.0 module; Pie Medical Imaging, the Netherlands), volumetric evaluation of the heart chambers was made using Syngo.via software (Siemens AG, Germany). The evaluation of MA surface, entire circumference, projected circumference, trigone-to-trigone distance and septal-to lateral distances for saddle-shaped and D-shaped mitral annulus, and annulus height for saddle-shaped annulus, aortic-mitral annular angle, LA to LV axis angle and MA to papillary muscles distance was done for all patients in both groups for ten phases (CT data was reconstructed in 10% intervals throughout the entire cardiac cycle).

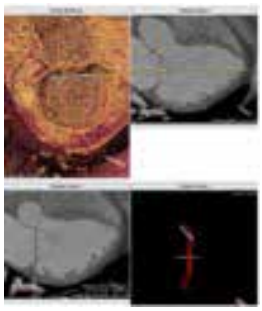

Mitral Valve annulus

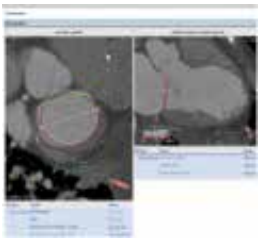

Saddle-shaped Mitral annulus

volume rendered Mitral annulus

Results: The mean MA annular circumference averaged 17 ± 7.4 mm in control group, 11 ± 13,9 mm in patients with FMR, being significantly different between two groups. Trigonum-to-trigonum distance was larger in healthy subjects than in patients with FMR; 6 ± 1.9 mm vs. 5 ± 1 mm (P<0,06). Aortic – mitral angle average for healthy subjects is 15 ± 6.2° vs. 12 ± 3.9°. There are also differences in the annulus to anterior papillary muscle distance, but not to the posterior papillary muscle. Additionally, the mobility of the mitral annulus is higher in healthy patients than in patients with FMR.
Conclusion: In the present study, MSCT data demonstrates significant differences in the mitral valve morphology in 2D and 3D assessments between healthy subjects and patients with FMR. Taking into account low mobility of the mitral annulus throughout the cardiac cycle in patients with FMR, multiphase MSCT might not be necessary for planning of transcatheter mitral valve interventions.

Determining the level of agreement for atherosclerotic cardiovascular disease risk stratification between coronary artery calcium score and traditional cardiovascular risk models

I. M. Kuria, S. Vinayak, K. Were, H. Otieno; Nairobi/KE

Purpose/Objectives: To determine the level of agreement between coronary calcium score and traditional cardiovascular risk models for coronary artery disease risk stratification in a multi-ethnic population at a tertiary institution in East Africa.
Methods and Materials: A cross-sectional study.
The data was collected retrospectively from the medical records of 200 patients referred to the Radiology department for a CT coronary artery calcium score. However, only 190 patients met the inclusion criteria were included in the analysis. Risk stratification comparisons were done according to Coronary Artery Calcium Score(CACS), Framingham Risk Score (FRS),

American Heart Association (AHA) and the American College of Cardiology guidelines (ACC/AHA) and World Health Organization/ International Society of Hypertension (WHO/ISH) and the agreement (Kappa) and correlation (Spearman rho) between them were calculated. Statistical significance was set at $p < 0.05$, and analyses were performed using the STATA 14.0 software.
Results: There was poor agreement (Kappa >0.191) between CACS and the clinical Cardiovascular Disease (CVD) risk models. In relation to this, 83.6%, 81.8 % and 66.2% of the intermediate risk group according to FRS, ACC/AHA and WHO/ISH, respectively, were down-classified by CACS while 9.1%, 13.6% and 13.8% of the same cohort were up-classified to high risk by CACS. Moreover, CACS recommended aggressive management, which includes statin therapy to 5.8%, 5.5% and 8.9% of the subjects who would not have been aggressively managed as per FRS, ACC/AHA and WHO/ISH, respectively. Conversely. 81.6%, 84.6% and 66.7% of those who would qualify for aggressive management as per FRS, ACC/AHA, and WHO/ISH risk-based algorithms, respectively, would not qualify for the same management as per the CACS as a tool for risk categorization.
Conclusion: The poor agreement between CACS and the clinical CVD risk scores suggests that the clinical CVD risk tools currently used in our East African population might be incorrectly stratifying risk in patients and a prospective study is needed to help improve risk predictions and set appropriate population-wide thresholds that are necessary to facilitate better clinical decision making.

Can Cardiac Magnetic Resonance Feature Tracking Predict Clinical Cardiovascular Events in Asymptomatic Aortic Stenosis Patients with Normal Ejection Fraction?

M. Y. Kim, E.-A. Park, W. Lee, S.-P. Lee; Seoul/KR

Purpose/Objectives: To determine the most valuable cardiac magnetic resonance (CMR) strain parameters for evaluating aortic stenosis (AS) and to assess whether they predict clinical cardiovascular events (CVEs) in asymptomatic AS patients with normal ejection fraction (EF).
Methods and Materials: As a prospective study, 123 moderate to severe AS patients (60 males, age 68.6±9.20) and 32 control subjects (14 males, age 67.9±4.35) were enrolled. They underwent echocardiography and 3 T CMR imaging. Short axis and 2-, 3-, and 4-chamber cine images were analyzed using feature tracking software (Circle, cvi42, Canada) to assess left ventricle (LV) radial, circumferential and longitudinal strain parameters including peak strain (PS), time to peak of strain (T2PS), PS rates, peak displacement, time to peak of displacement and peak velocities in 2-and 3-dimensional manners (Figure 1). After obtaining CMR imaging, CVEs, including cardiac death, heart failure, and AS-associated symptom development, were followed up for the median 32.6 months (8.7-53.2 months). The prognostic factor of CVE in asymptomatic AS patients with normal EF was chosen by logistic regression.

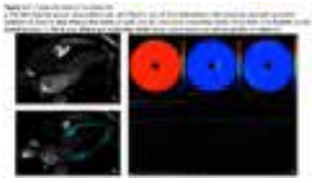

Figure 1 LV strain assessment.

Results: All global PSs were lower and four global T2PSs were longer in AS patients than in controls ($p<.05$, Table 1). Severe AS patients showed more impaired PS values than moderate AS ($p<.05$, Table 1). Trend analysis demonstrated that two-dimensional (2D) long-axis (LAX) global radial and longitudinal PSs and LAX radial T2PS revealed the significant gradual increasing or decreasing trend in the order of control, moderate, and severe AS groups ($p<.000$, Table 1). There were significant linear correlations between global PS parameters and other several cardiac functional indices ($p<.05$, Table 2). Twenty two of 60 asymptomatic AS patients with normal EF experienced CVEs during the follow-up period. Using logistic regression, 2D LAX global longitudinal PS remained as the only risk factor for CVE among various clinical and imaging parameters ($p=.019$). The receiver operative characteristic (ROC) curve analysis for 2D LAX global longitudinal PS for predicting CVE revealed area under the ROC curve (AUC) of 0.656 and criterion of -17.89% (Figure 2). The relative risk for CVE was 3.9 ($p=.016$, 95% confidential interval: 1.2-11.9) based on LAX global longitudinal PS with a cutoff of -17.89%.

Table 1 Differences of feature tracking global parameters between control and AS subjects and between moderate and severe AS subjects.

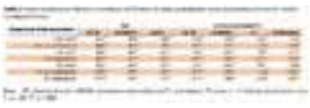

Table 2 Linear correlation (Pearson correlation coefficient) between global peak strain parameters and other cardiac functional indices.

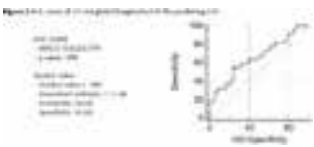

Figure 2 ROC curve of 2D LAX global longitudinal PS for predicting CVE.

Conclusion: Two-dimensional LAX global longitudinal PS, and 2D LAX global radial PS and T2PS can reflect cardiac dysfunction according to the degree of AS. Two-dimensional LAX global longitudinal PS may be one of the most potent predictive factor for CVE in asymptomatic AS patients with normal EF.

3D multimodal image fusion – combined information about cardiac morphology, coronary FFR, myocardial perfusion, and scar

J. von Spiczak[1], M. Mannil[1], R. Manka[1], S. Oebel[1], S. Hamada[2], H. Alkadhi[1]; [1]Zurich/CH, [2]Aachen/DE

Purpose/Objectives: To allow for comprehensive diagnostics of coronary artery disease (CAD) by 3D image fusion of CT coronary angiography (CT-CA, for morphological information), CT-CA derived fractional flow reserve (CT-FFR, for stenosis assessment), dynamic whole-heart 3D cardiac MR stress perfusion (CMR-Perf, for ischemia diagnostics), and MR late gadolinium enhancement (CMR-LGE, depicting myocardial scar).
Methods and Materials: 10 patients (63±14 years, one female) who underwent CT-CA, CMR, and catheter coronary angiography (CA) in our hospital due to suspected CAD were included retrospectively. A method facilitating 3D fusion of multimodal cardiac image data was developed. Postprocessing of CT data included: a) automatic segmentation of the coronary tree and heart contours; b) automatic calculation of CT-FFR values applying machine learning based on a coronary artery model database; c) color-coding of the coronary tree according to CT-FFR. Postprocessing of CMR data included: a) manual segmentation of the left ventricle (LV) in CMR-Perf and CMR-LGE datasets, b) semi-automatic co-registration of CMR datasets (acquired in short-axis geometry) to CT data (axial acquisition), c) mathematical projection of CMR-Perf and CMR-LGE values onto the high-resolution LV derived from CT datasets. For CMR-Perf, signal intensities of more than 2 standard deviations below the mean value of healthy remote tissue were considered as pathologic hypoperfusion. For CMR-LGE, values above half the overall maximum were considered as scar (“full-width-half-maximum” criterion). CMR-LGE values were graduated according to the degree of transmurality. Multiple color tables encoding complementary information were chosen carefully to avoid confusion. All resulting datasets (i.e., heart contours, coronary tree with color-coded FFR, LV with perfusion values and transmurality of myocardial scar) were combined and visualized in 3D volume rendering software. Results of hybrid 3D analysis were compared to separate readouts from CT-CA, CMR, and results from CA.
Results: Multimodal 3D image fusion was feasible in all cases. 3/10 patients showed no pathologic findings. 7/10 patients showed coronary stenosis, perfusion deficits, and/or myocardial scar to different extents. Perfusion deficits and myocardial scar could be correlated to culprit coronary lesions where applicable. Relevance of stenoses seen in CT-CA was re-judged in 4/10 cases. Assumed supply territories of CMR-Perf perfusion deficits were refined in 2/10 cases. In one case with myocardial hypoperfusion but no coronary stenosis (assumed false positive in conventional readout), ischemia could be explained by a narrow coronary artery with pathologic FFR (Figure 1). Results from CT-CA were in good accordance with CA.

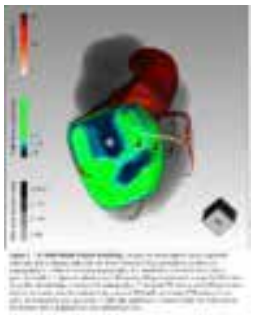

Figure 1. 3D Multi-Modal Volume Rendering.

Conclusion: Hybrid 3D cardiac imaging is feasible and offers comprehensive, non-invasive CAD diagnostics.

A new approach to manage the absence of full recovery of the longitudinal magnetization between the Look-Locker blocs in MOLLI sequence: Temporal registration, in vitro and in vivo

H. Rebbah[1], T. Galas[1], A. Menini[2], G. Soulat[1], C. A. A. Cuenod[1], E. Mousseaux[1]; [1]Paris/FR, [2]Munich/DE

Purpose/Objectives: The Modified Look-Locker Inversion recovery (MOLLI) is a well-established sequence for T1 mapping. However, the absence of full recovery of the longitudinal magnetization before a new inversion pulse leads to discrepancies between signals of each Look-Locker (LL) and consequently to a lower accuracy of T1 estimates. This point is particularly met for long T1.
Two main solutions were proposed to limit this issue of the MOLLI sequence. A first technique, The ShMOLLI assumes that for long T1, the signal of the first LL is enough for T1 estimation and a second technique uses the dynamic of the first LL’s signal for all the LL blocs, so the non-recovery of the signal of first LL doesn’t impact the estimation.
Methods and Materials: The signals of each LL are used independently while assuming that they should have the same parameters, with a simple time shift of the affected LL’s signal defined by: $Si(t) = Ai - Bi \exp(-(t+tOi)/T1i^*)$, where tOi is the shift of the ith LL. To estimate tOi we used the variation of the signal between the previous LL’s equation and the observations of the current one and then we applied a temporal registration to the signal.
Tubes with growing concentration of Gadolinium based agent and the hearts of 5 volunteers were scanned on a 3T GE system, with

different MOLLI schemes at different heartrate, see table 1. T1 values obtained with the widely used basic fit (Levenberg-Marquardt) without (BF) and with the aforementioned temporal registration (BFR) were compared with reference IR-Spin-Echo (IR) based on the mean value of the ROIs and the relative mean error and their reproducibility (coefficient of variation).

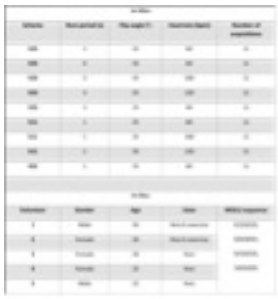

Table 1 - Liste of experiments in vitro and in vivo

Results: As compared to BF, BFR resulted in a significant decrease of error (around 10%) overall the schemes in regard to the IR (subfigure 1b). They also show an increase of reproducibility between MOLLIs (figure 2). This last point is also observed in the in vivo experiments, where it leads to a higher stability of the T1 map (figure 3).

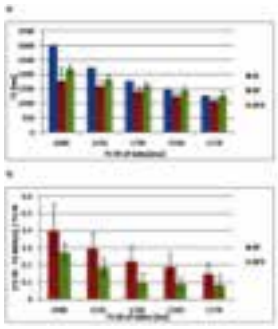

Figure 1 - Tubes results: a) IR values and Mean and SD of T1 overall the schemes at all the different heartrate for the BF and basic fit with temporal registration (BFR); b) Relative error as compared to the IR with SD for BF and BFR.

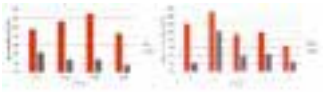

Reproducibility overall the schemes at all the heartrates for BF and BFR in vitro (left) and in vivo (right).

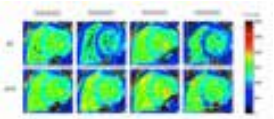

Figure 3 – T1 mapping BF based (first line) and BFR based (second line) for different MOLLI schemes (columns) applied on the first volunteer.

Conclusion: To handle the absence of full recovery between LLs (long T1, high heartrate and short acquisition time) we used a time registration before fitting all data set of the MOLLI sequence. The proposed technique resulted in a higher accuracy of T1 estimates and a better reproducibility than the basic fitting of all the data as performed usually.

Performance of visual Splenic Switch-off sign, splenic and myocardial T1-reactivity in the assessment of stress adequacy during adenosine Cardiac Magnetic Resonance Imaging

R. van Dijk[1], D. T. J. A. Kuijpers[2], M. van Assen[1], D. Kaandorp[2], P. van Dijkman[2], R. Vliegenthart[1], P. van der Harst[1], M. Oudkerk[1]; [1]Groningen/NL, [2]The Hague/NL

Purpose/Objectives: Caffeine is a known adenosine receptor antagonist and a possible cause of false negative cardiac Magnetic Resonance Perfusion Imaging (CMR) results due to insufficient stress. The splenic Switch-Off sign (SSO), splenic and myocardial rest-stress T1-mapping have been proposed as methods to assess stress adequacy. The purpose of our study was to compare these potential methods for stress adequacy assessment in patients with recent coffee intake.
Methods and Materials: We retrospectively assessed the occurrence of SSO and performed rest-stress T1-mapping in patients who underwent adenosine perfusion CMR at 1.5T and compared patients with recent coffee intake (<4h prior to the examination) to patients without recent coffee intake. Visual attenuation of the spleen during adenosine stress was assessed by two independent observers. Native rest-stress T1-mapping of the spleen and myocardium was performed and T1-reactivity was calculated.

Flowchart of the study population.

Results: The study population consisted of 146 patients (22 patients with and 124 patients without recent coffee intake). SSO, Splenic T1 rest, splenic T1 stress and splenic T1-reactivity values were not significantly different when comparing patients with recent coffee intake to patients without recent coffee intake. Myocardial T1 stress and myocardial T1-reactivity were significantly lower in patients with recent coffee intake (924 [879;946] and -5.2 [-8.1;-3.6]) as compared to patients without recent coffee intake (1015[998;1045] and 4.0[2.8;5.7]) both at p-value <.001.

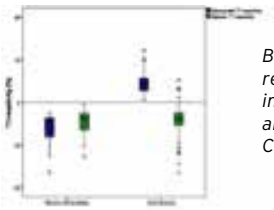

Boxplot of myocardial and splenic T1-reactivity (←T1) in patients with coffee intake <4h prior to the examination and patients with normal perfusion CMR and no recent coffee intake.

Conclusion: The SSO and splenic T1-mapping failed to accurately assess stress adequacy. Myocardial T1-reactivity were able to differentiate between patients with and without recent coffee intake.

Myocardial T1-mapping: The effects of coffee intake on the response to regadenoson as compared to adenosine during Cardiac Magnetic Resonance Perfusion Imaging

R. van Dijk[1], D. T. J. A. Kuijpers[2], D. Kaandorp[2], P. van Dijkman[1], R. Vliegenthart[1], P. van der Harst[1], M. Oudkerk[1]; [1]Groningen/NL, [2]The Hague/NL

Purpose/Objectives: The antagonistic adenosine receptor effects of caffeine are a potential cause for inadequate stress during cardiac vasodilator perfusion Imaging. Two of the most widely used vasodilator agents are adenosine and regadenoson. The purpose of this study was to assess the effects of recent coffee intake on the response to regadenoson during Cardiac Magnetic Resonance Perfusion Imaging (CMR). Furthermore, the effects of recent coffee intake on the response to regadenoson were compared to the effects on adenosine.
Methods and Materials: Patients referred for either adenosine or regadenoson perfusion CMR with suspected coronary artery disease (CAD) were included in the analysis. The following groups were recognized: patients with recent coffee intake (<4h prior to the examination) and patients without recent coffee intake. Native rest-stress T1-mapping was performed using a modified-look-locker inversion recovery sequence and T1-reactivity was calculated as the percentage of change from rest to stress.

Overview of the cardiac CMR protocol.

Results: 98 patients were included in the final analysis (24 with recent coffee intake and 74 patients without recent coffee intake). There was no significant difference between T1-rest, T1-stress, and T1-reactivity in the regadenoson perfusion CMR group when comparing patients with recent coffee intake (n=9) with patients without recent coffee intake (n=24). In patients with recent coffee intake both T1-stress and T1-reactivity were significantly lower in patients undergoing adenosine perfusion CMR (898±51ms, and -7.8±5.0%) as compared to regadenoson perfusion CMR (1019±48ms, and 4.4±3.2%).

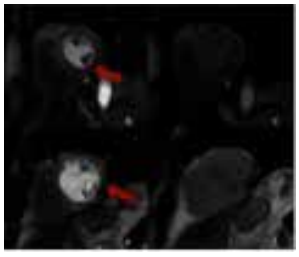

Myocardial ischemia assessment in two patients who consumed coffee several hours before Regadenoson perfusion CMR study. In both patients ischemia detection was still possible despite of recent coffee intake.

Conclusion: In contrast to adenosine, coffee intake prior to regadenoson perfusion CMR has no effect on myocardial T1-reactivity.

Association of Lung Volume and Subclinical Cardiac Impairment using Whole-body MR Imaging: A Population-based Cohort Study

R. von Krüchten[1], R. Lorbeer[2], T. Zitzelsberger[3], C. Schuppert[1], C. Storz[3], H. Schulz4, H.-U. Kauczor[1], S. Karrasch[4], F. Bamberg[3], C. L. Schlett[1]; [1]Heidelberg/DE, [2]Munich/DE, [3]Tübingen/DE, [4]Neuherberg/DE

Purpose/Objectives: Several studies have shown that obstructive lung disease (COPD) is associated with cardiac impairment. Recently, we showed that whole-body MR-derived lung volume best correlates with residual capacity as derived by pulmonary function tests, and is associated with chronic obstructive lung disease in a population-based cohort. Thus, our aim was to determine the association between MR-derived lung volume and cardiac impairment in a general population.
Methods and Materials: A total of 400 subjects from the population-based KORA-FF4 study with no history of cardiovascular disease underwent whole-body MR imaging. Lung volumes were derived from coronal acquired T1w sequences with semi-automatic segmentation using an in-house developed algorithm. Standard MR parameters of the right(RV)- and left-ventricle(LV) were derived from cine-SSFP sequences using cvi42 (v4.1.5), while LV filling rates were assessed using an in-house developed algorithm (pyHeart). Cardiac volumes and mass were standardized to body surface index. Associations were assessed by Pearson correlation and multivariate linear regression adjusting for age, sex, smoking status and BMI.
Results: MR-derived RV and LV parameters as well as lung volumes were available in 356 subjects (56.1±9.1 years, 43% female). The total MR-based lung volume was 4.0±1.1L; most cardiac parameters ranged within standard values (Figure 1). LV peak ejection rate was 359.9±132.6 (ml/s), while the early diastolic filling rate was not significantly higher than the late diastolic filling rate (231.5±115.7 vs 230.0±109.3, p=0.82). In univariate analysis, particularly RV and LV stroke volume were negatively correlated with lung volume (Figure 2). After multivariate adjustment, MR-based lung volumes were negatively associated with end-diastolic volumes and stroke volumes for both RV (β=-2.14, p=0.02; β=-1.45, p=0.004, respectively) and LV (β=2.75, p=0.001; β=1.73, p=0.001; respectively), but not with ejection fraction (all p≥0.32, Figure 1). All associations were stronger for LV than for RV. For LV, early but not late diastolic filling rate was negatively associated with MR-based lung volumes (β=-17.3, p=0.006 and β=-11, p=0.08, Figure 1). Peak ejection rate and myocardial mass were not significantly associated with lung volumes (all p≥0.18).

Figure 1. Association of MR-based Lung Volume with Cardiac Measurements

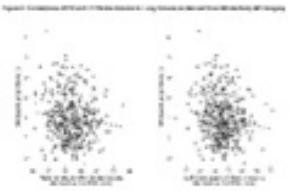

Figure 2. Correlations of RV and LV Stroke Volume to Lung Volume as derived from Whole-Body MR Imaging

Conclusion: Using whole-body MR imaging to assess both pulmonary and cardiac function, we found a significant negative association between lung volumes and subclinical changes in certain cardiac parameters and hemodynamics in subjects without cardiovascular disease. On multivariate analyses, biventricular end-diastolic and stroke volumes but not ejection fractions, and early diastolic LV filling rate were negatively associated with lung volume.

Vascular thoracic outlet syndrome: A focus on Time-Resolved MR Angiography

S. Wassef, A. Stolpen; Iowa City, IA/US

Purpose/Objectives: The purpose of this presentation is to review the role of contrast-enhanced time-resolved MR Angiography (TR-MRA) in the evaluation of vascular thoracic outlet syndrome (TOS). After reviewing this exhibit, the reader will be able to recognize (1) the pathology underlying vascular TOS, (2) the characteristic findings of vascular TOS on TR-MRA, and (3) the strengths and weaknesses of TR-MRA for evaluating TOS.
Methods and Materials: Thoracic outlet syndrome (TOS) is caused by compression of either the subclavian vessels (vascular TOS) or the brachial plexus (neurogenic) most commonly in the costoclavicular
area. Vascular TOS can lead to pulmonary embolism, venous gangrene, primary effort thrombosis, digital ischemia and stroke. Serious complications of arterial TOS include critical digital ischemia and rarely stroke from retrograde embolism. Therefore early diagnosis and treatment is important.

Thoracic outlet syndrome (TOS) is caused by compression of either the subclavian vessels (vascular TOS) or the brachial plexus (neurogenic TOS). This table highlights the difference between them.

Coronal MIP images from a direct venous TR-MRA show stenosis of the right subclavian vein with the right arm raised overhead (A). The stenosis resolves when the right arm arm is down (BI)

Results: The diagnosis of TOS is made by history and physical exam. Imaging studies can only support the diagnosis and suggest an etiology. Provocative tests are usually needed, such as imaging with the arm in multiple positions. However, positional changes in vessel caliber without corresponding symptoms are not diagnostic of TOS. Studies such as electrodiagnostic tests and brachial plexus neurography can also be helpful.
Recently Time-Resolved 3D MR Angiography (TR-MRA) has been shown to be an excellent noninvasive alternative to DSA. Provocative arm positions can be employed to determine the presence and degree of vascular compression and associated complications. TR-MRA is useful to identify postoperative complications such as restenosis or residual vascular compression. For arterial TOS studies the contralateral arm is injected with undiluted gadolinium-based contrast agent (GBCA). For the venous TOS study the ipsilateral arm is injected with GBCA diluted 1:10 in saline.

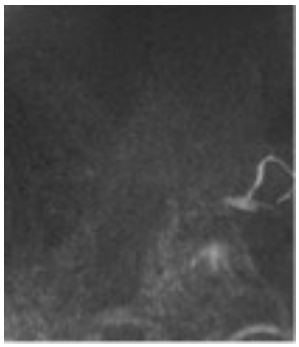

Coronal MIP cine loop from contrast-enhanced time-resolved 3D MRA shows focal stenosis of the right subclavian artery with the right arm raised overhead (A).

The stenosis resolves with the right arm down (B)

Conclusion: Time-resolved 3D MR Angiography (TR-MRA) has recently become an excellent, robust and reliable noninvasive alternative to DSA for evaluating patients with suspected vascular TOS. Provocative arm positions are employed to determine the presence, severity and site of vascular impingement and any associated complications. For unilateral arterial TOS studies, the contralateral arm is injected with undiluted gadolinium-based contrast agent. For unilateral venous TOS studies, the ipsilateral arm is injected with dilute gadolinium-based contrast. The latter technique, which is known as direct MR venography, can be performed on one or both arms. Venous TOS can also be evaluated using the arterial TOS technique, but allowing TR-MRA image acquisition to continue through the venous phase.

A new method for predicting splenic „switch-off" sign: Splenic T2-mapping

T. D'angelo[1], J. L. Wichmann[2], E. Elen[3], C. Arendt[2], S. Mazziotti[1], A. Blandino[1], G. Cicero[1], V. Puntmann[2], E. Nagel[2]; [1]Messina/IT, [2]Frankfurt am Main/DE, [3]Jakarta/ID

Purpose/Objectives: In a relevant proportion of patients undergoing myocardial first-pass perfusion cardiac magnetic resonance (FPP-CMR) inadequate adenosine stress may occur. This may cause false-negative results and a suboptimal clinical management. "Splenic switch-off" has recently been proposed as a sign to detect effective adenosine response after first-pass imaging is performed. Novel methods are emerging to detect reduction of splenic blood volume during adenosine stress and prior to contrast administration. We sought to determine the feasibility of using splenic T2-mapping as a marker to assess adenosine-stress effect.
Methods and Materials: Fifty-five consecutive patients (29 males, mean age 56.1±11.5) with clinical indications underwent FPP-CMR at 1.5T (n=16) and 3T (n=39). Splenic T1- and T2-values were assessed, using respectively MOLLI and FLASH sequences, performed at rest and during adenosine stress (140μg/kg/min, 4 min) along one mid-ventricular short-axis slice. Changes of T1- (ΔT1) and T2-values (ΔT2) were calculated and expressed as percentages. FPP-CMR was performed after intravenous injection of gadobutrol (0.1mmol/kg body-weight). Images were analyzed with the use of a semiautomatic software (Circle CMR42, Calgary, Canada) to quantify splenic and myocardial enhancement. Spleen-to-myocardium perfusion ratio (s/mΔSI) was calculated to obtain splenic relative enhancement during FPP-CMR. The presence of "switch-off" sign was evaluated in consensus by two readers and used as standard of reference. Accuracy of s/mΔSI, ΔT1 and ΔT2 in predicting the splenic switch-off sign was assessed.
Results: Mean splenic rest native T1- and T2-values were respectively 1256.7±96.5(ms) and 60.3±11(ms) at 3T, and 1149.1±75.1(ms) and 80±10.1(ms) at 1.5T, versus stress native T1- and T2-values of 1198.5±85.8(ms) and 54.1±11.2(ms) at 3T, and 1100.4±85.1(ms) and 73.3±10.9(ms) at 1.5T (all p<0.001). Splenic relative enhancement (s/mΔSI) showed a correlation of 0.701 and 0.504 respectively with ΔT2 and ΔT1 (all p<0.001). The best accuracy for predicting "switch-off" sign was obtained with ΔT2 (AUC=0.987), followed by s/mΔSI (AUC=0.962) and ΔT1 (AUC=0.912) (all p<0.001) (Fig.1). The largest difference in terms of accuracy was observed between ΔT2 and ΔT1 (0.0732; p=0.076). Cut-offs were 8.3% for ΔT2 (sensitivity: 95%; specificity 94%) and 3.6% for ΔT1 (sensitivity: 84%; specificity: 83%).

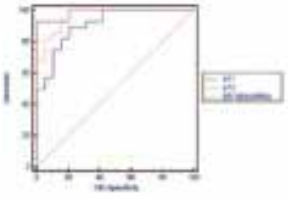

ROC Analysis

Conclusion: Splenic T2-mapping may be a helpful tool to predict splenic "switch-off" sign in FPP-CMR. This may be useful to predict an effective adenosine response and, eventually, to allow for preventive dose adaption and less false-negative results.

Compressed Sensing real-time cine imaging in patients with cardiac arrhythmia: Does it help to reduce mis-triggering artifacts?

F. Pontana[1], A. Bridoux[1], P.-E. Allard[1], M. Schmidt[2], C. Forman[2], A. Monnet[1], V. Silvestri[1], J. Pagniez[1], B. Longere[1]; [1]Lille/FR, [2]Erlangen/DE

Purpose/Objectives: To evaluate the impact of a Compressed Sensing (CS) real-time prototype cine sequence (Sparse 2D cine, Siemens Healthineers) on mis-triggering artefacts and image quality in patients with arrhythmia, in comparison with the reference cine-imaging technique.
Methods and Materials: 71 consecutive adult patients (41 males; mean age = 59 ± 20.6 years), referred for cardiac magnetic resonance (CMR) examination with concomitant irregular heart rate (defined by R-R interval variation > 10%) during scanning, were prospectively enrolled. For each patient, two series of cine images were systematically acquired: (a) a standard segmented multi-breath-hold steady-state free precession (bSSFP) sequence including short-axis stack, one four-chamber slice, one two-chamber slice (Group 1) and (b) an additional real-time CS single-breath-hold prototype sequence (Group 2) providing the same slice number, position and thickness as the reference technique. Two radiologists independently assessed mis-triggering artefacts, objective and subjective image quality for both acquisition techniques.
Results: The mean heart rate variation was 38% ± 22.8 (range: 11 - 122). A total of 609 cine slices were evaluated in each Group (mean number of slices per patient = 8.6 ± 1.9). The average number of slices with mis-triggering artefacts per patient was higher in Group 1 than in Group 2 (4.5 ± 2.9 vs 0.1 ± 0.5, p<0.0001). The European CMR registry standardized artefact score was lower in Group 2 than in Group 1 (1.0 ± 1.2 vs 2.37 ± 1.2 respectively, p<0,0001). Subjective image quality score was improved in Group 2 compared to Group 1 (3.3 ± 0.9 vs 2.7 ± 1.0 respectively, p=0.0002).
Conclusion: Compressed Sensing real-time cine imaging drastically reduces mis-triggering artefacts and improves image quality of CMR cine acquisition in patients with arrhythmia.

Assessment of left-ventricular-wall motion disorders after myocardial infarction using Compressed Sensing real-time cine imaging

F. Pontana[1], M.-H. Chavent[1], V. Silvestri[1], M. Schmidt[2], C. Forman[2], A. Monnet[1], J. Pagniez[1], B. Longere[1]; [1]Lille/FR, [2]Erlangen/DE

Purpose/Objectives: To evaluate the reliability of a compressed sensing (CS) real-time prototype cine sequence (Sparse 2D cine, Siemens Healthineers) for the detection of left ventricle (LV) wall motion disorders after myocardial infarction (MI) in clinical practice.
Methods and Materials: 100 consecutive adult patients (77 males; mean age = 63.1 ✣ 11.3 years) referred for either initial work-up or follow-up by cardiac magnetic resonance (CMR) in the clinical context of MI were prospectively included. Each patient underwent the same CMR protocol: (a) the reference segmented multi-breath-hold steady-state free precession cine sequence including short-axis stack, one four-chamber slice, one two-chamber slice (Group 1) and (b) a CS real-time single-breath-hold sequence (Group 2) providing the same slice number, position and thickness. In both groups, wall motion disorders were independently and blindly assessed by two radiologists, based on the American Heart Association LV segmentation. Paired Wilcoxon signed-rank test was used to analyze the statistical difference. ROC study was performed to assess the differential diagnosis performance.
Results: All patients presented at least one segmental wall motion abnormalities in Group 1 and in Group 2. The 1700 segments read in Group 1, were rated as normokinetic (n = 360; 21. 2%), hypokinetic (n= 783; 46. 1%), akinetic (n= 526; 30. 9%) or dyskinetic (n= 31; 1. 8%). No significant difference was assessed regarding wall motion disorder depiction in Group 2 compared to Group 1 (p = 1. 0). The CS prototype sequence sensitivity and specificity were 99.6% (95%CI [99.1-99.9]) and 99.7% (95%CI [98.5-100]), respectively. Area under the curve was 0.997 (95%CI [0.993-0.999]; p < 0.0001).
Conclusion: The single-breath-hold compressed sensing real-time cine sequence is reliable to assess wall motion abnormalities in the context of myocardial infarction. Since patients suffering from MI may present shortness of breath or arrhythmia due to myocardial fibrosis, the use of CS cine imaging can significantly reduce scan time without compromising detection accuracy of LV-wall motion disorders.

First-pass myocardial perfusion using dual-layer detector CT in healthy subjects: Impact of spectral reconstructions

D. C. Rotzinger[1], S. A. Si-Mohamed[2], M. Matzuzzi[2], L. Boussel[2], L. Hanquier[2], P. Douek[2]; [1]Lausanne/CH, [2]Lyon cedex 03/FR

Purpose/Objectives: (a) to measure the homogeneity of iodine distribution in healthy myocardium at first-pass perfusion imaging using dual-layer CT (DLCT) derived iodine maps in healthy myocardial segments; (b) to evaluate the impact of virtual monochromatic images (VMI) on image noise and signal-to-noise ratio (SNR).
Methods and Materials: Twenty consecutive patients underwent spectral coronary CT-angiography on a 64-row DLCT system using a standard injection protocol. To evaluate first-pass perfusion, iodine maps and VMI (between 40 and 90 keV in 10 keV increments) were reconstructed. Circular regions-of interest of 20mm2 were manually drawn on 9 pre-specified myocardial segments, carefully avoiding obvious artifacts, and mean values as well as standard deviation were recorded for each reconstructed series. Abnormal segments were excluded. Iodine concentration was measured on 2-material decomposition (iodine-water) maps in mg/mL.

Objective image quality was evaluated by measuring standard deviation (SD) and SNR on VMI. Statistical analysis was conducted using R for windows (R v. 3.4.3, R Foundation for Statistical Computing, Vienna, Austria), using the Kruskal-Wallis and Dunn's multiple comparison test as post hoc.
Results: On a total of 180, two abnormal segments were excluded (infarct scars). The median iodine concentration across the 9 myocardial segments was 2.1 mg/mL (interquartile range [IQR] 1.6-2.9). No significant difference in iodine concentration was found between segments (p=0.971). Image noise (median, [IQR]) on VMI (40-90 keV) was as follows (Fig. 1): 16.8 (10.6), 12.8 (7.1), 10.9 (5.4), 10.4 (5.0), 10.2 (5.1), 10.2 (4.7), with significant differences in multiple group testing (p<0.001). Post-hoc testing revealed non-significant results between combinations of 60, 70, 80 and 90 keV images. SNR (median, [IQR]) on VMI (40-140 keV) was as follows (Fig. 2): 9.8 (7.9), 9.8 (5.4), 8.6 (5.1), 7.3 (4.5), 6.8 (4.1), 6.0 (3.4), with significant differences in multiple group testing (p=0.003). Post-hoc testing revealed non-significant results in the following groups: 40 vs 50, 40 vs 60, 50 vs 60, 70 vs 80, and 80 vs 90 keV.

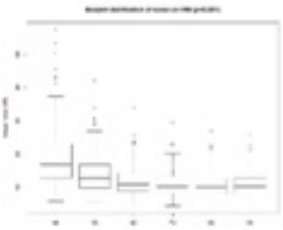

Figure 1

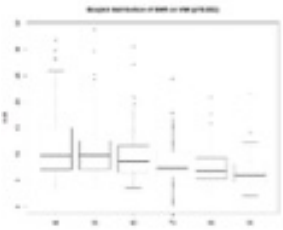

Figure 2

Conclusion: Spectral DLCT yields homogenous first-pass myocardial iodine maps in healthy subjects. VMI keep image noise constant from 60 to 90 keV, with a mild increase on 40 and 50 keV reconstructions. SNR gradually improves when decreasing VMI energy, and is optimal at 40 keV, demonstrating the potential of spectral DLCT to improve objective image quality.

Late gadolinium enhancement patterns in patients with hypereosinophilia: Does CMR help identifying the etiology?

J. Pagniez[1], M. Dubois[1], G. Lefevre[1], L. Averlant[1], J.-E. Kahn[2], V. Silvestri[1], B. Longere[1], F. Pontana[1]; [1]Lille/FR, [2]Suresnes/FR

Purpose/Objectives: The purpose of this study was to assess the prevalence and the patterns of cardiac abnormalities detected by cardiac magnetic resonance (CMR) in patients with hypereosinophilia according to the underlying disease.
Methods and Materials: 62 consecutive patients (36 males; mean age = 51.6 ±18.2) referred for hypereosinophilia, without history of ischemic cardiopathy, were prospectively enrolled. For each patient the etiological diagnosis determination was performed by the internal medicine staff of our institution according to a contemporary consensus on the classification of eosinophilic disorders. Patients were categorized in three groups (Group 1: including hypereosinophilia (HE) and hypereosinophilic syndrome (HES), n=31; Group 2: eosinophilic granulomatosis with polyangiitis (EGPA), n=14; Group 3: other underlying diseases, n=17). Cine functional parameters, T1 and T2 values on parametric mapping and late gadolinium enhancement (LGE) were independently assessed by two radiologists.
Results: Left ventricle (LV) and right ventricle (RV) ejection fractions were altered in 26 patients (42%) and 13 patients (21%) respectively. LV and RV dilatation was observed in 11 patients (18%) and 5 patients (8%) respectively. Increased myocardial T1 and T2 values were found respectively in 10/33 patients (30%) and 5/48 patients (10%). LGE was detected in 18 patients (29%). Among them, 5 patients presented a myocarditis enhancement pattern (Group 1: n=2; Group 2: n=2; Group 3: n=1), 7 patients presented a vasculitis enhancement pattern (Group 1: n=2; Group 2: n=3; Group 3: n=2), 3 patients presented an endomyocardial fibrosis pattern (Group 1: n=1; Group 2: n=1; Group 3: n=1) and 3 patients presented no specific pattern; p = 0.67
Conclusion: LGE was observed in almost one third of the patients with hypereosinophilia with three different patterns (myocarditis, vasculitis and endomyocardial fibrosis), independently of the etiological diagnosis, suggesting a non-specific myocardial toxicity of the eosinophils.

4D flow MRI evaluation of a new technique of valve-sparing aortic root replacement (VSARR)

V. Silvestri, E. Gabiano, A. Monnet, B. Longere, J. Pagniez, D. Montaigne, T. Modine, F. Pontana; Lille/FR

Purpose/Objectives: The aim of this study was to evaluate hemodynamics and blood flow patterns by 4D flow MRI after a modified VSARR in comparison with the standard David procedure. The new technique is conceived to ease the operative procedure, avoid prosthesis and annular deformation and facilitate coronary reimplantation.
Methods and Materials: 27 patient (23 males; mean age= 59.5 ± 13.14) including 13 patients after David procedure (group 1) and 14 patients after the modified one (group 2) underwent 4D flow evaluation 8.7 ± 1.7 years after surgery. Analysis included (a) wall shear stress (WSS) measurements performed at different levels of the thoracic aorta (neo-sinuses, sinotubular junction, ascending aorta and proximal arch), (b) qualitative assessment of flow pattern (laminar, helical or turbulent) and (c) flow eccentricity using a 3-point scale.

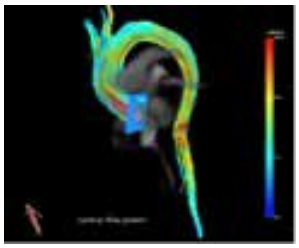
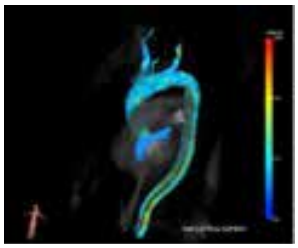
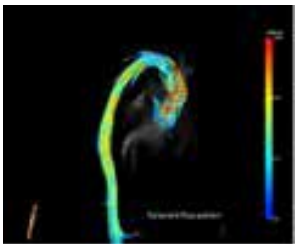

Results: No significant differences were found between the two groups in terms of: (a) WSS (neo-sinuses: 1183 mPa ± 610 vs 1418 ± 664, p=0.35; sinotubular jonction: 1577 ± 519 vs 1864 ± 673, p=0.23; ascending aorta: 1464 ± 598 vs 1697 ± 430, p=0.25; arch: 835 ± 401 vs 898 ± 214, p=0.62) and (b) flow pattern mainly rated as turbulent in both groups (p=0.12). A higher overall degree of flow eccentricity was observed in group2 mainly rated as moderate (6/14, 43%) without significant difference with group1 (6/13, 46% rated as central; p=0.34).
Conclusion: MRI 4D flow allows a detailed analysis of post-surgical hemodynamic profile of the thoracic aorta, demonstrating no significant difference of the modified David procedure compared with the classical one.

Relative myocardial perfusion on cardiac magnetic resonance for the assessment of lesion-specific coronary artery ischemia

O. Ghekiere[1], J.-N. Dacher[2], W. Dewilde[3], T. Couvreur[1], I. Mancini[1], P. Dendale[4], P. Vanhoenacker[5], A. de Roos[6], A. Nchimi Longang[1]; [1]Liege/BE, [2]Rouen/FR, [3]Bonheiden/BE, [4]Hasselt/BE, [5]Aalst/BE, [6]Leiden/NL

Purpose/Objectives: Fractional flow reserve (FFR) represents the current standard of reference for lesion-specific coronary artery ischemia. Invasive FFR equals the ratio of the mean distal coronary to the mean aortic pressure during hyperemia. In clinical practice, FFR values ≤ 0.8 identify inducible ischemia and require coronary revascularization, The concept of FFR was initially validated as a relative flow reserve, the ratio of hyperemic flow in a stenotic coronary artery to the hyperemic flow in a normal coronary artery. In contrast to FFR, stress perfusion cardiac magnetic resonance (CMR) is highly sensitive to microvascular disease. Correcting the myocardial perfusion downstream a coronary stenosis (culprit) for perfusion in normal (non-culprit) myocardium during hyperemia on CMR defines the relative myocardial perfusion index, which is potentially unaffected by microvascular obstruction.
The aim of this study was to assess the value of relative adenosine myocardial perfusion by CMR in predicting lesion-specific coronary artery ischemia as defined by FFR.
Methods and Materials: Forty-six patients (mean age 61 ± 9 years; 33 men) underwent stress perfusion CMR and FFR measurement distal to 49 coronary artery stenoses. The average FFR value was 0.84 ± 0.09 (0.60-0.98 range), 31% (n = 15) were ≤ 0.80. Subendocardial time-enhancement maximal upslopes, normalized by respective left ventricle cavity upslopes, were evaluated in culprit and non-culprit myocardium during adenosine and rest perfusion.
Results: The relative myocardial perfusion index (culprit/non-culprit upslopes) resulted in better correlations with the FFR value than uncorrected culprit upslopes (0.587 vs 0.273) and the myocardial perfusion reserve index (stress/rest upslopes) (0.587 vs 0.289). Using a cut-off value of 0.84 of the relative subendocardial perfusion index revealed an area under ROC curve of 0.88 to predict FFR ≤ 0.80 stenosis.
Conclusion: Using adenosine perfusion CMR, the relative myocardial perfusion enabled the best prediction of FFR-defined lesion-specific coronary artery ischemia.

Non-binary Myocardial Infarct Quantification Technique Accounting for Partial Volume Averaging – Feasibility of Application of Percent Infarct Mapping in Patients

D. Mastrodicasa[1], G. A. Elgavish[2], U. J. J. Schoepf[1], P. Suranyi[1], M. H. Albrecht[3], C. N. de Cecco[1], R. J. van der Geest[4], R. Hardy[1], B. Ruzsics[5], A. Varga-Szemes[1]; [1]Charleston/US, [2]Birmingham/US, [3]Frankfurt am Main/DE, [4]Leiden/NL, [5]Liverpool/UK

Purpose/Objectives: To assess the technical feasibility of myocardial infarct (MI) quantification using percent infarct mapping (PIM), a prototype non-binary algorithm, in patients with suspected MI.
Methods and Materials: Patients (n=171, 64±14 years) referred for 1.5T cardiac MRI were prospectively enrolled in this IRB-approved study. The MRI protocol included late gadolinium enhancement (LGE) imaging and post-contrast T1 mapping. MI size was expressed as both MI volume (IV) and MI fraction of the left ventricle (IF). Two obesrvers quantified MI based on LGE images with manual delineation, binary approaches (2-5 standard deviations [SD] and full-width at half-maximum [FWHM] thresholds), and T1 and LGE images applying the PIM algorithm (PIMT1 and PIMLGE, respectively) using an in-house developed application integrated into the Research Mass Software. ANOVA, Pearson's correlation, intraclass correlation coefficient (ICC), and Bland-Altman (BA) tests were used for data analysis.

Results: MI was observed in 89 (54.9%) patients and 185 (38%) short-axis slices. IF with binary 2-, 3-, 4-, 5SDs and FWHM techniques was 15.7±6.6, 13.4±5.6, 11.6±5.0, 10.8±5.2, and 10.0±5.2%, respectively. The 5SD and FWHM techniques showed the best agreement with manual MI delineation (P=0.1426 and P=0.8094, respectively). However, 2SD and 3SD algorithms significantly overestimated manual IF (P<0.0001, respectively). PIMLGE measured significantly lower IF (7.8±3.7%) compared to manual measurements (P<0.0001) but showed the best agreement with the PIMT1 reference (7.6±3.6%, P=0.3156). Inter-observer assessment was good to excellent for IV (ICCs between 0.727 and 0.820) and fair to good for IF (range 0.589–0.736).
Conclusion: The in-human application of PIMLGE technique for MI quantification is feasible. PIMLGE provides significantly smaller IF than any thresholding technique due to its ability to account for voxel-wise MI content and shows excellent agreement with the validated T1-based reference.

Microvascular perfusion in infarcted and remote myocardium after successful primary PCI: Angiographic and CMR findings

A. Bethke, L. Shanmuganathan, J. Eritsland, G. Ø. Andersen, D. Swanson, N.-E. Klow, P. Hoffmann; Oslo/NO

Purpose/Objectives: The aim of this study was to investigate myocardial perfusion with TIMI myocardial perfusion (TMP) grading in the acute setting and with cardiac magnetic resonance (CMR) first-pass perfusion subacute and at four months in a cohort of patients with ST-segment-elevation myocardial infarction treated with primary percutaneous coronary intervention (PCI).
Methods and Materials: 198 patients with ST-segment-elevation myocardial infarction treated with primary PCI were recruited from the POSTEMI study. TMP grade was assessed at the end of the PCI procedure, and CMR was performed at day 2 (1-5) and after 4 months. On first-pass perfusion images signal intensity was measured in the infarcted and in the remote myocardium and maximum contrast enhancement (MCE) index was calculated.
Results: Patients with TMP grade 2-3 (n=108) after PCI had significantly better CMR outcome at four months compared with patients with TMP grade 0-1 (n=81) for EDV 170 ± 47 vs. 187 ± 56; p= 0,022, ESV 72 ± 35 vs. 96 ± 52; p=0,00016; EF 59 ± 10 vs. 51 ± 13, p=0,000003, myocardial salvage 60 ± 22 vs. 45 ± 21; p=0,000027 and relative infarct volume, 12 ± 8 vs. 19 ± 12 %, p=0,0000002.
MCE in the infarcted (MCEi) and in the remote myocardium (MCEr) improved from baseline to follow-up, MCEi from 94 ± 56 to 126 ± 59, p=0,00008; and MCEr from 112 ± 51 to 127 ± 50, p=0,000001). In patients with the lowest perfusion in the subacute phase, perfusion at four months remained decreased compared to the other groups, MCEi 108 ± 75 vs. 133 ± 51, p=0,01 and MCEr 115 ± 41 vs. 131 ± 52, p=0,047.
Conclusion: Both TMP grade at angiography after the PCI and early CMR first-pass perfusion correlated with CMR outcomes of global function of the left ventricle at four months. After 4 months the first-pass perfusion was reduced in both the infarcted and the remote myocardium, particularly in those patients with the lower first-pass perfusion at the early CMR.

Detection of Occult Myocardial Scars with Cardiovascular Magnetic Resonance imaging in Patients with asymptomatic type 2 Diabetes Mellitus: The ACCREDIT study

S. M. Ko, J.-W. Kang, S. I. Choi; Seoul/KR

Purpose/Objectives: The main objective was to determine the prevalence of occult myocardial scars (OMS) on contrast-enhanced cardiovascular magnetic resonance imaging (CMR) in asymptomatic patients with type 2 diabetes mellitus (DM). The relationship between the occurrence of OMS detected with CMR and coronary atherosclerosis observed with contrast-enhanced coronary computed tomography angiography (CCTA) was also evaluated.
Methods and Materials: This multi-center (6 centres in South Korea), prospective, open-label study included asymptomatic patients with type 2 DM and at least two identified cardiac risk factors, scheduled to undergo a CMR and a CCTA procedures. CMR and CCTA were performed with gadoteric acid (Dotarem®, Guerbet) and iobitridol (Xenetix®, Guerbet), respectively. The prevalence of OMS was calculated on CMR examination. For each main coronary artery, stenosis degree and plaque characteristics (calcified, non-calcified or mixed) were assessed on CCTA. For each myocardial segment with OMS, the corresponding infarct-related artery (IRA) was identified, according to the AHA (American Heart Association) recommendations. The characteristics of the coronary plaques located in IRA were compared to those located in non-IRA.
Results: A total of 322 patients who completed both CMR and CCTA procedures were included in the study (mean age [±SD]: 60.3±6.5 years [range: 35 75]; male: 61.0%; mean body mass index: 25.4±3.2 kg/m^2 [range: 18.6-36.4]). At least one OMS was detected by CMR in 23 patients (7.1%). The coronary assessment by CCTA showed a significant stenosis (>50% diameter reduction) or occlusion for 13 (56.5%) of the 23 patients with OMS and for 67 (22.4%) of the 299 patients without OMS.
Sixty-two IRA plaques and 52 non-IRA plaques were identified with CCTA in 23 patients with OMS. In IRA, 10 (16.1%) plaques were non-calcified, 14 (22.6%) mixed and 31 (61.3%) calcified while in the non-IRA, 16 (30.8%) were non-calcified, 9 (17.3%) mixed and 27 (51.9%) calcified. There was no significant difference in plaque characteristics between IRA and non-IRA (p=0.175, Chi^2).
Conclusion: In this multi-center study, OMS were identified with CMR in 7.1% of asymptomatic patients with type 2 DM and at least two identified cardiac risk factors. No significant difference was demonstrated in plaque characteristics between IRA and non-IRA in patients with OMS. Further investigations are still required to determine whether the occurrence of OMS is related to atherosclerosis detected with CCTA.

Computational Quantitative Flow Ratio to assess hemodynamic relevance of coronary artery disease

D. Ties, R. van Dijk, G. Pundziute, E. Lipsic, T. Vonck, A. F. M. van Den Heuvel, R. Vliegenthart, M. Oudkerk, P. van der Harst; Groningen/NL

Purpose/Objectives: Fractional flow reserve (FFR) is currently considered the reference standard for the functional assessment of coronary artery disease (CAD) in the catheterization laboratory. FFR procedures are associated with additional complication risk and peri-procedural costs, related to the introduction of a sophisticated invasive pressure wire in the coronary artery and induction of hyperemia. Computational quantitative flow ratio (QFR) can be derived from the coronary angiogram by 3-dimensional quantitative coronary angiography (3D QCA) analysis and frame counting of resting angiography images, without the need for pressure wire introduction. This study aims to evaluate the diagnostic performance of QFR in comparison to wire-based FFR and 3D QCA analysis and to validate the previously reported QFR cut-off value of >0.90 to safely rule out functionally significant CAD.
Methods and Materials: Contrast-flow QFR (cQFR) was retrospectively derived from standard-care coronary angiograms using dedicated QFR software (Medis Medical Imaging Systems, Leiden, The Netherlands). Pearson's correlation coefficient of cQFR with wire-based FFR was calculated. Diagnostic performance of QFR was evaluated by receiver operating characteristic curve analysis at various QFR cut-off values ruling out significant CAD (FFR≤0.80).
Results: 101 vessels in 96 patients, who underwent FFR, were studied. Mean FFR was 0.87 ± 0.08 and hemodynamically significant CAD (FFR ≤0.80) was present in 21 of 101 (21%) vessels. Correlation between cQFR and FFR was r=0.70 (p<0.001). Sensitivity, specificity, positive predictive value and negative predictive of cQFR were 67%, 96%, 82%, and 92%, respectively, at a QFR cut-off value >0.80 ruling out significant CAD. cQFR>0.90 was present in 39 (39%) vessels. None of the vessels with cQFR >0.90 had an FFR ≤0.80.
Conclusion: In this retrospective study, QFR was able to safely rule out significant CAD when applying a QFR threshold of >0.90 to rule out significant CAD. QFR might function as an effective gatekeeper to wire-based FFR. Further prospective research is required to establish QFR in the real-life setting of functional CAD assessment in the catheterization laboratory.

[11C]mHED PET-MRI to evaluate cardiac re-innervation in long term heart transplant patients: Preliminary results

A. Wielandner, S. Rasul, C. Loewe, M. Hacker, K. Uyanik-Ünal, A. Zuckermann, D. Senn, C. Vraka, V. Pichler, D. Beitzke; Vienna/AT

Purpose/Objectives: Potential cardiac re-innervation after heart transplantation (HTX) was described from the first year after transplantation1 and associated with an improved cardiac function.2 Hybrid cardiac positron emission tomography/magnetic resonance imaging (PET/MRI) seems to be a promising method to evaluate cardiac function, tissue characteristics as well as re-innervation.
Therefore, this pilot study aimed to evaluate cardiac re-innervation and its correlation to function and tissue characteristics in heart transplant patients using PET/MRI.
(1) Buendia-Fuentes et al. 2011, Transplant Proc; (2) Bengel et al. 2001, N Eng J Med
Methods and Materials: Seven patients, 4 to 21 years after cardiac transplant, were included in this study. Cardiac PET/MRI using [11C]-meta-hydroxy-ephedrine ([11C]mHED) for presynaptic, sympathetic nerve imaging and a standard MRI protocol including T1 mapping was obtained. Cardiac re-innervation was assessed on a segmental base by the presence of myocardial [11C]mHED uptake. Re-innervated and non-re-innervated segments were compared in regards to wall motion(WM) and wall thickening(WT) as well as results from T1 mapping. The number of re-innervated segments and T1 values were additionally correlated to the time from transplant.
Results: WM did not differ between re-innervated and non-re-innervated segments (re-innervated vs. non-re-innervated: WM mean 8.17 mm, SD ±3.79 vs. WM mean 8.02 mm, SD ±3.2, p=0.116). There was a significant difference in WT between re-innervated and non-re-innervated segments. (mean 115.01%, SD ±79.07 vs. WT mean 82.96% ±45.71, p=0.46). The number of re-innervated segments increased over the years (min 1 segment after 4 years post HTX, to 9 segments after 7 years post HTX). Native T1 values correlated with the number of years post-transplant (k=0.6). However, there was no significant difference in T1 between re-innervated and non-re-innervated segments (re-innervated vs. non-re-innervated: T1 mean 1264.74, SD ±103.26 vs. T1 mean 1282.66, SD ±96.48).
Conclusion: Imaging of cardiac re-innervation using a hybrid PET-MRI system with carbon-11 is feasible showing increasing numbers of re-innervated segments over the time. WM as well as T1 values did not correlate with the presence of re-innervation. Re-innervation seems to have an effect on WT. T1 values correlated with the number of years post-transplant suggesting an interstitial disease over the time, independent from the presence or absence of re-innervation.

[11C]mHED image of a 58 years old male patient, 21 years post HTX, shows re-innervation over the anterior wall segments

Early detection of diabetic cardiomyopathy by using MRI-based multidirectional strain analysis - Differences in Subjects with Prediabetes, Diabetes and Healthy Controls

T. Zitzelsberger[1], A. Scholz[1], R. Lorbeer[2], F. Bamberg[1], W. Rathmann[3], S. Rospleszcz[2], K. Nikolaou[1], M. F. Reiser[2], A. Peters[4], C. L. L. Schlett[5]; [1]Tübingen/DE, [2]Munich/DE, [3]Düsseldorf/DE, [4]Neuherberg/DE, [5]Heidelberg/DE

Purpose/Objectives: According to the Framingham Heart Study the risk of heart failure a is 2.4-fold and 5-fold higher in diabetic patient(1). In addition, persons with hyperglycemia even below the diagnostic threshold for diabetes, so called prediabetes, are known to be at high risk for cardiovascular events. Therefore the aim of this study was to evaluate early changes in myocardial strain using MR-based feature tracking in patients with diabetes, pre-diabetes and controls.

(1)Kannel WB, Hjortland M, Castelli WP. Role of diabetes in congestive heart failure: the Framingham study. Am J Cardiol. 1974;34(1):29-34.

Methods and Materials: Subjects without history of cardiocerebrovascular disease were enrolled in a sub-study of the population-based KORA (Cooperative Health Research in the Region of Augsburg) cohort. In all participants with absence of late gadolinium enhancement, radial and circumferential global systolic and diastolic strain were measured on midventricular short-axis Cine SSFP imaging (TR: 29.97ms, TE: 1.46ms, ST: 8mm), using a semiautomatic segmentation algorithm (CVI42, Circle, Canada). Differences in strain values according diabetes status were derived using linear regression analysis.

Results: Radial and circumferential strain analysis was performed in in total 347 subjects, of which 41 (11.8%) suffered from diabetes, 92 (26.5%) from pre-diabetes and 214 (61.7%) controls. Mean HbA1c of diabetic subjects was 6.5±1mmol/mol Hb. Pre-diabetic subjects showed a significantly higher systolic global and endocardial radial strain compared to controls (p=0.036 and p=0.011 respectively), whereas diabetic subjects didn't show any significant difference (p=1.00 and p=0.811). Similarly we detected significant lower systolic global and endocardial circumferential strain values in pre-diabetic subjects (p=0.044 and p=0.009), whereas diabetic subjects didn't show a significant difference (p=1.00 and p=0.580). Regarding diastolic radial and circumferential strain we didn't find any significant difference.

Conclusion: In our cohort of well-treated diabetic subjects we didn't find any changes in strain values whereas pre-diabetic subjects showed early changes. Therefore early treatment of diabetes seems to be cardioprotective and should be considered.

Multiparametric Cardiac Magnetic Resonance in short-term monitoring of Patients with acute myocarditis: Preliminary results

G. Benedetti, A. Palmisano, A. Cristofano, A. Del Maschio, F. de Cobelli, A. Esposito; Milan/IT

Purpose/Objectives: To evaluate early changes in T1 and T2 mapping, ECV and T2-ratio in acute myocarditis (AM) related to morpho-functional and clinical parameters.

Methods and Materials: Histologically confirmed AM patients underwent basal and one-month CMR, evaluating: end-diastolic volume (EDV); ejection fraction (EF); STIR-edema (T2-ratio, T2-Nosegments); T2mapping; T1mapping; ECV; LGE%. Clinical presentation (cardio-vascular arrest, chest pain, flu-like), T-Troponin (TT) and creatin-phospho-kinase (CPK) values were collected. Basal and 1 month' clinical and CMR parameters correlation was tested.

Results: Eleven ppatients were enrolled (37.2 years): 1 cardiovascular arrest, 6 chest pain, 4 flu-like. Basal and 1month CMR parameters were: T2-ratio=2.9 vs 2.3, p=0.01; T2-Nosegments=8.2 vs 5.0, p=0.05; T2 mapping=61.6 vs 52.3 ms, p=0.04; T1 mapping=1121 vs 1071ms, p=0.03; ECV=30.1 vs 29.9, p=0.94; LGE%=12.6 vs 10.8, p=0.73. Basal T2-ratio was significantly correlated with TT (mean TT=614.3ng/L; p=0.011); basal T2mapping with CPK (mean CPK=295.5U/L; p=0.037). At 1month FU, higher T1mapping were associated with higher EDV (p=0.021). Flu-like presentation was associated with higher basal T1mapping (1184 vs 1100 ms, p=0.02), T2-ratio (3.3 vs 2.7, p=0.04), T2-Nosegments (10.5 vs 7.1, p=0.04) and higher T1mapping- improvement (DeltaT1=-120 vs -25 ms, p=0.038) compared to other presentations.

Conclusion: CMR tissue-characterization parameters (ECV, T1 and T2 mapping) may help stratifying patients according to their clinical presentation, as well as evaluating persistent myocardial inflammation associated with short-term cardiac remodeling. Patient population will be enlarged to confirm these results.

Intraobserver and interobserver variability in 3D printing and 3D model measurement of the aortic annulus

R. Faletti, A. Cosentino, M. Gatti, G. Pennisi, A. Depaoli, P. Fonio; Turin/IT

Purpose/Objectives: To determine the reproducibility and reliability of using CCT to print individual models of the aortic annulus.

Methods and Materials: Retrospective study on 20 patients who underwent aortic valve replacement with available records of pre-surgery annulus assessment by CCT and of intra-operative assessment by Hegar dilators. CCT was used to acquire and segment the 3D cardiovascular anatomy. Models were fabricated by fused deposition modelling of flexible polylactic acid filaments. A radiologist and a radiology technician independently segmented, modelled and printed all the 3D models. Two blinded cardiac surgeons performed the 3D model measurements and one of them after a month re-performed the measurements on randomly rearranged models of all patients. Each measure was made on a "naïve" model in order to avoid the possible bias of 3D-model deformation. Data were analysed using Wilcoxon signed-rank test.

Results: There were no intraobserver variability in the 3D model aortic annulus measurement (p=0.60). No significant differences were found when compared either the 3D model measurement made by each cardiac surgeon (p=0.59) or the measurement made on the 3D model printed by different observer (p>0.11). There was agreement between the annulus dimensions measured by 3D models derived from CCT either to the surgical reference of intra-operative sizing (p=0.12) or to the CCT measurement (p=0.91).
Conclusion: The use of 3D printing for the aortic annulus measurement it's a reliable and reproducible technique and the measurement performed well when compared either to the surgical reference of intraoperative or to the CCT sizing.

Quantification of the Extracellular Volume Fraction (ECV) with Cardiac CT - Comparison with Cardiac MR

D. Vignale, A. Esposito, A. Palmisano, D. Flouri, A. Del Maschio, F. de Cobelli; Milan/IT

Purpose/Objectives: Cardiac MR with T1 mapping allows for the quantification of the myocardial extracellular volume fraction (ECV). An increase in the ECV indicates the expansion of the interstitial fibrous matrix, which may represent the expression of many diseases. In fact, ECV has a growing diagnostic and prognostic role. The aim of this study is to compare cardiac CT to cardiac MR in the quantification of myocardial ECV.
Methods and Materials: 10 patients (F:M=7:3; age 56.4±16.1), affected by heterogeneous diseases (5 myocarditis; 2 idiopathic dilated cardiomyopathy; 1 hypertrophic cardiomyopathy; 1 ischemic cardiomyopathy; 1 amyloidosis), underwent a cardiac CT study (SOMATOM DEFINITION, Siemens) with a triphasic technique including basal acquisition and late acquisition after 10 minutes (low kilovoltage, prospective gating, no padding), in addition to the standard angiographic acquisition. In all patients an 85-mL bolus of high concentration iodinated contrast media was injected.
The same patients underwent cardiac MR (1.5 T Ingenia, Philips) with T1 mapping acquisition before and after administration of a standard Gadolinium dose.
The ECV-CT has been calculated comparing the density difference of the myocardium to the density difference of the blood pool before and after contrast media injection. The result was then weighted to the haematocrit of the patient.
Using MATLAB®, we registered the CT images before and after contrast injection to create a 2D map of the heart ECV on a short axis mid-ventricular slice.
The ECV-MR has been calculated comparing the relaxivity difference of the myocardium to the relaxivity difference of the blood pool before and after contrast media injection. The result was then weighted to the haematocrit of the patient.
With the same MATLAB® toolkit, we registered the MR images before and after contrast injection to create a 2D map of the heart ECV on the same short axis mid-ventricular slice used for the CT map.
We manually segmented the CT and MR maps to extract the ECV values of septum and left ventricular free wall.
Results: 20 ECV values have been analysed and compared.
The ECV-CT range was 25.5-72.3%, with a mean value of 36.1±10.6%.
The ECV-MR range was 26.3-75.2%, with a mean value of 36.5±12.1%.
The concordance between CT and MR was optimal (Spearman correlation coefficient =0.836, p<0.001; Pearson correlation coefficient =0.934, p<0.001).
Conclusion: Cardiac CT allows for the quantification of myocardial ECV, with an optimal correlation with the ECV calculated with cardiac MR.

MR-compatible Echocardiography and Predictive Slice Tracking For Feasibility of Ultrasound-driven Cardiovascular MRI

L. A. Crowe[1], F. Santini[2], L. Gui[1], P. Guillemin[1], O. Lorton[1], M. Roth[1], G. Manasseh[1], O. Bieri[2], J.-P. Vallee[1], R. Salomir[1]; [1]Geneva/CH, [2]Basel/CH

Purpose/Objectives: Cardiac MRI has the potential for high-resolution cardiac valve function evaluation. Morphology for surgical planning is assessed by echocardiography. Ultrasound quality is patient dependent and geometry often limited to a single plane. Improving accuracy of MRI for valve morphology would significantly advance valvular disease evaluation. We suggest an ultrasound-guidance method for motion compensation during MR acquisition with in-bore ultrasound, and a future-predicting algorithm illustrated in high-resolution cine MRI of a 'breathing' phantom.
Methods and Materials: US images from a clinical Siemens ACUSON Antares, with modified, MR-compatible, linear-array probe, were sent to an external PC. The extracted average motion vector (optical-flow-based tracking OpenCV2.3.1), with a non-parametric algorithm predicting future position (+60ms) was communicated to the MR on-the-fly. A cardiac-triggered segmented balanced-SSFP sequence was modified to adapt slice positioning according to the tracking information. Real-time balanced-SSFP determined the optimum algorithm for high-resolution 'cine' (>1min). Quantification of cine image improvement required a gold-standard static image. A gel-filled bottle, attached to an Innomotion robot simulating respiratory motion (amplitude 20mm), was imaged in a Siemens 3T PRISMA scanner.

In-vivo imaging (healthy volunteer, prone, spine/Body18 coil) used a 3D VIBE breathold to localise the US imaging plane. The probe was held in place in a 3D-printed support with 6 MRI-visible markers for localisation by MRI image and allowing 3 degrees of freedom. A customised wedge platform on the MRI table allowed optimal prone position for the best acoustic path. Cardiac valve US was acquired during MRI acquisition.

Figure 1. Set up of coil and robot, and phantom US image. US parameters: field depth 14-16cm, frame rate 25-30 images/second, 5mm slice, carrier frequency 3.3MHz, receive central frequency 6.6MHz (second harmonic).

Results: Quantitatively, on real-time images, the standard deviation of motion was 8.86mm uncorrected, 0.68mm on-the-fly, 0.53mm predictive. Visually, cine image quality was significantly improved with predictive correction and the edge sharpness increase is clear on gradient images. Visible motion artifacts are seen at the superior/inferior edges of the phantom with the on-the-fly correction and were reduced with predictive correction throughout the cardiac cycle. The predictive correction image was almost identical to the static gold-standard.
In vivo, there were no confounding US-based artifacts on MRI nor on the US during MR acquisition. Cardiac valves were visible in-vivo and trackable on ultrasound images during MR acquisition. The acoustic window did not interfere with the ECG patches.

Figure 2. A: bSSFP cine with flip angle 57, TR/TE 18/1.5ms, simulated RR 1000ms, 0.7mm resolution, 50 cardiac phases, 1 minute 'breathold', elliptical filter; B: Gradient image; C: Subtraction from static image.

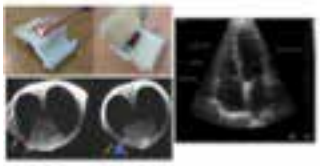

Figure 3. Left: Probe holder with probe; artifact-free images showing probe position on 3D VIBE in vivo. The overlay shows the probe and US imaging plane position. Right: Artifact-free cardiac valve ultrasound image acquired during MRI acquisition.

Conclusion: This multimodal method can correct all movements combined (respiration, contraction, valve function) as the anatomy of interest is directly observed. The volunteer acquisition demonstrated MR-compatibility and workflow of echocardiography in-situ. Dynamic MRI motion correction was quantified with a moving phantom. The future-predicting algorithms yielded dramatically improved "cine" images

Duration of Vortices in 4D Flow MRI Compared to Pulmonary Artery Mean Pressure

L. A. Crowe, A.-L. Hachulla, G. Guglielmi, M. Beghetti, F. Lador, J.-P. Vallee; Geneva/CH

Purpose/Objectives: A robust non-invasive method to estimate increased pulmonary artery mean pressure (mPAP) is needed. Recently, a 2D velocity encoding MRI study has shown that vortex duration in the pulmonary artery (PA) was related to mPAP (Reiter, 2105). This present study investigated the potential of 4D flow MRI to assess pulmonary artery hypertension.
Methods and Materials: Eighteen patients with suspected Chronic Thromboembolic Pulmonary Hypertension (CTEPH) had clinical routine right heart catheterization (RHC) and cardiac MRI, and including a 4D phase contrast flow sequence, on a Siemens 3T PRISMA. Parameters: 2mm isotropic, temporal resolution 20-40ms (both depending on patient anatomy and physiology), 60 slices, and 3 directions of flow encoding with venc 150cm/s.
For the 4D Flow analysis, streamlines were reconstructed in the pulmonary artery. The duration of a vortex (closed concentric rings parallel to the pulmonary artery (PA)), was measured as a % of the cardiac cycle with both Siemens 4DFlow and Gyrotools GTFlow analysis software.
Regression analysis compared MRI-parameters from standard clinical routine (right ventricular volume (RVV), PA diameter PA distensibility), 4D vortices and mPAP.
Results: CTEPH was confirmed in 11 / 18 patients (mPAP 28.7+14.6mmHg). On the 4D flow data, a vortex was observed in most of the patients to a greater or lesser extent.
Vortex duration measurement was reproducible, with intraobserver ICC=0.94 and interobserver ICC = 0.88.
Vortex duration correlated excellently with mPAP with R2=0.69,p=0.000018 and outperformed all the other parameters (mPAP correlations with; RVV: R2=0.13,p=0.14; PA diameter: R2=0.409,p=0.008; PA distensibility: R2=0.17,p=0.09).
Vortex duration correlations with the other 2D derived MRI parameters were only moderate for PA diameter (RVV: R2=0.11,p=0.19; PA diameter: R2=0.47,p=0.003; PA distensibility: R2=0.14,p=0.13).
Using the second software package (GTFlow), no significant difference was found to the Siemens software (p=0.675) and the correlation between vortex duration and mPAP was maintained at R2=0.66,p=0.00015. This is an important criterion for introducing this parameter in clinical routine.

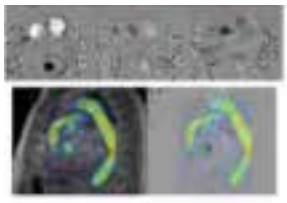

Figure 1. 2D representation of vortex in the 3 encoding directions and the full 4D flow streamline reconstruction. The pulmonary trunk (between arrows) dilated with a flow showing a vortex (vortex during 29% of cycle, mPAP 26mmHg).

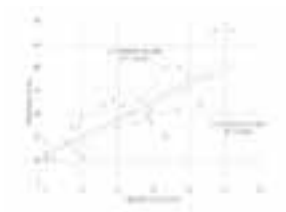

Figure 3. MRI 4D Flow Vortex duration showed excellent correlation with mPAP using both analysis software packages (blue, Siemens 4D Flow; orange, Gyrotools GTFlow).

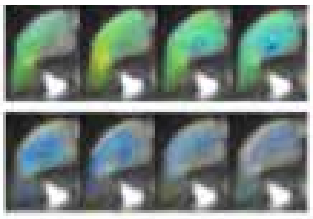

Figure 2. Streamline vortex frames, selected from the full cardiac cycle to illustrate vortex development.

Conclusion: Computational Fluid Dynamics suggests that a change from narrow to wider vessel (PA dilatation) would cause a vortex. This could also explain the moderate correlations of mPAP and vortex duration with PA diameter. Additionally, a pressure increase could cause an outflow obstruction.
The acquisition of the 3D volume and the complete velocity field in the 4D flow protocol is ideally adapted for analysis of complex vortical flow patterns.
Vortex duration derived from 4D flow MRI was the most promising MRI parameter to assess PA pressure.

Modification of left ventricle myocardial perfusion reserve after the implantation of coronary sinus stent: A stress-rest CMR study

A. Palmisano, A. Esposito, G. Benedetti, F. Giannini, L. Baldetti, A. Colombo, A. Del Maschio, F. de Cobelli; Milan/IT

Purpose/Objectives: Refractory angina is becoming an increasingly clinical challenge, impacting on patients productivity and lifestyle. The implantation of a coronary sinus stent named "Reducer" showed to improve patient' symptoms and quality of life, but objective data demonstrating an impact of Reducer implantation on the physiology of myocardial perfusion reserve are lacking and discordant and, therefore, many doubts remain about the effective pathophysiological mechanism of the device. Aim of the study was to evaluate the modification in myocardial perfusion reserve occurring after Reducer implantation using a stress-rest CMR study.
Methods and Materials: 15 patients eligible for implantation of the "Reducer" underwent clinical evaluation [Canadian Cardiovascular Society grading of angina pectoris (CCSA Class) and six minutes walking test (6minWT)] and CMR studies before and 3 months after Reducer implantation. All CMR examination were performed at 1.5 T, including first-pass perfusion sequences acquired during pharmacological stress (Dypiridamole) and at rest, followed by LGE assessment. Segmental and global Myocardial Perfusion Reserve index (MPRi) was measured.
Results: Thirteen out of 15 patients reported an improvement of $\geq$ 2 CCSA class ($p < 0.0001$) and a 60% increase in the average distance during the 6minWT ($p=0,004$). The global value of MPRi increased from 1.29 to 1.48 ($p =0.047$). The ischemic territories increased by 62% in MPRi ($p = 0.03$) with a reduction of the number of ischemic segment ($p=0.023$) and of the transmural involvement of myocardial wall ($p=0.0001$). While non-ischemic and scarred segments did not show significant changes in MPRi ($p>0.05$).
Conclusion: Using stress/rest CMR imaging, this study showed an improvement of myocardial perfusion reserve after 3 months from coronary sinus Reducer implantation. According to our best knowledge, this is the first study demonstrating a clear change in myocardial perfusion physiology induced by Reducer implantation. Segmental assessment of myocardial perfusion with qualitative evaluation and MPRi measurement, strongly suggest that clinical benefit subsequent to Reducer implantation is mostly driven by an increased perfusion reserve in most ischemic segments. These results will be confirmed enlarging our patients population.

CMR diagnosis of right ventricular myocarditis (RVM) vs arrhythmogenic right ventricle dysplasia: Overlapping phenotypes

G. de Rubeis, F. Vullo, F. Cilia, N. Galea, I. Carbone, C. Catalano, M. Francone; Rome/IT

Purpose/Objectives: Isolated Right Ventricular (RV) involvement in acute myocarditis is an uncommon event, sharing overlapped clinical and morphological manifestations with Arrhythmogenic right ventricular displasia (ARVC) consisting with regional wall motion abnormalities, RV enlargement, impaired ejection fraction (EF) and late gadolinium enhancement (LGE) of the free wall. The condition has shown to be misdiagnosed with Cardiac Magnetic Resonance (CMR) in approximately 50% of cases with relevant clinical implications on patient's prognosis and therapeutic management.

Methods and Materials: From a database of 15 consecutive patients undergoing endomyocardial biopsy (EMB) with an initial CMR suspicion of ARVC, we retrospectively identified 11 cases with an histological diagnosis of ARVC and 4 with RVM. In all cases, biventricular performances, CMR tissue abnormalities and clinical-laboratory data were systematically compared and matched with current CMR diagnostic criteria of ARVC.
Results: Clinical indication to the exam was given by the presence of a long-standing history of syncope in 2 ARVC cases whereas 1 RVM patient presented with acute chest pain and troponin raise followed by a cardiac arrest occurred during an access of VF. In the remaining 12 cases, clinical presentations were highly overlapped consisting with ECG abnormalities, variably associated with palpitations, and no troponin raise. CMR data showed comparably enlarged Right Ventricular End Diastolic Volume (RVEDV) between ARVC and RVM (EDV/BSA respectively (107.3 ± 36.5 vs 128.4 ± 57.2; p > 0.05) and reduced ejection fraction for both group (EF: 42.01 ± 14.98 vs 27.4 ± 13.6; p>0.05). LGE was noted in overall 7/15 cases (n=3 ARVC; n=4 RVM) with non ischemic pattern of distribution predominately involving RV free wall; homogeneus intraventricular thickening was also observed in 1/4 RVM patients, consisting with overlapped tissue edema. According to current diagnostic criteria, a diagnosis of ARVC with CMR was established overall in 1/11 (9%) patients with ARVC and 3/4 (75%) with RVM (p=0.04)

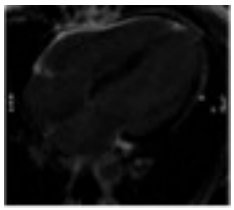

Figure 1. Patient with right ventricular isolated myocarditis presented with acute chest pain, the LGE 4 chamber view shows an hyperintese LGE enhancement of right ventricle free wall.

Figure 2. Patient with arrhythmogenic right ventricular displasia presented with syncope, the CINE SSFP short axis (A) shows a RV enlargement (EDV/BSA 143.9 ml/m^2). The LGE 4 chamber view (B) confirms the RV enlargement without positive LGE enhancement.

Conclusion: Our retrospective evaluation confirmed highly overlapped morho-functional and tissue manifestation of both pathological entities, introducing a relevant interpretation bias recalling the need of an invasive characterization in selected cases.

A phantom-based validation method for myocardial perfusion imaging: Initial results in CT

M. E. Kamphuis[1], G. J. Pelgrim[2], M. Greuter[2], C. Slump[1], R. Slart[2]; [1]Enschede/NL, [2]Groningen/NL

Purpose/Objectives: Myocardial perfusion imaging (MPI) is a common test method to diagnose obstructive coronary artery disease. Institutional variations due to different imaging modalities, vendors and protocols result in different standards in MPI. In line with proper clinical decision-making, it is essential to validate institutional MPI by evaluating absolute myocardial blood flow (MBF) using a proper reference. This research focuses on the development of a multimodality quantitative MPI validation method.
Methods and Materials: Basic requirements for the myocardial perfusion phantom, flow circuit and validation method were specified. The prototype (figure 1) includes a piston pump (Superpump, VivitroLabs) that generates a pulsatile flow (sine, 60 bpm) for varying stroke volumes (20-35 mL/stroke). The static myocardial perfusion phantom is placed in an anthropomorphic thorax phantom (QRM-thorax, QRM GmbH). Experiments were performed in contrast enhanced dynamic first-pass CT (SOMATOM, Force, Siemens). MPI was validated by comparing computed MBF from Perfusion CT software and measured flow (FCH-mini POM Flowmeter, Biotech) as reference.
The MBF was computed according to the upslope method, whereby dividing the maximum slope of the myocardial time intensity curve (TIC) by the maximum intensity of the arterial input function (AIF).

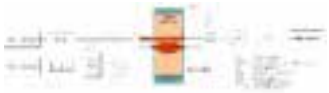

Figure 1: Measurement setup.

Results: Requirements for the myocardial perfusion phantom, flow circuit and MBF quantification method were met. The obtained TIC from the phantom was compared to the TIC of healthy patients (Figure 2). Similar contrast enhancement was observed for the AIF, though the upslope myocardial perfusion rate was higher in the phantom setup compared to the in vivo situation. The computed and measured MBF showed a moderate correlation (Figure 3).

Figure 2: Arterial input function (AIF) and myocardial time intensity curve obtained from dynamic CT-MPI in a healthy patient4 and prototype myocardial perfusion phantom.

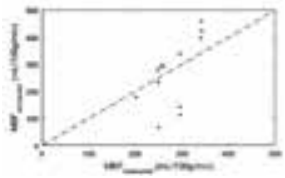

Figure 3: Correlation plot between computed and measured myocardial blood flow (MBF).

Conclusion: We developed a novel, multimodal and multivendor myocardial perfusion phantom using measured sensor flow as reference. Initial results showed a moderate correlation between computed and measured MBF on CT.

Comparison of the different imaging time points in delayed phase cardiac CT for myocardial scar assessment and ECV fraction estimation in patients with old myocardial infarction

A. Hamdy[1], K. Kitagawa[1], Y. Goto[1], A. Yamada[2], S. Nakamura[1], M. Takafuji[3], H. Sakuma[1]; [1]Tsu/JP, [2]Mie/JP, [3]Tsu Mie/JP

Purpose/Objectives: Delayed enhancement cardiac CT is a potential tool for myocardial viability assessment and is essential for extracellular volume fraction (ECV) estimation with CT. The timing of the delayed acquisition is important to obtain good quality images. The objective of this study is to determine the optimal time point/s for acquisition of the delayed CT scans.
Methods and Materials: 35 patients with enhancement pattern typical of previous myocardial infarction on delayed CT and 17 control subjects comprised the final study population. Delayed scans were acquired at 3, 5 and 7 minutes after contrast material injection for CT coronary angiography. Image quality, CT density of the infarcted and remote myocardium and the left ventricular cavity, contrast-to-noise ratio and signal-to-noise ratio were assessed for the three time points. The estimated ECV fractions were compared among the three time points in the infarcted and the remote myocardium and in control subjects.
Results: For observer 1, the best image quality was noted at 5 and 7 minutes with no statistically significant difference (2.9±0.9 at 5 minutes and 3±0.8 at 7 minutes, p = 0.5). For observer 2, the best image quality was noted at 5 minutes and was significantly higher than the 7 minutes (3.1±0.8 at 5 minutes, and 2.9±0.95 at 7 minutes, p = 0.015). Absolute CT densities of the different regions within the same time point and the same region at the different time points were significantly different (p < 0.0001). in the infa5cted tissue, CNR at 7 minutes was significantly higher than at 3 minutes (6.36±2.5 vs 4.96±1.87, p < .0001) but not than at 5 minutes (6.06±2.2, p = 0.08). The SNR at 5 minutes (15.23±1) was slightly higher than that at 3 and 7 minutes (13.57±1, p < .0001 and 14.88±1 respectively, p = 0.0015). ECV values in the infarcted myocardial segments were slightly but significantly higher at 5 and 7 minutes (39.6%±5.3% and 39.8%±.5.6%, respectively, p = 0.66) than at 3 minutes (38.7%±5%, p = 0.03). For the scar-free myocardium, no significant difference in global ECV values was found among different time points.
Conclusion: At delayed enhancement cardiac CT, myocardial scars are equally best visualized at 5 and 7 minutes post contrast administration. For ECV measurement, the common bolus injection protocol achieved equilibrium in control and remote myocardium as early as 3 minutes but was slightly delayed to 5 minutes in focal scars of myocardial infarction.

Correlation between haptoglobin phenotypes and myocardial reperfusion injury in consecutive ST-elevation myocardial infarction as detected by cardiac magnetic resonance

M. Guglielmo[1], A. Baggiano[1], G. Muscogiuri[1], S. Mushtaq[1], E. Conte[1], A. Formenti[1], E. Mancini[1], D. Andreini[1], A. I. Guaricci[2], G. Pontone[1]; [1]Milan/IT, [2]Bari/IT

Purpose/Objectives: Primary percutaneous coronary intervention (pPCI) has significantly reduced cardiovascular mortality of ST-segment elevation myocardial infarction (STEMI) patients. However, even rapid and complete restoration of culprit vessel flow may not guarantee adequate perfusion with consequential myocardial reperfusion injury. Recent studies on animal models showed that different variants of haptoglobin could play a role in the myocardial reperfusion injury. Cardiac magnetic resonance (CMR) has emerged as the gold standard technique for the measurement of the myocardial salvage index (MSI) and microvascular obstruction (MVO) over the traditional risk stratification.
Aim of this study is to evaluate the correlation between variants of haptoglobin and myocardial reperfusion injury as detected by CMR in consecutive STEMI patients who underwent successful pPCI.
Methods and Materials: Consecutive STEMI patients reperfused by primary PCI were enrolled in this study. For each patient, the characterization of different phenotypes of haptoglobin was evaluated. Moreover, a CMR was performed by 1 week after STEMI evaluating the following parameters: left ventricle ejection fraction (LVEF), MSI and prevalence and amount of MVO. The primary endpoint of study was to evaluate the correlation between different phenotypes of haptoglobin and myocardial reperfusion injury as detected by CMR.
Results: One-hundred forty five consecutive STEMI were enrolled in this study (mean age: 62∔10 years; male:114). The three different phenotypes Hp 1-1, Hp 1-2, Hp 2-2 were observed in 15 (10%), 62 (43%) and 68 (47%) patients, respectively. CMR showed a LVEF and MSI of 52∔10% and 0.43±0.3, respectively. The MVO was observed in 38 patients (26%) with a mean value of 1.6±3.8% of left ventricle myocardial mass. The patients with phenotype Hp 1-1 or Hp 1-2 showed no differences in terms of LVEF (50.2±9.8% vs. 48±11.1%, p:0.42) and MSI (0.44±0.35 vs. 0.42±0.30, p:0.7) but higher prevalence (27% vs. 11%, p<0.01) and amount (2.5 ±4.5% vs. 0.8±2.7% of left ventricle mass, p<0.05) of MVO as compared to phenotype Hp 2-2. After correction for baseline characteristics the presence of phenotype Hp 2-2 was an independent predictor of MVO [HR:0.63 (0.54-0.72), p<0.01]
Conclusion: Different variants of haptoglobin may play a crucial role in cardiac repair responses by reducing oxidative stress, maintaining microvascular integrity and proper scar formation. Further studies should be performed to evaluate if different therapeutic strategies should be developed based on phenotypes of haptoglobin of patients.

Stress computed tomographic perfusion improve diagnostic accuracy of coronary computed tomographic angiography in intermediate to high risk patients for coronary artery disease

A. Baggiano[1], G. Muscogiuri[1], M. Guglielmo[1], S. Mushtaq[1], E. Conte[1], A. D. Annoni[1], E. Mancini[1], D. Andreini[1], A. I. Guaricci[2], G. Pontone[1]; [1]Milan/IT, [2]Bari/IT

Purpose/Objectives: Coronary computed tomographic angiography (CCTA) was approved as alternative to functional strategy in patients with suspected coronary artery disease (CAD) and low to intermediate risk (prevalence of CAD<50%) thanks to its excellent negative predictive value. Unfortunately, in the intermediate to high risk population (prevalence of CAD≥50%), the presence of multiple lesions and coronary artery calcium could limit the diagnostic accuracy of CCTA regarding the assessment of flow limiting obstructive CAD. Static stress computed tomographic perfusion (CTP) may represent an opportunity to overcome this limitation.
The aim of this study is to evaluate the incremental diagnostic value of CTP over CCTA in intermediate to high risk patients scheduled for invasive coronary angiography (ICA) plus clinically indicated invasive fractional flow reserve (FFR) for suspected CAD.
Methods and Materials: Consecutive symptomatic patients with intermediate to high pre-test probability of CAD and scheduled for clinically indicated ICA+FFR, were prospectively enrolled. All patients underwent rest-CCA followed by stress-CTP protocol with adenosine (Revolution CT Scanner, GE Healthcare, Milwaukee, WI) with injection of 70 ml of Iodixanol 320 (Visipaque 320 mg/ml, GE Healthcare, Oslo, Norway) as additional test. CCTA and CTP were defined positive for the presence of 50% stenosis and for the presence of subendocardial hypoenhancement encompassing ≥25% of transmural myocardial thickness within a specific coronary territory, respectively. At ICA, obstructive CAD was defined by the presence of ≥50% stenosis and hemodynamically significant CAD was defined by the presence of >50% stenosis on left main coronary artery, severe (>80%) or occlusive stenosis or FFR<0.80. The additive value of CTP versus CCTA to rule out the presence of hemodynamically relevant stenosis were performed on a per-vessel basis.
Results: One hundreds patients [mean age: 66±9 years, male: 69 (69%)] were included in our study. Obstructive CAD was found in 34% (136/400) of vessels and in 72% (72/100) of patients. Hemodynamically significant CAD was present in 29% (117/400) of vessel and in 44% (44/100) of patients. In a vessel-based model, CCTA alone and CTP showed a sensitivity and specificity of 98% [CI95%:95-100)], 76% [CI95%:71-82)] and 91% [CI95%:85-97)], 94% [CI95%:93-99)], respectively. CTP showed a higher area under the curve (AUC) as compared to CCTA alone to rule out hemodinamically significant CAD (0.93 vs. 0.83, p:0.002).
Conclusion: In patients with intermediate to high pre-test likelihood of CAD, CTP had incremental value over CCTA alone, to diagnose the presence of hemodynamically significant CAD.

Accuracy of coronary computed tomographic angiography to detect obstructive coronary artery disease by using stress versus rest dataset in patients referred to stress computed tomo

A. Baggiano[1], G. Muscogiuri[1], M. Guglielmo[1], S. Mushtaq[1], E. Conte[1], A. Formenti[1], E. Mancini[1], D. Andreini[1], A. I. Guaricci[2], G. Pontone[1]; [1]Milan/IT, [2]Bari/IT

Purpose/Objectives: The combined evaluation with coronary computed tomographic angiography (CCTA) and stress computed tomographic perfusion (CTP) is emerging as robust tool to provide anatomical and functional information in intermediate to high risk patients with suspected coronary artery disease (CAD). Unfortunately, this approach requires two acquisitions with double iodine contrast agent injection and radiation exposure.
The aim of this study is to compare the diagnostic accuracy of CCTA to detect obstructive CAD between stress versus rest dataset as compared to invasive coronary angiography (ICA).
Methods and Materials: One hundred consecutive symptomatic patients [mean age: 66±9 years, male: 69 (69%)] with intermediate to high pre-test probability of CAD and scheduled for clinically indicated ICA, were prospectively enrolled. All patients underwent rest-CCTA followed by stress-CTP protocol with adenosine (Revolution CT Scanner, GE Healthcare, Milwaukee, WI) with injection of 70 ml of Iodixanol 320 (Visipaque 320 mg/ml, GE Healthcare, Oslo, Norway). For both datasets, the image quality was evaluated with Likert score [score 1: non-diagnostic; score 2: adequate; score 3: good; score 4: excellent]. Moreover, the severity of coronary lesions was quantified in multi-planar curved reformatted images by identifying the minimum diameter and reference diameter for all stenoses, and the percentage of stenosis will be derived according to the following formula: (Dref − Dmin)/Dref · 100, where Dref is the reference diameter and Dmin is the minimum diameter. For CCTA and ICA, the obstructive CAD was defined as the presence of coronary artery stenosis≥50%.
Results: Obstructive CAD was found in 69% (69/100) of patients at ICA. The stress CTP was successfully performed in all patients. In a vessel-based model, the stress dataset showed a higher heart rate as compared to the rest dataset (76±14 vs 62±9 bpm, p<0.001) with similar image quality (3.0±1.0 vs. 3.4±0.9, p < 0.05). The stress dataset showed similar sensitivity (100% [CI95%:100-100)] vs. 96% [CI95%:91-100)] but slight lower specificity (72% [CI95%:56-89)] vs. 86% [CI95%:74-99), p>0.05] as compared to rest dataset. However, in both vessel and patient based model, stress and rest dataset showed similar area under the curve (AUC) (0.89 vs. 0.92 and 0.92 vs. 0.93).
Conclusion: In static stress CTP, the new generation scanner allows to perform the coronary artery imaging in the stress dataset with the same accuracy of rest dataset. This preliminary evidence opens the potential scenario to perform a single stress acquisition providing anatomical and functional information without the need of additional scan.

Left atrial appendage closure guided by 3D printed patient-specific models

G. Muscogiuri[1], M. Guglielmo[1], A. Baggiano[1], M. Conti[2], S. Marconi[2], F. Auricchi[2], G. Fassini[1], D. Andreini[1], A. I. Guaricci[3], G. Pontone[1]; [1]Milan/IT, [2]Pavia/IT, [3]Bari/IT

Purpose/Objectives: Percutaneous left atrial appendage (LAA) occlusion has emerged as an alternative therapeutic approach to medical therapy for stroke prevention in patients affected by atrial fibrillation. Thanks to 3D printing is nowadays possible to manufacture patient-specific models of any given anatomical portion of the heart reconstructed by medical images such as Computed Tomography Angiography (CTA). Moving from our preliminary experience, the present study aims at assessing whether the sizing of the implanted occluder device, based on the sole medical image analysis, is in accordance with the sizing obtained using the 3D printing models.
Methods and Materials: We retrospectively analysed our database to identify 13 cases of LAA occlusion. For each case, we segmented the pre-operative CTA scan by ITK-snap [2] creating a LAA 3D model (Caretronik, Prato, Italy), that after smoothing, refining, and improvement of the mesh quality was considered suitable for 3D stereolithography printing (SLA) technique (Form 2 Desktop, Formlabs Inc., MA, USA). Two independent observers measured the LAA landing zone, major and minor axis using a digital caliper. The measurements were used for sizing. A rehearse occlusion was then accomplished using the 3D printed LAA and the occluder device models; the resulting values were subsequently compared with the size of the implanted device to assess agreement, over or underestimation and its correlation with post-operative drawbacks.
Results: Thirteen patients, undergoing percutaneous LAA occlusion, were retrospectively analyzed; for each of them a patient-specific 3D LAA printed model was manufactured using pre-operative CTA images. The comparison between the 3D printed model sizing and the actual sizing revealed that: i) in 54% of the cases (n=7) the actual sizing was underestimated when compared to the 3D printed model; ii)in 38% of the cases (n=5) the two sizing approaches matched; iii) only in 1 case (8%) an overestimation of the actual size compared to the 3D printed model was detected. It is worth noticing that in all underestimated cases a drawback, such as leakage or device migration was observed; consequently, the results suggest that the use of 3D printing models help in finding the correct size of the device, potentially avoiding the negative outcome of the surgery.
Conclusion: This report demonstrates that 3D printing LAA model may contribute in sizing the device, finding its correct position and guiding the choice of the device, providing additional data to angiography and TEE.

EDUCATIONAL POSTER

P-0003 **Modern technologies in diagnostics of tracheomalacia in patients with cicatricial stenosis of the trachea in the perioperative period**
I. Koroleva, M. Mishchenko, V. Parshin; Moscow/RU

P-0005 **MDCT in the diagnosis of pulmomary infiltration with eosinophilia (PIE-syndrom)**
I. Koroleva; Moscow/RU

P-0007 **Radiomics and Lung cancer**
A. Farchione, A. R. Larici, A. Ottavianelli, J. Lenkowicz, L. Calandriello, G. Cicchetti, A. del Ciello, G. Sica, L. Bonomo, R. Manfredi; Rome/IT

P-0010 **Various imaging spectrum of pulmonary cryptococcosis: A pattern analysis**
J. H. Kim, K. H. Lee, H. Y. Lee, Y. J. Kim, G. R. Kim, Y. S. Jeon, S. G. Cho; Incheon/KR

P-0016 **Paradoxical movement of the interventricular septum. Physiological and pathological conditions that may cause anomalous interventricular septal movement. Cardiac-MR study**
C. Saborido Avila, M. Rodríguez Álvarez, B. Nieto Baltar; Vigo/ES

P-0019 **A radiologic review of acute aspiration pneumonia in the elderly**
E.-Y. Kang[1], H. S. Yong[1], K. Y. Lee[2], Y. W. Oh[1]; [1]Seoul/KR, [2]Ansan/KR

P-0021 **Lung cancer staging: Update**
T. J. Kim; Seoul/KR

P-0028 **Imaging Spectrum of Primary Malignant Chest Wall Tumors**
B. Alami, C. A. Beiba, S. Boujraf, Y. Alaoui Lamrani, M. Boubou, M. Maaroufi; Fes/MA

P-0029 **Bronchial Carcinoid Tumors of the Thorax**
B. Alami, S. Boujraf, Y. Alaoui Lamrani, M. Boubou, M. Maaroufi; Fes/MA

P-0032 **Radiologic finding of pulmonary histoplasmosis: Pictorial review**
S. J. Hong[1], Y. Lee[2]; [1]Guri-si/KR, [2]Guri/KR

P-0033 **Recurrent pneumothorax: Important to investigate the cause of secondary spontaneous pneumothorax**
S. Y. Shin, D. W. Sung; Seoul/KR

P-0036 **Percutaneous transthoracic needle biopsy: Various techniques and complications**
C. H. Park, Y. T. Kim, S. S. Jou; Cheonan/KR

P-0037 **Drug-Induced Pulmonary Toxicity: High Resolution Computed Tomography Findings**
C. Valdesi[1], L. Mazzamurro[2], L. Fabrizio[3], M. Scutti[4], M. Mereu[5], R. L. Patea[5], A. R. Cotroneo[5]; [1]Palermo/IT, [2]Pescara/IT, [3]San Salvo/IT, [4]Guardiagrele/IT, [5]Chieti/IT

P-0042 **Non-tumorous disease of the mediastinum: Radiologic features**
K. Y. Lee[1], H. Lee[1], C. Kim[2], E.-Y. Kang[2], Y. W. Oh[2], H. S. Yong[2], S. H. Hwang[2]; [1]Ansan/KR, [2]Seoul/KR

P-0045 **Asbestos related pleural and parenchymal pathologies: Computed Tomography findings**
N. Isiksalan Ozbulbul, M. Metintas, G. Ak; Eskisehir/TR

P-0048 **Pulmonary calcifications: Imaging features and differential diagnosis**
L. Mazzamurro[1], C. Valdesi[2], L. Fabrizio[3], M. Scutti[4], M. Mereu[5], R. L. Patea[5], A. R. Cotroneo[5]; [1]Pescara/IT, [2]Palermo/IT, [3]San Salvo/IT, [4]Guardiagrele/IT, [5]Chieti/IT

P-0050 **A comparison of lung cancer ablation modalities and review of imaging findings**
E. Skondras, M. Efstathiou, P. Dalal; London/UK

P-0051 **Hyperenhancing Mediastinal Masses: Spectrum of Causes and Imaging Features**
Y. W. Oh[1], S. H. Hwang[1], S. Y. Ham[1], E.-Y. Kang[1], K. Y. Lee[2]; [1]Seoul/KR, [2]Ansan/KR

P-0053 **Multimodality imaging follow-up after radiofrequency ablation (RFA) in patients with non-small cell lung cancer (NSCLC): An our experience-based pictorial review**
A. del Ciello, L. Leccisotti, A. Ottavianelli, V. Scolozzi, A. Farchione, L. Calandriello, M. L. Calcagni, A. R. Larici, R. Manfredi; Rome/IT

P-0057 **Lung imaging in acute respiratory distress syndrome's evolution**
L. Fabrizio[1], M. Scutti[2], C. Valdesi[3], L. Mazzamurro[4], R. L. Patea[5], M. Mereu[5], A. R. Cotroneo[5]; [1]San Salvo/IT, [2]Guardiagrele/IT, [3]Palermo/IT, [4]Pescara/IT, [5]Chieti/IT

P-0058 **CT findings of smoking-related lung disease**
A. L. Amado da Costa[1], R. Gaio[1], P. Campos[2], J. Fonseca Santos[1]; [1]Lisbon/PT, [2]Cascais/PT

P-0061 **Vascular complications of chronic liver disease and portal hypertension: Thoracic Imaging Findings**
H. Lee, V. Cardinal, C. Tavares, M. Wanderley, M. V. Y. Sawamura, R. Guerrini; Sao Paulo/BR

P-0062 **Clinicoradiologic significance of chronic pulmonary aspergillosis that a thoracic radiologist should know — based on the updated guideline by ERS/ESCMID**
K. E. Shin[1], J. S. Park[2]; [1]Bucheon-si, Gyeonggi-do/KR, [2]Bucheon/KR

P-0064 **Unwelcome Guests! The imaging findings of non-thrombotic pulmonary emboli**
S. Hesni, S. Hare; London/UK

P-0067 **What every radiologist should know about subsolid nodules (SSNs): Evaluation and management**
G. Cicchetti[1], P. Franchi[2], G. Sica[1], A. del Ciello[1], A. Farchione[1], L. Calandriello[1], L. Bonomo[1], A. R. Larici[1], R. Manfredi[1]; [1]Rome/IT, [2]Teramo/IT

P-0071 **TNM Staging System for Esophageal Cancer: Up To Date**
S. L. Betancourt[1], D. M. Palacio[2]; [1]Houston/US, [2]Tucson, AZ/US

P-0072 **Mediastinal Tumours: Compartment Anatomy and Use of Cardiovascular Magnetic Resonance Imaging Techniques**
M. Arzanauskaite[1], R. H. Mohiaddin[2]; [1]Liverpool/UK, [2]London/UK

P-0077 **Thoracic Manifestations Of Connective Tissue Diseases**
L. M. A. QUENUM, S. KOLANI, A. L. M. Youssef, M. Boubbou, M. Maaroufi, B. ALAMI; FES/MA

P-0078 **Noninfectious aortitis must be differentiated with AAS**
K. Banioniene; Kaunas/LT

P-0082 **Reversed Halo Sign (RHS) in chronic thrombo-embolism complicated by pulmonary infarction**
F. Landolfi[1], G. M. Barelli[1], C. De Dominicis[1], A. Laghi[2]; [1]Rome/IT, [2]Latina/IT

P-0083 **Acute Respiratory Distress Syndrome: Spectrum of Imaging Findings and Radiologic Mimics**
N. Antunes, R. Santos, C. Leal, O. Fernandes, L. Figueiredo; Lisbon/PT

P-0084 **A Pattern-based approach in the diagnosis of small airways diseases using MDCT**
Z. Moqbel, A. Rizk, A. Elnekeidy, A. Baess; Alexandria/EG

P-0086 **Multivariable appearance of LAC and its subtypes on CT images**
J. Petkevicius, I. Simeliunaite, J. ZAVECKIENE; Kaunas/LT

P-0087 **Diaphragmatic hernias: Emphasis on CT imaging features**
P. C. D. M. Pereira, I. Marques, L. Batista, D. Castelo; Vila Nova de Gaia/PT

P-0089 **Congenital pulmonary airway malformations: Postnatal radiologic findings and differential diagnosis**
L. Tamkevičiūtė, A. Tumenas, J. ZAVECKIENE; Kaunas/LT

P-0090 **Pulmonary complications of illicit drug abuse**
I. Willekens, J. de Mey; Brussels/BE

P-0092 **Learning from superior vena cava**
A. L. Sanchez Martinez, D. Varona Porres, O. Persiva Morenza, J. Andreu, E. Pallisa; Barcelona/ES

P-0093 **Quantitative CT imaging of the lung: Current applications and future perspectives in diagnostics of nodule and diffuse lung disease**
E. Casilli, M. Silva, G. Milanese, N. Sverzellati; Parma/IT

P-0095 **Bronchial and Vascular Anastomoses in Lung Transplant – Normal Findings and Complications using CT**
J. M. Almeida, V. Carvalho, N. Antunes, C. Leal, O. Fernandes, P. Calvino, L. Semedo, L. Figueiredo; Lisbon/PT

P-0096 **Imaging of Partial anomalous pulmonary vein connection with multislice compruted tomography (MDCT): A pictorial review**
S. Kampanarou[1], S. Katsilouli[2], O. Karapanagiotou[2], D. Panagiotidou[3], I. Mastorakou[2]; [1]Kallithea/GR, [2]Athens/GR, [3]Thessaloniki/GR

P-0097 **HRCT features of radiation-induced lung disease**
M. Scutti[1], L. Fabrizio[1], C. Valdesi[1], L. Mazzamurro[2], M. Mereu[1], R. L. Patea[1], A. Travaglini[1], A. R. Larici[3]; [1]Chieti/IT, [2]Pescara/IT, [3]Rome/IT

P-0103 **Fontan circulation in an adult: A guide for the radiologist**
M. Arzanauskaite[1], E. Nyktari[2], I. Voges[3]; [1]Liverpool/UK, [2]Athens/GR, [3]London/UK

P-0104 **Idiopathic pulmonary fibrosis, when things go south: HRCT findings**
M. Scutti[1], L. Fabrizio[1], C. Valdesi[1], L. Mazzamurro[2], M. Mereu[1], R. L. Patea[1], A. R. Larici[3]; [1]Chieti/IT, [2]Pescara/IT, [3]Rome/IT

P-0105 **Pulmonary tuberculosis: Still a first line diagnosis in Portugal**
P. M. Costa[1], A. C. Silva[2], N. Rodrigues[2], A. M. F. P. Reis[2], R. Correia de Abreu[2], M. J. Ribeiro[1], J. A. Machado[2]; [1]Matosinhos/PT, [2]Porto/PT

P-0106 **Hold your breath! Inhalational lung disease - imaging findings**
V. Burovienė[1], M. Arzanauskaite[2], J. ZAVECKIENE[1]; [1]Kaunas/LT, [2]Liverpool/UK

P-0107 **Radiology of Eponymous Thoracic Diseases**
J. G. Colville, B. Bhartia, A. L. Johnstone, M. Darby, S. Karthik; Leeds/UK

P-0108 **Large vessels vasculitis – Multimodal imaging in diagnosis and follow-up**
A. L. M. Lourenço, C. A. S. Ruano, L. F. S. B. Torres, C. Leal, S. Pinheiro, M. Silva, S. I. C. Silva, Â. Marques, O. Fernandes; Lisbon/PT

P-0111 **Systemic disorders affecting lung and heart: Key points for diferential diagnosis using cardiac magnetic resonance and multidetector computed tomography**
J. M. Gutiérrez[1], L. Jimenez-Juan[1], L. kha[1], D. Vargas[2], I. Roifman[1], L. Guo[1], A. Oikonomou[1]; [1]Toronto/CA, [2]Colorado/US

P-0113 **Blastomycosis - The great pretender**
M. D. Martin, J. P. Kanne, C. Meyer; Madison, WI/US

Abstracts appear as submitted to the abstract/poster submission system and have not been checked for correctness and completeness.

SCIENTIFIC POSTER

P-0001 **Low field cardiac MRI**
H.-M. Klein; Burbach/DE

P-0002 **Image quality and radiation dose of cardiac CTA in overweight and obese patients**
D. Golubickas, E. Naujokaite, A. Jankauskas, R. Slapikas, A. Basevicius; Kaunas/LT

P-0004 **Diaphragm thickness measurements on computed tomography**
F. Ufuk, P. Cakmak, B. Yagci; Denizli/TR

P-0006 **Chest CT reports: How the clinician wants them - referrer preference on content, format and key images**
D. Serich[1], L. Xu[1], S. Hashoul[2], Y. D. Weerakkody[1]; [1]Perth/AU, [2]Haifa/IL

P-0008 **Computed tomography evaluation of aberrant right subclavian artery: Anatomy and clinical implications**
M. Krupinski, M. Irzyk, Z. Moczulski, R. P. Banys, M. Urbańczyk-Zawadzka; Kraków/PL

P-0009 **‚COPD: CT Thorax - friend or foe': Clinical utility of CT in diagnosing co-morbidities**
A. Vohra, S. Raza, P. Dalal, S. Kaul; London/UK

P-0011 **Left atrium, left atrial appendage and pulmonary veins anatomical variants in patients with atrial fibrillation versus patients with sinus rhythm**
M.-L. Cobzeanu, A. C. Rusu, R. O. Chistol, D. Negru; Iasi/RO

P-0012 **Prevalence of bronchial wall thickening and air trapping in patients without known respiratory tract disease or smoking habits**
E. Detorakis[1], M. Raissaki[1], A. Papachristodoulou[2], R. Illing[3]; [1]Iraklion/GR, [2]Thessaloniki/GR, [3]Budapest/HU

P-0013 **Cardiovascular magnetic resonance (CMR) imaging in patients with acute myocarditis and a preceding upper respiratory tract infection**
E. Detorakis[1], M. Raissaki[1], A. Papachristodoulou[2], I. Papadopoulou[3], R. Illing[4]; [1]Iraklion/GR, [2]Thessaloniki/GR, [3]Heraklion/GR, [4]Budapest/HU

P-0014 **Reproducibility of the automatic calculation of average intima-media thickness (IMT) in the carotids' ultrasound study**
F. Secchi, G. Lastella, F. Wiedenmann, M. Alì, F. Sardanelli; Milan/IT

P-0015 **Evaluation of the anatomical distribution of pulmonary emboli on CT pulmonary angiography**
S.-M. O'Hanlon, T. Wooding, A. Mittal, Y. D. Weerakkody; Perth/AU

P-0017 **Low level of Albumin and Zinc (Zn) Serum in patients Tuberculosis with and without destroyed lung**
A. D. Messah; Tulang Bawang/ID

P-0018 **Magnetic Resonance Imaging Detects Mosaic Perfusion in Early Cystic Fibrosis Lung Disease**
P. Leutz, M. Stahl, H. U. Kauczor, A. Alrajab, M. Puderbach, S. Triphan, O. Sommerburg, M. Mall, M. Eichinger, M. O. Wielpütz; Heidelberg/DE

P-0020 **Prediction of Prognosis for Idiopathic Pulmonary Fibrosis with Thin-Section CT findings: Visual and Simple Quantitative Assessment**
J. J. Woo, Y. S. Kim, J. K. An; Seoul/KR

P-0022 **Fast thoracic MRI as an alternative to chest X-ray radiography: A retrospective evaluation of 287 patients**
M. Alì, F. Secchi, C. B. Monti, G. Di Leo, F. Sardanelli; Milan/IT

P-0023 **Planning of CT-guided Percutaneous Lung Biopsy Trajectory: Comparison Using Axial Images with Additional Sagittal Images for upper lobe lesions**
S. S. Jou, C. H. Park, Y. T. Kim; Cheonan/KR

P-0024 **A comparative analysis of PACS/RIS reporting efficiency from a user perspective**
A. Chandrashekar[1], A. Devaraj[1], L. Dixon[1], S. Copley[1], C. A. Ridge[2], S. P. G. Padley[1]; [1]London/UK, [2]Dublin/IE

P-0025 **A retrospective analysis of CT pulmonary angiograms in the emergency department: Demographic, clinical and radiological features in a single centre**
A. Carvalho, P. Leitão, J. Ferreira-Coimbra, L. Flores, J. Rebelo, R. Cunha; Porto/PT

P-0026 **A combination of unroofed coronary sinus and intracavitary course of the right coronary artery detected by CT angiography**
M. J. Rafiee[1], F. Babaki Fard[1], S. Mohammadi[2]; [1]Tehran/IR, [2]Québec/CA

P-0027 **An automatic algorithm for left ventricular function quantification in cardiac MRI: Inter-method and inter-reader reproducibility**
M. Zanardo[1], F. Messina[1], G. Di Leo[2], M. Codari[2], S. D. Fabiano[2], F. Secchi[1], F. Sardanelli[1]; [1]Milan/IT, [2]San Donato Milanese/IT

P-0030 **Image quality of a 1-Tesla open MRI scanner for evaluation of cardiac diseases**
F. Secchi[1], B. Gold[1], C. B. Monti[1], P. M. Cannao'[2], M. Alì[1], S. Papa[1], F. Sardanelli[1]; [1]Milan/IT, [2]San Donato Milanese/IT

P-0031 **Association between small pulmonary vascular area and mild airflow limitation in healthy smokers**
M. J. Park[1], K. N. Jeon[2]; [1]Jinju/KR, [2]Changwon/KR

P-0034 **Sensitivity of chest X-ray in detection of pulmonary emphysema, Preliminary results from Czech Multicenter Register of Chronic Obstructive Pulmonary Disease**
M. Hyrsl, E. Kocova, V. Koblizek; Hradec Králové/CZ

P-0035 **Balloon Pulmonary Angioplasty in Chronic Thromboembolic Pulmonary Hypertension: The role of MultiDetector Computed Tomography**
O. Karapanagiotou[1], S. Katsilouli[1], S. Kampanarou[2], P. Karyofyllis[1], I. Mastorakou[1]; [1]Athens/GR, [2]Kallithea/GR

P-0038 **Low dose CT of the lung using iterative reconstruction: Our experience**
C. Valdesi, A. Giammarini, A. Delli Pizzi, L. Fabrizio, M. Scutti, M. Mereu, R. L. Patea, A. R. Cotroneo; Chieti/IT

P-0039 **Image quality and radiation dose at routine unenhanced chest-CT using a tin filter in a new single-source CT model: Comparison with other chest-CT scans in the same patient**
J. Arenas-Jimenez, E. García-Garrigós, E. Pinilla Soler, C. A. Duarte Obando, M. Sirera Matilla, M. C. Planells Alduvin; Alicante/ES

P-0040 **Left circumflex artery originating from right sinus vasalva with left atrial diverticulum and left-sided atrial septal pouch: 128-slice computed tomography findings**
N. Isiksalan Ozbulbul, E. Emekli, K. U. Mert; Eskisehir/TR

P-0041 **Myocardial CT-derived Extracellular Volume (ECV): A Systematic Review and Meta-analysis**
C. B. Monti[1], M. Zanardo[1], S. Schiaffino[2], F. Secchi[1], P. M. Cannao[1], G. Di Leo[3], F. Sardanelli[1]; [1]Milan/IT, [2]Genova/IT, [3]San Donato Milanese/IT

P-0043 **Relationship between OSA and presence of subclinical coronary artery disease predicted by calcification of coronary artery and thoracic aorta and epicardial fat volume**
K. Y. Lee[1], S. Kim[1], S. H. Kim[1], C. Kim[2], C. Shin[2], S. K. Lee[1]; [1]Ansan/KR, [2]Seoul/KR

P-0044 **Quantitative versus qualitative evaluation of static stress computed tomographic perfusion to detect hemodinamically significant coronary artery disease in intermediate to high ris**
A. Baggiano[1], G. Muscogiuri[1], M. Guglielmo[1], S. Mushtaq[1], E. Conte[1], A. D. Annoni[1], A. Formenti[1], D. Andreini[1], A. I. Guaricci[2], G. Pontone[1]; [1]Milan/IT, [2]Bari/IT

P-0046 **Prognostic relevance of subclinical coronary and carotid atherosclerosis in asymptomatic at-risk adult population**
G. Muscogiuri[1], M. Guglielmo[1], A. Baggiano[1], S. Mushtaq[1], E. Conte[1], A. D. Annoni[1], E. Mancini[1], D. Andreini[1], A. I. Guaricci[2], G. Pontone[1]; [1]Milan/IT, [2]Bari/IT

P-0047 **Salvage of suboptimal enhancement of pulmonary artery in chest CT: Experience using a dual-layer detector spectral CT**
K. N. Jeon, K. Bae, S. B. Cho, S. E. Park, J. I. Moon, H. J. Baek, B. H. Choi, K. H. Ryu; Changwon/KR

P-0049 **A new post-processing algorithm named adaptive statistical iterative reconstruction (ASIR-V) has been recently introduced. The aim of this manuscript is to analyze the impact of AS**
G. Muscogiuri[1], A. Baggiano[1], M. Guglielmo[1], S. Mushtaq[1], E. Conte[1], A. Formenti[1], E. Mancini[1], D. Andreini[1], A. I. Guaricci[2], G. Pontone[1]; [1]Milan/IT, [2]Bari/IT

P-0052 **Peripheral small lung nodules with pleural tag detected on lung CT scans remain stable in follow-up: Clinical and radiological characteristics in a series of 40 patients**
J. Arenas-Jimenez, E. García-Garrigós, M. Sirera Matilla, C. Gracia Serrano, A. Barredo Sanchez; Alicante/ES

P-0054 **Bronchopulmonary carcinoid tumours: CT appearance and multifocal occurrence of central and peripheral lesions**
K. Peldschus[1], T. H. Schröder[1], L. Welker[2], G. Adam[1], C. Weber[1]; [1]Hamburg/DE, [2]Grosshansdorf/DE

P-0055 **Prevalence and Clinical Outcomes of Extracardiac Findings on Cardiac MRI from a Large Single-Centre Cohort**
E. R. Hurst, D. Oswal, R. Chittal; Wakefield/UK

P-0056 **Quantification of Emphysema using Hybrid and Full Iterative Model Reconstruction in low dose HRCT scans and correlation with Pulmonary Lung Function tests**
E. De Boer, G. Ismailova, S. Walen, I. Nijholt, M. A. Edens, J. W. van den Berg, M. F. Boomsma; Zwolle/NL

P-0059 **FDG-PET in Infections and Inflammatory Pathologies Associated with Cardiovascular Diseases**
A. A. Albweady[1], S. Raja[1], S. George[2], M. ALHARBI[1], K. ALDOSSARI[1]; [1]Riyadh/SA, [2]Houston/US

P-0060 **Differentiation between lymphangioleiomyomatosis and Birt-Hogg-Dubé syndrome: Analysis of pulmonary cysts on CT**
E. J. Chae, H. J. Park, J. W. Song, K.-H. Do, C. Kim, S. M. Lee; Seoul/KR

P-0063 **CT findings and prognostic CT features of seasonal influenza viral pneumonia in adults**
K. E. Shin[1], J. S. Park[2]; [1]Bucheon-si, Gyeonggi-do/KR, [2]Bucheon/KR

P-0065 **Pleural invasion classification of primary lung cancer by a 3T MRI with radial T1-weighted 3D spoiled gradient echo sequence**
W. Kwon; Wonju/KR

P-0066 **3D printing of the aortic root based on cardiac computed tomography and cardiac magnetic resonance imaging: Preliminary experience on pre-procedural planning for aortic valve sizin**
R. Faletti, A. Cosentino, M. Gatti, G. Pennisi, A. Depaoli, P. Fonio; Turin/IT

P-0068 **Comparative analysis of 256-slice dual source CT coronary angiography with catheter coronary angiography in evaluation of coronary in-stent restenosis**
A. K. Sinha[1], N. Nischal[1], R. Gupta[2], S. Arya3, N. Goyal[1], S. K. Puri[1]; [1]New Delhi/IN, [2]Patna/IN, [3]Delhi/IN

P-0069 **Evaluation with quantitative measurement developing airway-related physio-biologic marker using chest HRCT in COPD patients**
Y. S. Kim, Y. H. Kim, J. Cho, J. Kim, Y. K. Kim; Gwangju/KR

P-0070 **The feasibility of low radiation and low contrast agent in coronary CT angiography with knowledge-based iterative model reconstruction**
T. H. Kim, S. J. Kim, C. H. Park, J. Lee; Seoul/KR

P-0073 **Differences in the CT findings between vulnerable plaque and culprit lesions in acute coronary syndrome**
J. Y. YOO[1], E. J. Chun[2], S. M. Yoo[3], I. S. Song[4]; [1]Cheongju-si/KR, [2]Seongnam-Si/KR, [3]Bundang/KR, [4]Chunju/KR

P-0074 **Clinical significance of lobe-specific emphysema index for prediction of prolonged air leak after anatomical segmentectomy**
S. J. Kim, T. H. Kim, D. H. Moon, C. H. Park, D.-Y. Kang, H. S. Lee, M. K. Kang, S. Lee; Seoul/KR

P-0075 **Idiopathic Pulmonary Fibrosis :- Correlation of HRCT findings with Pulmonary Function Tests**
R. Pothera[1], C. P. Mathew[2], A. V. Nair[3], S. Karumathil Pullara[1], D. Viswam[1], S. Moorthy[1]; [1]Kochi/IN, [2]Kochi, Ke/IN, [3]Trivandrum, Kerala/IN

P-0076 **Influence of radiation dose and iterative reconstruction on pulmonary nodule volumetric measurement: A phantom study using wide-volume axial scan**
H. N. Lee; Seoul/KR

P-0079 **Adult Type ALCAPA syndrome: CT-Imaging of a rare coronary artery anomaly**
A. Patrianakos, A. Hatzidakis, M. Marketou, A. Kostaki, E. D. Savva, F. Parthenakis; Heraklion/GR

P-0080 **Computed tomography angiography in children with low left ventricular ejection fraction**
A. Skripnik, V. Fokin, G. E. Trufanov, R. R. Mironchuk, T. Loevets, T. Vershinina, E. Vasichkina; Saint-Petersburg/RU

P-0081 **Pulmonary regurgitation volume versus pulmonary regurgitation fraction in congenital heart disease**
C. B. Monti[1], F. Secchi[2], M. Alì[2], A. Ziouziou[1], M. Petrini[1], F. Sardanelli[2]; [1]San Donato Milanese/IT, [2]Milan/IT

P-0085 **Diffusion-Weighted Magnetic Resonance Imaging (DWI-MRI) can detect vessel wall inflammation in patients with large vessel Giant Cell Arteritis (GCA)**
A. Napolitano, G. Ironi, E. Tombetti, E. Incerti, M. Picchio, L. Gianolli, L. Dagna, A. Manfredi, F. De Cobelli; Milan/IT

P-0091 **Prevalence and patterns of lung abnormalities detected by chest CT in patients with vascular Ehlers Danlos Syndrome (vEDS)**
S. Boussouar[1], A. Benattia[1], J. B. Escudier[1], L. Gibault[1], F. Capron[1], P.-Y. Brillet[2], P. A. Grenier[1], M. Frank[1], E. Mousseaux[1], O. Sanchez[1]; [1]Paris/FR, [2]Bobigny/FR

P-0094 **CT dose reduction for epicardial fat measurement in obese patients: Effects of low-dose cardiac CT and adaptive statistical iterative reconstruction**
S. Mirafzal, C. Lahaye, A. Mulliez, Y. Boirie, L. Boyer, L. Cassagnes; Clermont-Ferrand/FR

P-0098 **CT Texture Analysis as an early biomarker of tumor response to immunotherapy in lung cancer: Preliminary results from a Δ-Radiomic study**
G. Ficarra[1], E. Barabino[1], C. Genova[1], S. Mennella[1], M. Verda[2], G. Pittaluga[1], F. Grossi[1], G. Cittadini[1]; [1]Genova/IT, [2]Imperia/IT

P-0099 **LGE pattern in cardiac sarcoidosis**
D. Piotrowska-Kownacka, M. Martusewicz-Boros, L. Kownacki, E. Wiatr, A. Kempisty, M. Golebiowski; Warsaw/PL

P-0100 **The use of Time-Resolved MR Angiography in the evaluation of Pelvic Congestion Syndrome**
S. Wassef, A. Stolpen; Iowa City, IA/US

P-0101 **Possibilities of computed tomography angiography in assessment of aortic valve in patients with the calcification of the aortic valve**
R. R. Mironchuk, A. Skripnik, V. Fokin, G. E. Trufanov; Saint-Petersburg/RU

P-0102 **Late Enhancement in Cardiac CT - Comparison with Cardiac MR**
D. Vignale, A. Esposito, A. Palmisano, G. Benedetti, A. Del Maschio, F. De Cobelli; Milan/IT

P-0109 **What is the cut-off value of CT attenuation for distinguishing PMF from lung cancer in pneumoconiosis patient?**
Y. Jo, E. S. Lee, J. I. Jung; Seoul/KR

P-0110 **Does the contrast enhancement influence diagnostic accuracy in coronary CT angiography using APS?**
Y. Jo[1], J. J. Kim[2], J. I. Jung[1]; [1]Seoul/KR, [2]Jeju/KR

P-0112 **Impact of added CT-venography performed in combination with CT pulmonary angiography on the detection of deep venous thrombosis and relevant occult CT-findings**
P. I. Douek, D. C. ROTZINGER, R. Meuli, V. Dunet, S. Schmidt; Lausanne/CH

Abstracts appear as submitted to the abstract/poster submission system and have not been checked for correctness and completeness.